bioRxiv preprint doi: https://doi.org/10.1101/2023.02.04.527149; this version posted February 4, 2023. The copyright holder for this preprint (which was not certified by peer review) is the author/funder, who has granted bioRxiv a license to display the preprint in perpetuity. It is made available under aCC-BY-NC-ND 4.0 International license.

Extended fractional-polynomial generalizations of diffusion and Fisher-KPP equations on directed networks: Modeling neurodegenerative progression

Arsalan Rahimabadi[a,b,*], Habib Benali[a,b]

[a] *PERFORM Centre, Concordia University, Montreal, QC, Canada*
[b] *ECE Department, Concordia University, Montreal, QC, Canada*

Abstract

In a variety of practical applications, there is a need to investigate diffusion or reaction-diffusion processes on complex structures, including brain networks, that can be modeled as weighted undirected and directed graphs. As an instance, the celebrated Fisher-Kolmogorov-Petrovsky-Piskunov (Fisher-KPP) reaction-diffusion equation are becoming increasingly popular for use in graph frameworks by substituting the standard graph Laplacian operator for the continuous one to study the progression of neurodegenerative diseases such as tauopathies including Alzheimer's disease (AD). However, due to the porous structure of neuronal fibers, the spreading of toxic species can be governed by an anomalous diffusion process rather than a normal one, and if this is the case, the standard graph Laplacian cannot adequately describe the dynamics of the spreading process. To capture such more complicated dynamics, we propose a diffusion equation with a nonlinear Laplacian operator and a generalization of the Fisher-KPP reaction-diffusion equation on undirected and directed networks using extensions of fractional polynomial (FP) functions. A complete analysis is also provided for the extended FP diffusion equation, including existence, uniqueness, and convergence of solutions, as well as stability of equilibria. Moreover, for the extended FP Fisher-KPP reaction-diffusion equation, we derive a family of positively invariant sets allowing us to establish existence, uniqueness, and boundedness of solutions. Finally, we conclude by investigating nonlinear diffusion on a directed one-dimensional lattice and then modeling tauopathy progression in the mouse brain to gain a deeper understanding of the potential applications of the proposed extended FP equations.

Keywords: Fractional polynomial, Fisher-KPP reaction-diffusion equation, Nonlinear diffusion, Anomalous diffusion, Directed networks, Tauopathies

1. Introduction

A generalization of the Fisher-Kolmogorov-Petrovsky-Piskunov (Fisher-KPP) reaction-diffusion equation [1, 2] to undirected networks has recently been employed to study the spreading of prion-like proteins within the brain [3–6]. In fact, the Fisher-KPP equation has

*Corresponding author
Email addresses: arsalan.rahimabadi@concordia.ca (Arsalan Rahimabadi), habib.benali@concordia.ca (Habib Benali)

bioRxiv preprint doi: https://doi.org/10.1101/2023.02.04.527149; this version posted February 4, 2023. The copyright holder for this preprint (which was not certified by peer review) is the author/funder, who has granted bioRxiv a license to display the preprint in perpetuity. It is made available under aCC-BY-NC-ND 4.0 International license.

been altered by replacing the continuous Laplacian operator with the conventional graph Laplacian operator. This generalization and the concept of nonlinear diffusion prompted us to propose a new nonlinear graph Laplacian operator that allows us to capture more complex diffusion phenomena on both undirected and directed networks. We also extend the reaction term of the Fisher-KPP equation to introduce a larger family of reaction-diffusion models.

The dynamics of linear Laplacian operators in directed graphs have been well studied [7–10]. In the literature, the standard graph Laplacian has been developed in a variety of ways to study spectral information, such as eigenvalues, eigenvectors, and Cheeger constants, for graphs and hypergraphs [11–18]. Aside from the extensions regarding spectral graph theory, several generalizations of the standard graph Laplacian exist particularly for exploring anomalous and nonlinear diffusion processes, most of which are restricted to undirected graphs [19–31], and for studying the dynamics of chemical reaction networks (CRNs) [32], which are directed networks [33, 34]. Fractional graph Laplacian operators constructed by raising the Laplacian matrix to a real power between 0 and 1 [19–22], d-path Laplacian operators defined by using path matrices accounting for the existence of shortest paths of length d between two nodes [23], and the Mellin-transformed d-path Laplacian operators $\sum_{d=1}^{\infty} L_d d^{-s}$ [24–26], where s is a nonnegative real number, have been applied to investigate superdiffusion with a linear differential equation. Besides the normal diffusion, in which the mean square displacement (MSD) of particles scales linearly with time, and the anomalous superdiffusion processes, in which $MSD\left(t\right)$ is proportional to t^{ζ} with $\zeta > 1$, there is a substantial body of knowledge about the subdiffusion processes for which $\zeta < 1$, especially observed in biological systems [35–41]. In a recent paper [27], Diaz-Diaz and Estrada presented a linear diffusion equation incorporating the Mellin-transformed d-path Laplacian operator, which utilizes fractional-time derivatives to describe subdiffusion on undirected networks. Some nonlinear generalizations of the standard graph Laplacian operator on undirected graphs are the p-Laplace operator $\left(\Delta_{\omega,p} f\right)\left(x_i\right) = \sum_{x_j \sim x_i} \omega\left(x_i, x_j\right)^{p/2} \left|f\left(x_j\right) - f\left(x_i\right)\right|^{p-2} \left(f\left(x_j\right) - f\left(x_i\right)\right)$ for a vertex x_i and its variants, which have been exploited to introduce a family of discrete-in-time diffusion equations used in image processing [28, 29]. In order to examine the dynamics of interacting random walkers moving over unweighted undirected graphs, a nonlinear graph Laplacian operator has been suggested as follows [30]: $\mathcal{L}_i\left(\rho\right) = \sum_j L_{ij}\left(f\left(\rho_j\right) g\left(\rho_i\right) - \left(k_j/k_i\right) f\left(\rho_i\right) g\left(\rho_j\right)\right)$ for the mean-field node density ρ_i, where $L_{ij} = a_{ij}/k_j - \delta_{ij}$ is the usual graph Laplacian and k_i represents the degree of node i. Given functions $f\left(x\right) = x^{\alpha}$ and $g\left(x\right) = \left(1-x\right)^{\sigma}$ for $0 \leq x \leq 1$ and zero elsewhere, it was illustrated that the diffusion equation formed by $\mathcal{L}_i\left(\rho\right)$ has a unique stationary solution under some assumptions. Nevertheless, the authors have not addressed the existence and uniqueness of solutions of the proposed diffusion equation in a broader sense. In a recent work [31], considering functions $f\left(x\right) = x^m$ and $g\left(x\right) = 1$, it has been shown that taking the continuum limit of the diffusion equation incorporating $\mathcal{L}_i\left(\rho\right)$ for an infinite q-homogeneous tree, where each node has degree $q+1$ and the distance between nodes is given by a, yields the nonlinear partial differential equation (PDE) $\partial_t \rho = a^2\left(q+1\right)\partial_{xx}\left(\rho^m\right) - a\left(q-1\right)\partial_x\left(\rho^m\right)$, where $\rho\left(x,t\right)$ is identified with $\rho\left(x,t\right) = \rho_i\left(t\right)$. In the case of an infinite regular lattice, i.e.,

bioRxiv preprint doi: https://doi.org/10.1101/2023.02.04.527149; this version posted February 4, 2023. The copyright holder for this preprint (which was not certified by peer review) is the author/funder, who has granted bioRxiv a license to display the preprint in perpetuity. It is made available under aCC-BY-NC-ND 4.0 International license.

$q = 1$, the aforementioned PDE reduces to the so-called porous medium equation $\partial_t \rho = \sigma \Delta (\rho^m)$, with $m > 1$, admitting a family of self-similar solutions (in a weak sense), called Barenblatt-Pattle solutions, representing diffusion from a point source [42, 43]. The article [31] also verified the uniqueness of the stationary solution under specific conditions. However, similar to [30], it did not discuss the existence and uniqueness of the solution of the graph diffusion equation $d\rho_i/dt = \mathcal{L}_i(\rho)$ with initial conditions $\rho_i(0) \geq 0$ in a more general sense. Recently, Veerman et al. [32] propounded a nonlinear Laplacian framework for CRNs, which leads to the polynomial system of differential equations $dx/dt = -SL_{out}^T \psi(x)$, where S is a non-negative matrix with no zero rows, L_{out} is an out-degree Laplacian matrix, and each element of vector ψ is a monomial. It has been demonstrated that for a componentwise strongly connected network when $Ker S \cap Im L^T = \{0\}$, the proposed polynomial system has exactly one positive equilibrium x^* in a specified invariant set X_z. Using a Lyapunov function, the authors concluded the (local) asymptotic stability of that equilibrium point x^* in X_z, and they also verified that the ω-limit set of any positive initial condition in X_z either equals x^* or is a bounded set contained in the boundary of the positive orthant.

Our generalizations of the diffusion and reaction terms result in systems of differential equations involving fractional polynomial (FP) functions whose definitions are restricted to the nonnegative orthant, which is a closed subset of the Euclidean space. Hence, we first extend these functions to functions on an open subset possessing a differentiable structure, empowering us to gain the common methods and theorems of dynamical systems theory to analyze the proposed FP equations. In addition, since the extended FP functions are continuously differentiable on the whole space, we can investigate the properties of solutions not only with nonnegative initial conditions but also negative ones whose practical importance can be realized by introducing the notion of active concentration. The elaboration of the details is continued in Subsection 3. The remainder of the paper is organized as follows; we propose a nonlinear Laplacian operator and its corresponding diffusion equation in Subsections 4.1 and 4.2, respectively. For the extended FP diffusion equation, the existence and uniqueness of solutions as well as positively invariant sets are discussed Subsubsection 4.2.1, and we also establish the convergence of solutions and stability of equilibria in Subsubsection 4.2.2. Next, our generalization of the Fisher-KPP equation and a family of its positively invariant sets are presented in Subsection 5. For the purpose of illustrating the potential applications of our model, we first examine nonlinear diffusion on a directed one-dimensional lattice in Section 6 and then proceed to model tauopathy progression in the mouse brain in Section 7.

2. Mathematical preliminaries

2.1. Definitions and notations

To delineate our model, we first need to introduce a few definitions and notations. The set of all real numbers will be denoted by $\mathbb{R}$, and given $\gamma \in \mathbb{R}$, we define $\mathbb{R}_{\geq \gamma} = [\gamma, \infty)$, $\mathbb{R}_{> \gamma} = (\gamma, \infty)$, $\mathbb{R}_{\leq \gamma} = (-\infty, \gamma]$, and $\mathbb{R}_{< \gamma} = (-\infty, \gamma)$. Accordingly, $\mathbb{R}^M$, $\mathbb{R}^M_{\geq \gamma}$, $\mathbb{R}^M_{> \gamma}$, $\mathbb{R}^M_{\leq \gamma}$, and $\mathbb{R}^M_{< \gamma}$ represent the sets of all M-tuples whose components belong to $\mathbb{R}$, $\mathbb{R}_{\geq \gamma}$, $\mathbb{R}_{> \gamma}$, $\mathbb{R}_{\leq \gamma}$, and $\mathbb{R}_{< \gamma}$, respectively. The

bioRxiv preprint doi: https://doi.org/10.1101/2023.02.04.527149; this version posted February 4, 2023. The copyright holder for this preprint (which was not certified by peer review) is the author/funder, who has granted bioRxiv a license to display the preprint in perpetuity. It is made available under aCC-BY-NC-ND 4.0 International license.

set of all M-by-M matrices over $\mathbb{R}$ is indicated by $\mathcal{M}_M(\mathbb{R})$, and $\boldsymbol{I}$ also denotes the identity matrix. Throughout the paper, boldface is used to distinguish vectors and matrices from scalars. Suppose $\boldsymbol{u}, \boldsymbol{v}, \boldsymbol{w} \in \mathbb{R}^M$, and let $\boldsymbol{\Lambda}(\boldsymbol{v})$ be a diagonal matrix whose diagonal elements are the elements of $\boldsymbol{v}$. Then, the vector $\boldsymbol{v} \odot \boldsymbol{w}$ defined by $\boldsymbol{v} \odot \boldsymbol{w} = \boldsymbol{\Lambda}(\boldsymbol{v})\boldsymbol{w}$ is called the Hadamard product of $\boldsymbol{v}$ and $\boldsymbol{w}$, which is commutative, i.e., $\boldsymbol{v} \odot \boldsymbol{w} = \boldsymbol{w} \odot \boldsymbol{v}$, associative, i.e., $\boldsymbol{u} \odot (\boldsymbol{v} \odot \boldsymbol{w}) = (\boldsymbol{u} \odot \boldsymbol{v}) \odot \boldsymbol{w}$, and distributive over vector addition, i.e., $\boldsymbol{u} \odot (\boldsymbol{v} + \boldsymbol{w}) = \boldsymbol{u} \odot \boldsymbol{v} + \boldsymbol{u} \odot \boldsymbol{w}$ [44]. We also define functions $(\cdot)^{\boldsymbol{n}} : \mathbb{R}^M_{>0} \to \mathbb{R}^M$ by $\boldsymbol{x}^{\boldsymbol{n}} = (x_1^{n_1}, x_2^{n_2}, ..., x_M^{n_M})^T$, $|\cdot|^{\boldsymbol{n}} : \mathbb{R}^M \to \mathbb{R}^M$ by $|\boldsymbol{x}|^{\boldsymbol{n}} = (|x_1|^{n_1}, |x_2|^{n_2}, ..., |x_M|^{n_M})^T$, $\boldsymbol{sgn}(\cdot) : \mathbb{R}^M \to \mathbb{R}^M$ by $\boldsymbol{sgn}(\boldsymbol{x}) = (sgn(x_1), sgn(x_2), ..., sgn(x_M))^T$, and $\boldsymbol{ln}(|\cdot|) : \mathbb{R}^M \to \mathbb{R}^M$ by $\boldsymbol{ln}(|\boldsymbol{x}|) = (\tilde{x}_1, \tilde{x}_2, ..., \tilde{x}_M)^T$ where

$$
\begin{aligned}
\boldsymbol{n} &= (n_1, n_2, ..., n_M)^T \in \mathbb{R}^M_{>0}, \\
x_i^{n_i} &= \begin{cases} exp(n_i ln(x_i)) & x_i > 0, \\ 0 & x_i = 0, \end{cases} \\
sgn(x_i) &= \begin{cases} 1 & x_i \geq 0, \\ -1 & x_i < 0, \end{cases} \\
\tilde{x}_i &= \begin{cases} ln(|x_i|) & x_i \neq 0, \\ 0 & x_i = 0, \end{cases}
\end{aligned}
\tag{1}
$$

and $|x_i|$ is the absolute value of x_i. For notational simplicity, we will use $\boldsymbol{x}^n$ and $|\boldsymbol{x}|$ rather than $\boldsymbol{x}^{n\mathbf{1}}$ and $|\boldsymbol{x}|^{\mathbf{1}}$, respectively, where $\mathbf{1}$ is an all-ones vector with an appropriate dimension. It is also obvious that $\boldsymbol{x} = \boldsymbol{\Lambda}(\boldsymbol{sgn}(\boldsymbol{x}))|\boldsymbol{x}|$ and $|\boldsymbol{x}|^{\boldsymbol{n}} = \boldsymbol{\Lambda}(|\boldsymbol{x}|^{\boldsymbol{n}})\mathbf{1}$.

2.2. Autonomous systems of ODEs

Now, we recall some theorems and results concerning autonomous systems of differential equations, which will be used in our analysis. Consider the system

$$
\dot{\boldsymbol{x}} := \frac{d\boldsymbol{x}}{dt} = \boldsymbol{f}(\boldsymbol{x}), \tag{2}
$$

where $\boldsymbol{f} : X \to \mathbb{R}^M$ is a continuously differentiable function from a domain (open and connected set) $X \subseteq \mathbb{R}^M$ into $\mathbb{R}^M$. Then, a point $\boldsymbol{x}_e$ is said to be an equilibrium point of (2) if $\boldsymbol{f}(\boldsymbol{x}_e) = 0$.

Theorem 2.1. *[45] Let Ξ be a compact (closed and bounded) subset of X, and $\boldsymbol{x}_0 \in \Xi$. If every solution of the system (2) with the initial condition $\boldsymbol{x}(0) = \boldsymbol{x}_0$ lies entirely in Ξ, then there is a unique solution that is defined for all $t \geq 0$.*

Theorem 2.2 (Lyapunov's stability theorem)**.** *[45] Suppose that $V : X^* \to \mathbb{R}$ is a continuously differentiable function defined in a domain $X^* \subseteq X$ which contains an equilibrium point $\boldsymbol{x}_e$ of the system (2), and let $\nabla V(\boldsymbol{x})$ be its gradient. If $V(\boldsymbol{x})$ and its derivative along the trajectories of the system (2), i.e., $\dot{V}(\boldsymbol{x}) = \nabla V(\boldsymbol{x})^T \dot{\boldsymbol{x}}$, satisfy the following conditions*

- *$V(\boldsymbol{x})$ is positive definite with respect to $\boldsymbol{x}_e$; and*
- *$\dot{V}(\boldsymbol{x})$ is negative semidefinite.*

bioRxiv preprint doi: https://doi.org/10.1101/2023.02.04.527149; this version posted February 4, 2023. The copyright holder for this preprint (which was not certified by peer review) is the author/funder, who has granted bioRxiv a license to display the preprint in perpetuity. It is made available under aCC-BY-NC-ND 4.0 International license.

Then $\boldsymbol{x}_e$ is stable in the sense of Lyapunov, and $V(\boldsymbol{x})$ is called a Lyapunov function.

We say that $V(\boldsymbol{x})$ is positive (resp., negative) definite with respect to $\boldsymbol{x}_e$ if $V(\boldsymbol{x}_e) = 0$ and $V(\boldsymbol{x}) > 0$ (resp., $-V(\boldsymbol{x}) > 0$) for all $\boldsymbol{x} \in X^* \setminus \{\boldsymbol{x}_e\}$. Further, if it satisfies the weaker condition $V(\boldsymbol{x}) \geq 0$ (resp., $-V(\boldsymbol{x}) \geq 0$), it is said to be positive (resp., negative) semidefinite. It is not difficult to check the sign definiteness of a quadratic function $\boldsymbol{x}^T\boldsymbol{P}\boldsymbol{x}$ where $\boldsymbol{P}$ is a real symmetric matrix. It can be shown that $\boldsymbol{x}^T\boldsymbol{P}\boldsymbol{x} > 0$ (resp., $\boldsymbol{x}^T\boldsymbol{P}\boldsymbol{x} \geq 0$) for all $\boldsymbol{x} \neq 0$ if and only if every eigenvalue of $\boldsymbol{P}$ is positive (resp., nonnegative), in which case the matrix $\boldsymbol{P}$ is called positive definite (resp., positive semidefinite) and denoted by $\boldsymbol{P} \succ 0$ (resp., $\boldsymbol{P} \succeq 0$).

Theorem 2.3 (LaSalle's invariance theorem)**.** *[46] Let $\Xi^* \subset X$ be a compact set that is positively invariant with respect to the system (2), i.e.,*

$$\forall \boldsymbol{x}(0) \in \Xi^* \Rightarrow \boldsymbol{x}(t) \in \Xi^* \quad \forall t \geq 0.$$

If an equilibrium point $\boldsymbol{x}_e$ belongs to Ξ^* and there exists a continuously differentiable function $V : X \to \mathbb{R}$ such that

$$\dot{V}(\boldsymbol{x}_e) = 0,$$
$$\dot{V}(\boldsymbol{x}) < 0, \quad \forall \boldsymbol{x} \in \Xi^* \setminus \{\boldsymbol{x}_e\},$$

then every solution starting in Ξ^* approaches $\boldsymbol{x}_e$ as t goes to infinity.

Note that Theorem 2.3 is actually a corollary of LaSalle's theorem [46], customized to the situation that the set $\{\boldsymbol{x} \in \Xi^* : \dot{V}(\boldsymbol{x}) = 0\}$ is equal to $\{\boldsymbol{x}_e\}$.

Despite the fact that this manuscript has been devoted to explore systems with continuously differentiable right-hand side functions, we need to recall some concepts and results concerning Filippov's differential inclusion [47–50], having been particularly developed to analyze nonsmooth systems, since they enable us to study the convergence of solutions using nonsmooth functions. Due to the continuity of $\boldsymbol{f}$ [48], the system (2) can be replaced with the following Filippov differential inclusion: $\dot{\boldsymbol{x}} \in \{\boldsymbol{f}(\boldsymbol{x})\}$. If there is a locally Lipschitz function $V : \mathbb{R}^M \to \mathbb{R}$ that can be written as a pointwise maximum of a set of smooth functions, called a max function, such as $\|\boldsymbol{x}\|_1 = \mathbf{1}^T|\boldsymbol{x}|$, then the derivative of V along the trajectories of the differential inclusion $\dot{\boldsymbol{x}} \in \{\boldsymbol{f}(\boldsymbol{x})\}$ exists almost everywhere and satisfies [49]:

$$\dot{V}(\boldsymbol{x}) \in^{a.e.} \dot{\tilde{V}}(\boldsymbol{x}) = \bigcap_{\varsigma \in \partial V(\boldsymbol{x})} \varsigma^T \{\boldsymbol{f}(\boldsymbol{x})\}, \tag{3}$$

where $\partial V(\boldsymbol{x})$ represents Clark's generalized gradient of V at point $\boldsymbol{x}$ which is defined as [51]

$$\partial V(\boldsymbol{x}) = co\{\lim_{i \to \infty} \nabla V(\boldsymbol{x}_i) : \boldsymbol{x}_i \to \boldsymbol{x},\ \boldsymbol{x}_i \notin Y \cup Z\},$$

where *co* denotes the convex hull, and Y is the set of Lebesgue measure zero where ∇V does not exist, and Z is also an arbitrary set of zero measure. For example, the function $V(x) = |x|$

bioRxiv preprint doi: https://doi.org/10.1101/2023.02.04.527149; this version posted February 4, 2023. The copyright holder for this preprint (which was not certified by peer review) is the author/funder, who has granted bioRxiv a license to display the preprint in perpetuity. It is made available under aCC-BY-NC-ND 4.0 International license.

with $x \in \mathbb{R}$ has the Clarke generalized gradient

$$\partial V(x) = \begin{cases} \{+1\} & x > 0, \\ [-1, 1] & x = 0, \\ \{-1\} & x < 0. \end{cases}$$

Theorem 2.4 (A nonsmooth version of LaSalle's invariance theorem)**.** *[49] Assume that $\Xi^* \subset X$ is a compact set that is positively invariant with respect to Eq. (2). If $V : X \to \mathbb{R}$ is a locally Lipschitz max function such that $v \leq 0$ for all $v \in \dot{\tilde{V}}(\boldsymbol{x})$ for all $\boldsymbol{x} \in \Xi^*$ (note that if $\dot{\tilde{V}}(\boldsymbol{x})$ is the empty set then this condition is trivially satisfied), then every solution in Ξ^* converges to the largest invariant set in the closure of $\{\boldsymbol{x} \in \Xi^* : 0 \in \dot{\tilde{V}}(\boldsymbol{x})\}$.*

It is worth noting that the original theorem [49] from which Theorem 2.4 was derived requires uniqueness of solutions, which is automatically established here by Theorem 2.1.

Once a system of differential equations is utilized to describe the temporal evolution of nonnegative variables such as concentrations, the system requires to preserve nonnegativity of solutions for nonnegative initial conditions on the maximal forward time interval of existence of each solution. This property is classically known as positivity, and if a system has it, then it is called a positive system [52]. It is intuitively evident and shown in [53] that the system (2) with $\mathbb{R}^M_{\geq 0} \subset X$ is positive if and only if $\boldsymbol{f}(\boldsymbol{x})$ satisfies

$$\forall \boldsymbol{x} \in \mathbb{R}^M_{\geq 0} \setminus \mathbb{R}^M_{>0} : x_i = 0 \Rightarrow f_i(\boldsymbol{x}) \geq 0, \tag{4}$$

which henceforth will be referred to as the positivity condition.

2.3. Weighted directed graphs

A weighted directed graph (or simply a digraph) G with no self-loops is a triple (N_G, E_G, ω_G), where N_G is a finite nonempty set of nodes (or vertices), $N_G = \{1, 2, ..., M\}$ with a positive integer M, E_G is a set of directed edges, $E_G \subseteq N_G \times N_G \setminus \{(k, i) \in N_G \times N_G : k = i\}$, and $\omega_G : E_G \to (0, \infty)$ is a function that associates each edge in G from vertex k to vertex i, $k \to i$, to a positive real number, ω_{ik}. If there is no such edge, we let $\omega_{ik} = 0$. When E_G also satisfies the symmetric condition which implies if $(k, i) \in E_G$, then $(i, k) \in E_G$, the digraph G is here referred to as a symmetric digraph. Note that in our context a weighted undirected graph G can be treated as a symmetric digraph when $\omega_{ik} = \omega_{ki}$ for all $(i, k) \in E_G$. Given a digraph G, a path from node k to node i is a sequence of successive edges $\{(k, k_1), (k_1, k_2), ..., (k_l, i)\} \subseteq E_G$, i.e.,

$$k \to k_1 \to k_2 \to ... \to k_l \to i,$$

and denoted by $k \rightsquigarrow i$, and node k is also said to be strongly connected to node i if either $k = i$ or there are both paths $k \rightsquigarrow i$ and $i \rightsquigarrow k$. Strong connectivity defines an equivalence relation on the set of nodes, whose equivalence classes are called the strongly connected components (SCCs) of G. Now, suppose $[i]_{SCC}$ and $[k]_{SCC}$ represent the SCC having the vertex i and the SCC containing the vertex k, respectively. We say that $[i]_{SCC}$ precedes $[k]_{SCC}$, denoted by

bioRxiv preprint doi: https://doi.org/10.1101/2023.02.04.527149; this version posted February 4, 2023. The copyright holder for this preprint (which was not certified by peer review) is the author/funder, who has granted bioRxiv a license to display the preprint in perpetuity. It is made available under aCC-BY-NC-ND 4.0 International license.

$[i]_{SCC} \leqslant [k]_{SCC}$, if $i' \rightsquigarrow k'$ for some $i' \in [i]_{SCC}$ and some $k' \in [k]_{SCC}$. Since the relation $\leqslant$ on SCCs of G is transitive, reflexive, and antisymmetric, it is a partial order, and thus it enables us to determine terminal SCCs of G, which are those $[i]_{SCC}$ such that if $[i]_{SCC} \leqslant [k]_{SCC}$ then $[i]_{SCC} = [k]_{SCC}$ [54]. Here, $\mathcal{G}_{\mathcal{T}}$ denotes the set of all digraphs whose SCCs are all terminal. It is obvious that symmetric digraphs belong to $\mathcal{G}_{\mathcal{T}}$.

3. Extensions of fractional polynomial functions

Let $\mathbb{EF}\left(\mathbb{R}^M\right)$ represent the set of all functions from $\mathbb{R}^M$ to $\mathbb{R}$ which can be expressed in the form

$$\varphi(\boldsymbol{x}) = \xi_0 + \sum_k \xi_k \left(\prod_{l \in S_k} sgn\left(x_l\right) |x_l|^{n_l} \right), \tag{5}$$

with ξ_0, $\xi_k \in \mathbb{R}$, $n_l \in \mathbb{R}_{\geq 1}$, where the sum is over a finite number of k's, and S_k is a sub-multiset of the multiset $\{1, 1, 2, 2, ..., M, M\}$. A multiset is a set whose elements can be repeated more than once, and the number of times an element appears in a multiset is called its multiplicity [55]. Hence, the multiplicity of each element of the sub-multiset S_k can be at most two. Taking elements with multiplicity 2 into account allows a function $\varphi \in \mathbb{EF}\left(\mathbb{R}^M\right)$ to have terms including $\left(sgn(x_l)|x_l|^{n_l}\right)\left(sgn(x_l)|x_l|^{n_l}\right)$, which is equal to $|x_l|^{2n_l}$, and thus it makes the set $\mathbb{EF}\left(\mathbb{R}^M\right)$ closed under the standard multiplication of functions. Indeed, it can be shown that pointwise addition and multiplication of functions turn $\mathbb{EF}\left(\mathbb{R}^M\right)$ into a commutative ring and also a commutative and associative algebra over $\mathbb{R}$ if we define scalar multiplication by $\left(\gamma\varphi\right)\left(\boldsymbol{x}\right) := \gamma\varphi\left(\boldsymbol{x}\right)$ for any $\gamma \in \mathbb{R}$. Note that since proving the mentioned algebraic properties of $\mathbb{EF}\left(\mathbb{R}^M\right)$ is similar to proving those properties for the set of all continuous functions from $\mathbb{R}^M$ to $\mathbb{R}$ [56], we have deliberately avoided discussing their proofs in detail.

The restriction of $\varphi \in \mathbb{EF}\left(\mathbb{R}^M\right)$ to $\mathbb{R}^M_{\geq 0}$ is a FP function. Although FP functions have been used in various fields of research, such as statistical modeling [57, 58], fractional calculus [59, 60], non-integer summations [61–63], and b-function computing [64, 65], to the best of the authors' knowledge there has been no generalization of a FP function like (5) in previous published studies. The ultimate aim of this manuscript is to develop a framework for describing the spatiotemporal evolution of concentrations of different species, and since the concentration of a given species takes nonnegative values, at first glance it may appear that there would be no reason for proposing the set $\mathbb{EF}\left(\mathbb{R}^M\right)$, but we have had a theoretical as well as practical motivation behind this generalization. The theoretical reason was to provide continuously differentiable extensions of FP functions on the whole Euclidean space; see Lemma 3.1. Indeed, the conventional definition of a real-valued fractional polynomial function is confined to the nonnegative orthant, which is a closed subset of the Euclidean space, whereas in the literature most theorems and results concerning differentiable functions are only applicable to functions on open domains. To clarify, in any application of functions defined on a closed subset of the Euclidean space, which requires the consideration of their differentiability, it is generally needed either to customize the standard theorems of interest to their closed domains [66] or more typically to find continuous differentiable extensions of these functions to an open

bioRxiv preprint doi: https://doi.org/10.1101/2023.02.04.527149; this version posted February 4, 2023. The copyright holder for this preprint (which was not certified by peer review) is the author/funder, who has granted bioRxiv a license to display the preprint in perpetuity. It is made available under aCC-BY-NC-ND 4.0 International license.

subset including their domains [67], due to the fact that closed subsets of the Euclidean space normally lack a differentiable structure. For further investigation about such extensions and their existence, we refer to Whitney's extension problem [68, 69] and other relevant articles [70–72].

The practical motivation for introducing the set $\mathbb{EF}\left(\mathbb{R}^M\right)$ can be explained by defining the *active* concentration of a given species that is calculated by subtracting the normalized concentration of its annihilating (or neutralizing) species from its own concentration, where the normalization is done such that zero active concentration corresponds to neutralization. As a result, the active concentration may take negative values, and additionally, if no annihilating species exist, the concept of active concentration is simply equivalent to the usual concept of concentration. In fact, it allows us to simultaneously consider two species that can neutralize the effects of each other at the expense of accepting negative values. Generally speaking, biological studies on species affected by antibodies can benefit from the notion of active concentration. Let us note that although we have introduced the active concentration and will continue our theoretical discussion based on this notion, the simulations in this article are confined to nonnegative initial conditions due to brevity. Indeed, we intend to address more empirical aspects of this work, especially in the context of neurodegenerative diseases, in future articles.

Lemma 3.1. *Every function $\varphi \in \mathbb{EF}\left(\mathbb{R}^M\right)$ is continuously differentiable on $\mathbb{R}^M$.*

Proof. A function $\varphi : \mathbb{R}^M \to \mathbb{R}$ is said to be continuously differentiable on $\mathbb{R}^M$ if all its partial derivatives exist and are continuous at each point of $\mathbb{R}^M$. Hence, since a function $\varphi \in \mathbb{EF}\left(\mathbb{R}^M\right)$ consists of a finite number of additions and multiplications of the terms $sgn(x_i)|x_i|^{n_i}$, $i \in \{1, 2, ..., M\}$, and also the constants ξ_0 and ξ_k, it is sufficient, according to the linearity of differentiation and the chain rule, to show that the derivative of $sgn(x_i)|x_i|^{n_i}$ for each $i \in \{1, 2, ..., M\}$ with $n_i \in \mathbb{R}_{\geq 1}$ exists and is also continuous at every point of $\mathbb{R}$. Using the definition of derivative and applying the L'Hôpital's rule, it is not difficult to obtain

$$\frac{d}{dx_i}\left(sgn(x_i)|x_i|^{n_i}\right) = \begin{cases} n_i exp((n_i - 1)\, ln(|x_i|)) & x_i \neq 0, \\ 0 & x_i = 0, \end{cases} \tag{6}$$

which may be written more compactly as $n_i|x_i|^{n_i-1}$. Since it can be easily seen that $|x_i|^{n_i-1}$ with $n_i \geq 1$ is continuous on $\mathbb{R}$, the continuity of the partial derivatives of φ on $\mathbb{R}^M$ will be assured. □

Let $\mathbb{EF}\left(\mathbb{R}^M, \mathbb{R}^M\right)$ denote the set of all vector-valued functions from $\mathbb{R}^M$ to $\mathbb{R}^M$ whose all M real-valued components belong to $\mathbb{EF}\left(\mathbb{R}^M\right)$. Since a vector-valued function is continuously differentiable on $\mathbb{R}^M$ if and only if all its components are continuously differentiable on $\mathbb{R}^M$, Lemma 3.1 implies the following statement.

Lemma 3.2. *Any vector-valued function $\boldsymbol{\varphi} \in \mathbb{EF}\left(\mathbb{R}^M, \mathbb{R}^M\right)$ is continuously differentiable on $\mathbb{R}^M$.*

bioRxiv preprint doi: https://doi.org/10.1101/2023.02.04.527149; this version posted February 4, 2023. The copyright holder for this preprint (which was not certified by peer review) is the author/funder, who has granted bioRxiv a license to display the preprint in perpetuity. It is made available under aCC-BY-NC-ND 4.0 International license.

4. Extended FP diffusion equation on directed networks

4.1. A generalized nonlinear Laplacian operator on directed networks

We generalize the conventional graph Laplacian operator on a digraph G with M nodes as follows:

$$\boldsymbol{\mathcal{L}}_G(\boldsymbol{x}) = \boldsymbol{L}\left(\boldsymbol{sgn}(\boldsymbol{x}) \odot |\boldsymbol{x}|^{\boldsymbol{n}}\right), \tag{7}$$

where $\boldsymbol{x} \in \mathbb{R}^M$, and $\boldsymbol{n}$ is a constant vector belonging to $\mathbb{R}^M_{\geq 1}$, which implies $\boldsymbol{\mathcal{L}}_G \in \mathbb{EF}\left(\mathbb{R}^M, \mathbb{R}^M\right)$. The matrix $\boldsymbol{L} \in \mathcal{M}_M(\mathbb{R})$ is called the Laplacian matrix and defined by

$$[\boldsymbol{L}]_{ik} = \begin{cases} -\omega_{ik} & i \neq k, \\ \sum\limits_{i' \neq k} \omega_{i'k} & i = k, \end{cases} \tag{8}$$

where ω_{ik} is the weight of the edge $k \to i$. It can be directly deduced from the definition (8) that the Laplacian matrix satisfies the following equality $\mathbf{1}^T \boldsymbol{L} = 0$.

Lemma 4.1. *[7, 73] If G is a strongly connected digraph with M nodes, then the kernel of the Laplacian matrix $\boldsymbol{L}$, i.e., $ker(\boldsymbol{L}) = \{\boldsymbol{x} \in \mathbb{R}^M : \boldsymbol{L}\boldsymbol{x} = 0\}$, is one-dimensional [73], and there is also a vector $\boldsymbol{v} \in ker(\boldsymbol{L})$ whose elements are all positive [7].*

Note that [73] and [7] consider $-\boldsymbol{L}$ as the Laplacian matrix. However, since $-\boldsymbol{L}\boldsymbol{v} = 0$ implies $\boldsymbol{L}\boldsymbol{v} = 0$, their results are also applicable to $\boldsymbol{L}$.

Lemma 4.2. *[7] Assume that $G \in \mathcal{G}_{\mathcal{T}}$ has M nodes and m SCCs. Then, there is a permutation matrix $\boldsymbol{P}_d$ that transforms the Laplacian matrix $\boldsymbol{L}$ of G into a block diagonal form, i.e.,*

$$\boldsymbol{P}_d \boldsymbol{L} \boldsymbol{P}_d^T = \begin{pmatrix} \boldsymbol{L}_1 & 0 & \dots & 0 \\ 0 & \boldsymbol{L}_2 & \dots & 0 \\ \vdots & \vdots & \ddots & \vdots \\ 0 & \dots & 0 & \boldsymbol{L}_m \end{pmatrix},$$

where every block of $\boldsymbol{P}_d \boldsymbol{L} \boldsymbol{P}_d^T$ corresponds to a unique SCC of G.

4.2. A Model for Diffusion Processes

Given a digraph $G \in \mathcal{G}_{\mathcal{T}}$ having M nodes and m SCCs, let us study a diffusion process on G that may be described by

$$\dot{\boldsymbol{x}} = -\boldsymbol{\mathcal{L}}_G(\boldsymbol{x}), \quad \boldsymbol{x}(0) \in \mathbb{R}^M, \tag{9}$$

where the i-th element of $\boldsymbol{x}(t)$ is the active concentration of a given species at node i at time t, and accordingly, $x_{tot}(t) = \mathbf{1}^T \boldsymbol{x}(t)$ is their total active concentration on G at time t.

Lemma 4.3. *The total active concentration is preserved during a diffusion process governed by the differential equation (9).*

bioRxiv preprint doi: https://doi.org/10.1101/2023.02.04.527149; this version posted February 4, 2023. The copyright holder for this preprint (which was not certified by peer review) is the author/funder, who has granted bioRxiv a license to display the preprint in perpetuity. It is made available under aCC-BY-NC-ND 4.0 International license.

Proof. Using $\mathbf{1}^T \boldsymbol{L} = 0$, we obtain

$$\frac{d}{dt}\left(x_{tot}\right) = \mathbf{1}^T \dot{\boldsymbol{x}} = -\mathbf{1}^T \boldsymbol{L}\left(\boldsymbol{sgn}\left(\boldsymbol{x}\right) \odot |\boldsymbol{x}|^{\boldsymbol{n}}\right) = 0.$$

□

4.2.1. Existence and uniqueness of solutions and positively invariant sets

Proposition 4.1. *The set* $\Upsilon_\eta = \{\boldsymbol{x} \in \mathbb{R}^M : \|\boldsymbol{x}\|_1 \leq \eta\}$ *with* $\eta \in \mathbb{R}_{\geq 0}$ *is positively invariant with respect to the system (9).*

Proof. Suppose $\boldsymbol{\varepsilon} = (\varepsilon_1, ..., \varepsilon_M)^T$ where ε_i is either -1 or 1. Then, we define

$$\mathbb{O}^M_{\boldsymbol{\varepsilon}} = \{\boldsymbol{x} \in \mathbb{R}^M : \varepsilon_i x_i \geq 0,\ \forall i \in \{1, ..., M\}\}, \tag{10}$$

which is obviously an orthant of $\mathbb{R}^M$. Each boundary segment $\boldsymbol{\varepsilon}^T\boldsymbol{x} = \eta$ of the set Υ_η is totally contained in the orthant $\mathbb{O}^M_{\boldsymbol{\varepsilon}}$, and clearly, it can be seen that $\boldsymbol{\varepsilon}^T\boldsymbol{x} \geq 0$ for $\boldsymbol{x} \in \mathbb{O}^M_{\boldsymbol{\varepsilon}}$ due to $\varepsilon_i x_i \geq 0$. Calculating the derivative of $\boldsymbol{\varepsilon}^T\boldsymbol{x}$ along the trajectories of the system (9) yields

$$\begin{aligned}\frac{d}{dt}\left(\boldsymbol{\varepsilon}^T\boldsymbol{x}\right) &= -\sum_{i=1}^{M}\sum_{\substack{j=1\\ j\neq i}}^{M} sgn\left(x_i\right)|x_i|^{n_i}\omega_{ji}\left(\varepsilon_i - \varepsilon_j\right) \\ &= -\sum_{i=1}^{M}\sum_{\substack{j=1\\ j\neq i}}^{M} |x_i|^{n_i}\omega_{ji}\left(1 - sgn\left(x_i\right)\varepsilon_j\right) \leq 0,\ \forall \boldsymbol{x} \in \mathbb{O}^M_{\boldsymbol{\varepsilon}},\end{aligned} \tag{11}$$

which demonstrates that at any point on each boundary segment $\boldsymbol{\varepsilon}^T\boldsymbol{x} = \eta$, $\boldsymbol{\varepsilon}^T\boldsymbol{x}$ is nonincreasing along the trajectories of the system (9). Therefore, any solution $\boldsymbol{x}\left(t\right)$ with an initial condition $\boldsymbol{x}\left(0\right) \in \Upsilon_\eta$ cannot leave the set Υ_η, and the proof is concluded by Theorem 2.1. □

Corollary 4.1. *For any initial condition* $\boldsymbol{x}\left(0\right) \in \mathbb{R}^M$*, the system (9) has a unique bounded solution* $\boldsymbol{x}\left(t\right)$ *that is defined for all* $t \geq 0$*.*

Proof. For any initial condition $\boldsymbol{x}\left(0\right) \in \mathbb{R}^M$, it is seen that $\boldsymbol{x}\left(0\right) \in \Upsilon_\eta$ with $\eta \geq \|\boldsymbol{x}\left(0\right)\|_1$. The rest of the proof follows from Proposition 4.1 and Theorem 2.1. □

Proposition 4.2. *The sets*

$$\begin{aligned}\Psi_{x_{tot}} &= \{\boldsymbol{x} \in \mathbb{R}^M : \mathbf{1}^T\boldsymbol{x} = x_{tot}\},\ x_{tot} \in \mathbb{R}, \\ \Psi^+_{x_{tot}} &= \mathbb{R}^M_{\geq 0} \cap \Psi_{x_{tot}},\ x_{tot} \geq 0, \\ \Psi^-_{x_{tot}} &= \mathbb{R}^M_{\leq 0} \cap \Psi_{x_{tot}},\ x_{tot} \leq 0,\end{aligned}$$

are positively invariant with respect to the system (9).

Proof. For the set $\Psi_{x_{tot}}$, the conclusion follows directly from Lemma 4.3 and Proposition 4.1. Due to the fact that the system (45) is invariant under the change of variables $\boldsymbol{x} \to -\boldsymbol{x}$, its state space is symmetric under reflection through the origin. Hence, it is only sufficient to continue

bioRxiv preprint doi: https://doi.org/10.1101/2023.02.04.527149; this version posted February 4, 2023. The copyright holder for this preprint (which was not certified by peer review) is the author/funder, who has granted bioRxiv a license to display the preprint in perpetuity. It is made available under aCC-BY-NC-ND 4.0 International license.

the proof for the set $\Psi^+_{x_{tot}}$. According to Lemma 4.3, any solution $\boldsymbol{x}(t)$ of the system (9) with an initial condition $\boldsymbol{x}(0) \in \Psi^+_{x_{tot}}$ always satisfies $\mathbf{1}^T\boldsymbol{x}(t) = x_{tot}$. Additionally, $\boldsymbol{x}(t)$ cannot leave the set $\Psi^+_{x_{tot}}$ through the boundary of the nonnegative orthant, thanks to the fact that $-\boldsymbol{\mathcal{L}}_G(\boldsymbol{x})$ satisfies the positivity condition (4). Thus, the solution $\boldsymbol{x}(t)$ lies entirely in the compact set $\Psi^+_{x_{tot}}$ on the maximal forward time interval of its existence. Further, since the right-hand side of Eq. (9) is continuously differentiable on $\mathbb{R}^M$, Theorem 2.1 ensures the existence and uniqueness of the solution $\boldsymbol{x}(t)$ for all $t \geq 0$. Hence, it can be concluded that

$$\forall \boldsymbol{x}(0) \in \Psi^+_{x_{tot}} \Rightarrow \boldsymbol{x}(t) \in \Psi^+_{x_{tot}} \quad \forall t \geq 0.$$

□

Corollary 4.2. *For any initial state $\boldsymbol{x}(0) \in \mathbb{R}^M_{\geq 0}$ (resp., $\boldsymbol{x}(0) \in \mathbb{R}^M_{\leq 0}$), the system (9) has a unique solution $\boldsymbol{x}(t)$ remaining entirely in $\mathbb{R}^M_{\geq 0}$ (resp., $\mathbb{R}^M_{\leq 0}$) for all $t \geq 0$.*

Proof. Every solution $\boldsymbol{x}(t)$ of the system (9) with $\boldsymbol{x}(0) \in \mathbb{R}^M_{\geq 0}$ lies entirely in the compact set $\Psi^+_{x_{tot}}$ with $x_{tot} = \mathbf{1}^T\boldsymbol{x}(0)$ by Proposition 4.2. The rest of the proof is similar to that of Proposition 4.2. □

Compared to Corollary 4.2, a stronger conclusion can be drawn when G is strongly connected.

Proposition 4.3. *Assume G is strongly connected. For any initial condition $\boldsymbol{x}(0) \in \mathbb{R}^M_{\geq 0} \setminus \{0\}$ (resp., $\boldsymbol{x}(0) \in \mathbb{R}^M_{\leq 0} \setminus \{0\}$), the system (9) has a unique solution $\boldsymbol{x}(t)$ remaining entirely in $\mathbb{R}^M_{>0}$ (resp., $\mathbb{R}^M_{<0}$) for all $t > 0$.*

Proof. Owing to the fact that the state space is symmetric under reflection through the origin, it suffices only to proceed with the nonnegative orthant. Before we embark on the proof, let us rewrite the system (9) as

$$\dot{x}_i = a_i(t)\, x_i + b_i(t),$$

where

$$a_i(t) = -\sum_{k \neq i} \omega_{ki} |x_i|^{n_i - 1}, \;\; b_i(t) = \sum_{j \neq i} \omega_{ij}\, sgn(x_j)\, |x_j|^{n_j},$$

According to the solution formula for a first-order linear differential equation, we obtain

$$\begin{aligned} x_i(t) = & \, exp\left(\int_0^t a_i(\tau)\, d\tau\right) x_i(0) \\ & + \int_0^t exp\left(\int_{t'}^t a_i(\tau)\, d\tau\right) b_i(t')\, dt'. \end{aligned} \tag{12}$$

Due to $\boldsymbol{x}(0) \in \mathbb{R}^M_{\geq 0} \setminus \{0\}$, there is at least one component x_{i^*} for which $x_{i^*}(0) > 0$. Considering Corollary 4.2 and the fact that $\omega_{ij} \geq 0$, the initial condition $x_{i^*}(0) > 0$ implies $x_{i^*}(t) > 0$ for all $t > 0$ using Eq. (12). Since G is strongly connected, there is at least one edge from node i^* to another node j^*, which leads to $b_{j^*}(t) > 0$ for all $t > 0$. Thus, using again the formula (12), we deduce that $c_{j^*}(t) > 0$ for all $t > 0$. Continuing this reasoning yields $\boldsymbol{x}(t) \in \mathbb{R}^M_{>0}$ for all $t > 0$. □

bioRxiv preprint doi: https://doi.org/10.1101/2023.02.04.527149; this version posted February 4, 2023. The copyright holder for this preprint (which was not certified by peer review) is the author/funder, who has granted bioRxiv a license to display the preprint in perpetuity. It is made available under aCC-BY-NC-ND 4.0 International license.

Recalling Lemma 4.2, it can be demonstrated that the change of variables $y = \boldsymbol{P}_d\boldsymbol{x}$ and $\boldsymbol{n}^* = \boldsymbol{P}_d\boldsymbol{n}$ transforms the system (9) into

$$\dot{\boldsymbol{y}} = -\boldsymbol{P}_d\boldsymbol{L}\boldsymbol{P}_d^T\left(\boldsymbol{sgn}\left(\boldsymbol{y}\right)\odot|\boldsymbol{y}|^{\boldsymbol{n}^*}\right), \quad \boldsymbol{y}\left(0\right)\in\mathbb{R}^M, \tag{13}$$

where $\boldsymbol{n}^* \in \mathbb{R}^M_{\geq 1}$ due to the assumption $\boldsymbol{n} \in \mathbb{R}^M_{\geq 1}$. Note that $\boldsymbol{P}_d^{-1} = \boldsymbol{P}_d^T$, resulting from the fact that any permutation matrix is an orthogonal matrix. It is also easy to see that $x_{tot} = \boldsymbol{1}^T\boldsymbol{x} = \boldsymbol{1}^T\boldsymbol{y}$, and hence the set $\{\boldsymbol{y}\in\mathbb{R}^M : \boldsymbol{1}^T\boldsymbol{y} = x_{tot}\}$ is equal to the set $\Psi_{x_{tot}}$, which is positively invariant by Proposition 4.2. Since $\boldsymbol{P}_d\boldsymbol{L}\boldsymbol{P}_d^T$ has a block diagonal form, the analysis of a diffusion process on G governed by the differential equation (13) can be done for each SCC of G independently. Thus, let us rewrite the system (13) as follows:

$$\begin{aligned}&\dot{\boldsymbol{y}}_l = -\boldsymbol{L}_l\left(\boldsymbol{sgn}\left(\boldsymbol{y}_l\right)\odot|\boldsymbol{y}_l|^{\boldsymbol{n}_l^*}\right), \quad \boldsymbol{y}_l\left(0\right)\in\mathbb{R}^{M_l},\\ &\forall l\in\{1,...,m\},\end{aligned} \tag{14}$$

where $\boldsymbol{L}_l$ and $\boldsymbol{n}_l^*$ denote a block of $\boldsymbol{P}_d\boldsymbol{L}\boldsymbol{P}_d^T$ and a subvector of $\boldsymbol{n}^*$ corresponding to the l-th SCC of G, respectively. M_l is the number of nodes belonging to the SCC l, and subsequently, it follows that $\sum_{l=1}^m M_l = M$ and the Cartesian product $\prod_{l=1}^m \mathbb{R}^{M_l}$ is equal to $\mathbb{R}^M$ by defining the vector $(\boldsymbol{y}_1,...,\boldsymbol{y}_m) = ([\boldsymbol{y}_1]_1,...,[\boldsymbol{y}_1]_{M_1},...,[\boldsymbol{y}_m]_1,...,[\boldsymbol{y}_m]_{M_m})^T$ where $[\boldsymbol{y}_l]_k$ is the k-th element of $\boldsymbol{y}_l\in\mathbb{R}^{M_l}$. Furthermore, given $\boldsymbol{P}_d^T\boldsymbol{P}_d = \boldsymbol{I}$, the equality $\boldsymbol{1}^T\boldsymbol{L} = 0$ leads to

$$\begin{aligned}&\boldsymbol{1}^T\boldsymbol{P}_d^T\boldsymbol{P}_d\boldsymbol{L}\boldsymbol{P}_d^T = 0 \xRightarrow{\boldsymbol{1}^T\boldsymbol{P}_d^T=\boldsymbol{1}^T}\\ &\boldsymbol{1}^T\boldsymbol{P}_d\boldsymbol{L}\boldsymbol{P}_d^T = 0 \Rightarrow \boldsymbol{1}^T\boldsymbol{L}_l = 0.\end{aligned} \tag{15}$$

Generally, a fixed value of the total concentration on a digraph belonging to $\mathcal{G}_{\mathcal{T}}$ may correspond to more than one equilibrium point of the system (14). In other words, the set $\Psi_{x_{tot}}$ can contain more than one equilibrium point. For example, given a graph G with three nodes and with no edges, every point $\boldsymbol{y}\in\mathbb{R}^3$ is an equilibrium point of the system (14), and as long as the condition $\boldsymbol{1}^T\boldsymbol{y} = x_{tot}$ is satisfied, the equilibrium point $\boldsymbol{y}$ belongs to $\Psi_{x_{tot}}$. However, in Proposition 4.4 we show that if the total active concentration on each SCC of a digraph $G\in\mathcal{G}_{\mathcal{T}}$ is fixed, then the total active concentration on G will correspond to only one equilibrium point of the system (14).

Proposition 4.4. *Consider the system (14) and the sets*

$$\begin{aligned}&\tilde{\Psi}_{(y_1,...,y_m)} = \{(\boldsymbol{y}_1,...,\boldsymbol{y}_m)\in\prod_{l=1}^m\mathbb{R}^{M_l} : \boldsymbol{1}^T\boldsymbol{y}_l = y_l, \forall l\in\{1,...,m\}\},\\ &\tilde{\Psi}^*_{(y_1,...,y_m)} = \prod_{l=1}^m\mathbb{O}^{M_l}_{sgn(y_l)\boldsymbol{1}} \ \cap\tilde{\Psi}_{(y_1,...,y_m)},\end{aligned} \tag{16}$$

where the value y_l stands for the total active concentration on the l-th SCC of G. Then, each set in (16) contains exactly one equilibrium point of the system (14). Note that $\sum_{l=1}^m y_l = x_{tot}$ also leads to $\tilde{\Psi}_{(y_1,...,y_m)}\subseteq\Psi_{x_{tot}}$.

bioRxiv preprint doi: https://doi.org/10.1101/2023.02.04.527149; this version posted February 4, 2023. The copyright holder for this preprint (which was not certified by peer review) is the author/funder, who has granted bioRxiv a license to display the preprint in perpetuity. It is made available under aCC-BY-NC-ND 4.0 International license.

Proof. Due to brevity, we only provide a proof for the set $\tilde{\Psi}_{(y_1,...,y_m)}$. Let $\boldsymbol{y}_e \in \mathbb{R}^M$ be an equilibrium point of the system (14). Suppose that $\boldsymbol{y}_{e_l} \in \mathbb{R}^{M_l}$ is a subvector of $\boldsymbol{y}_e$ corresponding to the SCC l. Thus, $\boldsymbol{y}_{e_l}^{\boldsymbol{n}_l^*}$ belongs to the kernel of the block $\boldsymbol{L}_l$. Since each component of G is strongly connected, Lemma 4.1 implies that $ker\,(\boldsymbol{L}_l)$ has dimension one, and there is also a subvector $\boldsymbol{v}_l \in ker\,(\boldsymbol{L}_l)$ whose elements are positive. Hence, there exists a real nonnegative number ϱ_l such that

$$\begin{aligned} \boldsymbol{y}_{e_l}^{\boldsymbol{n}_l^*} &= \varrho_l \boldsymbol{v}_l \quad if \quad \boldsymbol{y}_{e_l} \in \mathbb{R}_{\geq 0}^{M_l}, \\ \left(-\boldsymbol{y}_{e_l}\right)^{\boldsymbol{n}_l^*} &= \varrho_l \boldsymbol{v}_l \quad if \quad \boldsymbol{y}_{e_l} \in \mathbb{R}_{\leq 0}^{M_l}. \end{aligned} \tag{17}$$

Assume without loss of generality that $\boldsymbol{y}_{e_l} \in \mathbb{R}_{\geq 0}^{M_l}$, and let us rewrite Eq. (17) as follows:

$$[\boldsymbol{y}_{e_l}]_k = \left(\varrho_l [\boldsymbol{v}_l]_k\right)^{1/[\boldsymbol{n}_l^*]_k} \quad \forall k \in \{1, ..., M_l\}, \tag{18}$$

where the index k means the k-th element. Note that $[\boldsymbol{n}_l^*]_k \geq 1$ for all k. Furthermore, if $\boldsymbol{y}_e \in \tilde{\Psi}_{(y_1,...,y_m)}$, then $\mathbf{1}^T \boldsymbol{y}_{e_l} = y_l$, and the substitution of Eq. (18) in $\mathbf{1}^T \boldsymbol{y}_{e_l} = y_l$ yields

$$\sum_{k=1}^{M_l} \left(\varrho_l [\boldsymbol{v}_l]_k\right)^{1/[\boldsymbol{n}_l^*]_k} = y_l. \tag{19}$$

Since the left-hand side of Eq. (19) is a strictly increasing function of ϱ_l for its nonnegative values, there is a one-to-one correspondence between ϱ_l and y_l, and it follows for a fixed value of y_l that there exists only one subvector $\boldsymbol{y}_{e_l}$ which corresponds to y_l. Therefore, there is a one-to-one correspondence between the vector $(y_1, ..., y_m)^T \in \mathbb{R}^m$ and the vector $\boldsymbol{y}_e = \left(\boldsymbol{y}_{e_1}, ..., \boldsymbol{y}_{e_m}\right) \in \mathbb{R}^M$, which leads to the conclusion that the set $\tilde{\Psi}_{(y_1,...,y_m)}$ includes exactly one equilibrium point of the system (14). □

Corollary 4.3. *Both sets in (16) are positively invariant with respect to the system (14).*

Proof. It can be proven by repeating the proof of the Proposition 4.2 for each SCC of G. □

4.2.2. Convergence of solutions and stability of equilibria

To investigate the convergence of solutions of the system (14), we first exploit the Lyapunov function candidate

$$V_{\mathcal{D}}(\boldsymbol{y}) = \sum_{l=1}^{m} \boldsymbol{y}_l^T \boldsymbol{\Lambda}^{-1}(\boldsymbol{v}_l) \left(\boldsymbol{sgn}(\boldsymbol{y}_l) \odot |\boldsymbol{y}_l|^{\boldsymbol{n}_l^*}\right), \tag{20}$$

where $\boldsymbol{v}_l \in \mathbb{R}_{>0}^{M_l}$ belongs to $ker\,(\boldsymbol{L}_l)$, and its existence is guaranteed by Lemma 4.1. Note that $\boldsymbol{\Lambda}^{-1}(\boldsymbol{v}_l)$ denotes the inverse of the matrix $\boldsymbol{\Lambda}(\boldsymbol{v}_l)$. The function $V_{\mathcal{D}}(\boldsymbol{y})$ can also be rewritten as follows $V_{\mathcal{D}}(\boldsymbol{y}) = \sum_{l=1}^{m} |\boldsymbol{y}_l|^T \boldsymbol{\Lambda}^{-1}(\boldsymbol{v}_l) |\boldsymbol{y}_l|^{\boldsymbol{n}_l^*}$, for which it is easy to notice the positive definiteness with respect to $\boldsymbol{y} = 0$, i.e.,

$$\begin{aligned} &V_{\mathcal{D}}(0) = 0, \\ &V_{\mathcal{D}}(\boldsymbol{y}) > 0, \quad \forall \boldsymbol{y} \in \mathbb{R}^M \setminus \{0\}. \end{aligned} \tag{21}$$

bioRxiv preprint doi: https://doi.org/10.1101/2023.02.04.527149; this version posted February 4, 2023. The copyright holder for this preprint (which was not certified by peer review) is the author/funder, who has granted bioRxiv a license to display the preprint in perpetuity. It is made available under aCC-BY-NC-ND 4.0 International license.

Considering $V_{\mathcal{D}} \in \mathbb{EF}\left(\mathbb{R}^M\right)$, this function is continuously differentiable on $\mathbb{R}^M$ by Lemma 3.1, and the calculation of its derivative along the trajectories of the system (14) yields

$$\begin{aligned}\dot{V}_{\mathcal{D}}\left(\boldsymbol{y}\right) = \frac{1}{2}\sum_{l=1}^{m}\Bigg(&\dot{\boldsymbol{y}}_l^T\boldsymbol{\Lambda}^{-1}\left(\boldsymbol{v}_l\right)\left(\boldsymbol{sgn}\left(\boldsymbol{y}_l\right)\odot\left|\boldsymbol{y}_l\right|^{\boldsymbol{n}_l^*}\right)\\ &+\boldsymbol{y}_l^T\boldsymbol{\Lambda}^{-1}\left(\boldsymbol{v}_l\right)\left(\boldsymbol{n}_l^*\odot\left|\boldsymbol{y}_l\right|^{\boldsymbol{n}_l^*-\mathbf{1}}\odot\dot{\boldsymbol{y}}_l\right)\\ &+\left(\boldsymbol{n}_l^*\odot\left|\boldsymbol{y}_l\right|^{\boldsymbol{n}_l^*-\mathbf{1}}\odot\dot{\boldsymbol{y}}_l\right)^T\boldsymbol{\Lambda}^{-1}\left(\boldsymbol{v}_l\right)\boldsymbol{y}_l\\ &+\left(\boldsymbol{sgn}\left(\boldsymbol{y}_l\right)\odot\left|\boldsymbol{y}_l\right|^{\boldsymbol{n}_l^*}\right)^T\boldsymbol{\Lambda}^{-1}\left(\boldsymbol{v}_l\right)\dot{\boldsymbol{y}}_l\Bigg).\end{aligned} \tag{22}$$

Using the change of variables $\boldsymbol{z}_l^* = \left(\boldsymbol{sgn}\left(\boldsymbol{y}_l\right)\odot\left|\boldsymbol{y}_l\right|^{\boldsymbol{n}_l^*}\right)$, and substituting Eq. (14) into Eq. (22), we have

$$\begin{aligned}\dot{V}_{\mathcal{D}}\left(\boldsymbol{y}\right) = -\frac{1}{2}\sum_{l=1}^{m}\Bigg(&\left(\boldsymbol{z}_l^*\right)^T\left(\boldsymbol{L}_l^T\boldsymbol{\Lambda}^{-1}\left(\boldsymbol{v}_l\right)+\boldsymbol{\Lambda}^{-1}\left(\boldsymbol{v}_l\right)\boldsymbol{\Lambda}\left(\boldsymbol{n}_l^*\right)\boldsymbol{L}_l\right)\boldsymbol{z}_l^*\\ &+\left(\boldsymbol{z}_l^*\right)^T\left(\boldsymbol{\Lambda}^{-1}\left(\boldsymbol{v}_l\right)\boldsymbol{L}_l+\boldsymbol{L}_l^T\boldsymbol{\Lambda}\left(\boldsymbol{n}_l^*\right)\boldsymbol{\Lambda}^{-1}\left(\boldsymbol{v}_l\right)\right)\boldsymbol{z}_l^*\Bigg).\end{aligned} \tag{23}$$

Finally, the change of variables $\boldsymbol{z}_l = \boldsymbol{\Lambda}^{-1}\left(\boldsymbol{v}_l\right)\boldsymbol{z}_l^*$ brings Eq. (23) into

$$\begin{aligned}\dot{V}_{\mathcal{D}}\left(\boldsymbol{y}\right) &= -\frac{1}{2}\sum_{l=1}^{m}\boldsymbol{z}_l^T\boldsymbol{\Gamma}_l\boldsymbol{z}_l,\\ \boldsymbol{z}_l &= \boldsymbol{\Lambda}^{-1}\left(\boldsymbol{v}_l\right)\left(\boldsymbol{sgn}\left(\boldsymbol{y}_l\right)\odot\left|\boldsymbol{y}_l\right|^{\boldsymbol{n}_l^*}\right),\end{aligned} \tag{24}$$

where

$$\boldsymbol{\Gamma}_l = \left(\boldsymbol{\Lambda}\left(\boldsymbol{n}_l^*\right)+\boldsymbol{I}\right)\boldsymbol{L}_l\boldsymbol{\Lambda}\left(\boldsymbol{v}_l\right)+\boldsymbol{\Lambda}\left(\boldsymbol{v}_l\right)\boldsymbol{L}_l^T\left(\boldsymbol{\Lambda}\left(\boldsymbol{n}_l^*\right)+\boldsymbol{I}\right). \tag{25}$$

It is easy to spot that $\boldsymbol{\Gamma}_l$ is a symmetric matrix, and thus to conclude that $\dot{V}_{\mathcal{D}}\left(\boldsymbol{y}\right) \leq 0$ for all $\boldsymbol{y} \in \mathbb{R}^M$ is equivalent to showing that $\boldsymbol{\Gamma}_l$ for all l is a positive semidefinite matrix. If the matrix $\boldsymbol{\Gamma}_l$ is positive semidefinite, then it must possess the following property: $\boldsymbol{w}_l^T\boldsymbol{\Gamma}_l\boldsymbol{w}_l = 0$ if and only if $\boldsymbol{\Gamma}_l\boldsymbol{w}_l = 0$ for all $\boldsymbol{w}_l \in \mathbb{R}^{M_l}$. See [44] for a proof of this property. Hence, since the relation $\boldsymbol{v}_l \in ker\left(\boldsymbol{L}_l\right)$ results in $\mathbf{1}^T\boldsymbol{\Gamma}_l\mathbf{1} = 0$, we must have $\boldsymbol{\Gamma}_l\mathbf{1} = 0$, which requires

$$\boldsymbol{L}_l^T\boldsymbol{n}_l^* = 0. \tag{26}$$

In fact, the equality (26) is a necessary condition for $\boldsymbol{\Gamma}_l$ to be positive semidefinite. Furthermore, since this equality ensures $\boldsymbol{\Gamma}_l\mathbf{1} = 0$, it is also a sufficient condition for $\boldsymbol{\Gamma}_l$ to be positive semidefinite by Lemma 4.4.

Lemma 4.4. *Let $\boldsymbol{B} \in \mathcal{M}_M\left(\mathbb{R}\right)$ be a symmetric matrix whose off-diagonal elements are nonpositive.*

- *If $\boldsymbol{B}\mathbf{1} \in \mathbb{R}_{\geq 0}^M$, then $\boldsymbol{B} \succeq 0$.*
- *If $\boldsymbol{B}\mathbf{1} \in \mathbb{R}_{> 0}^M$, then $\boldsymbol{B} \succ 0$.*

bioRxiv preprint doi: https://doi.org/10.1101/2023.02.04.527149; this version posted February 4, 2023. The copyright holder for this preprint (which was not certified by peer review) is the author/funder, who has granted bioRxiv a license to display the preprint in perpetuity. It is made available under aCC-BY-NC-ND 4.0 International license.

Proof. It is a corollary of Geršgorin circle theorem. Geršgorin circle theorem states that every eigenvalue λ of the matrix $\boldsymbol{B}$ belongs to the union of Geršgorin discs, i.e.,

$$\lambda \in \bigcup_{i=1}^{M} \{z \in \mathbb{C} : |z - B_{ii}| \leq \sum_{\substack{j=1 \\ j \neq i}}^{M} |B_{ij}|\}, \tag{27}$$

where $\mathbb{C}$ and B_{ij} denote the complex plane and the entry in the i-th row and j-th column of $\boldsymbol{B}$, respectively. Since $\boldsymbol{B}$ is symmetric, all its eigenvalues are real. Thus, given that its off-diagonal elements are also nonpositive, the relation (27) can be rewritten as follows:

$$\lambda \in \bigcup_{i=1}^{M} \{z \in \mathbb{R} : \sum_{j=1}^{M} B_{ij} \leq z \leq B_{ii} - \sum_{\substack{j=1 \\ j \neq i}}^{M} B_{ij}\}. \tag{28}$$

Considering the relation (28), $\boldsymbol{B}\mathbf{1} \in \mathbb{R}^{M}_{\geq 0}$ (resp., $\boldsymbol{B}\mathbf{1} \in \mathbb{R}^{M}_{> 0}$) ensures that all eigenvalues of $\boldsymbol{B}$ are equal to or greater than zero (resp., greater than zero), which confirms that $\boldsymbol{B}$ is positive semidefinite (resp., positive definite). □

Because $\boldsymbol{L}_l$ is a square matrix, the dimension of $ker\left(\boldsymbol{L}_l\right)$ is equal to the dimension of $ker\left(\boldsymbol{L}_l^T\right)$, which is a standard result in linear algebra. Hence, given that each component of G is strongly connected, Lemma (4.1) implies that $ker\left(\boldsymbol{L}_l^T\right)$ has dimension one. In addition, owing to the fact that $\boldsymbol{L}_l^T\mathbf{1} = 0$ (see Eq. (15)), the condition (26) can boil down to

$$\boldsymbol{n}_l^* = n_l^*\mathbf{1}. \tag{29}$$

considering $\boldsymbol{n}^* \in \mathbb{R}^{M}_{\geq 1}$, the coefficient n_l^* must be greater than or equal to one. An immediate conclusion from the foregoing discussion is that if the system (14) holds the condition (29) for all l, then by Theorem 2.2 the function $V_{\mathcal{D}}\left(\boldsymbol{y}\right)$ in Eq. (20) is a Lyapunov function to demonstrate the stability of the equilibrium point at the origin, which is of no practical interest in view of the fact that the equilibrium point $\boldsymbol{y}_e = 0$ corresponds to the zero total concentration. However, when the condition (29) is satisfied, Lemma 4.5 reveals more details about the derivative of $V_{\mathcal{D}}\left(\boldsymbol{y}\right)$ along the trajectories of the system (14) which will assist us in achieving a result concerning the convergence of solutions in the case of an arbitrary total concentration.

Proposition 4.5. *Assume that the system (14) satisfies the condition (29) for all l. Then, for any equilibrium point $\boldsymbol{y}_e \in \mathbb{R}^M$ and the set $\tilde{\Psi}_{(y_1,\ldots,y_m)} \supset \{\boldsymbol{y}_e\}$, the function $\dot{V}_{\mathcal{D}}\left(\boldsymbol{y}\right)$ in Eq. (24) meets the following conditions:*

$$\begin{aligned} &\dot{V}_{\mathcal{D}}\left(\boldsymbol{y}_e\right) = 0, \\ &\dot{V}_{\mathcal{D}}\left(\boldsymbol{y}\right) < 0, \quad \forall \boldsymbol{y} \in \tilde{\Psi}_{(y_1,\ldots,y_m)} \setminus \{\boldsymbol{y}_e\}. \end{aligned} \tag{30}$$

Proof. Assume that $\boldsymbol{y}_{e_l}$ is a subvector of $\boldsymbol{y}_e$ corresponding to the l-th SCC of G. Since $\boldsymbol{y}_e$ is an

bioRxiv preprint doi: https://doi.org/10.1101/2023.02.04.527149; this version posted February 4, 2023. The copyright holder for this preprint (which was not certified by peer review) is the author/funder, who has granted bioRxiv a license to display the preprint in perpetuity. It is made available under aCC-BY-NC-ND 4.0 International license.

equilibrium point of the system (14), it must satisfy

$$\boldsymbol{L}_l \left(\boldsymbol{sgn} \left(\boldsymbol{y}_{e_l} \right) \odot |\boldsymbol{y}_{e_l}|^{\boldsymbol{n}_l^*} \right) = 0, \tag{31}$$

for all l, from which it follows that $\dot{V}_{\mathcal{D}}(\boldsymbol{y}_e) = 0$. Considering the condition (29), the function $\dot{V}_{\mathcal{D}}(\boldsymbol{y})$ in Eq. (24) can be rewritten as

$$\begin{aligned} \dot{V}_{\mathcal{D}}(\boldsymbol{y}) &= -\frac{1}{2} \sum_{l=1}^{m} (n_l^* + 1)\, \boldsymbol{z}_l^T \boldsymbol{\Gamma}_l^* \boldsymbol{z}_l, \\ \boldsymbol{z}_l &= \boldsymbol{\Lambda}^{-1}(\boldsymbol{v}_l) \left(\boldsymbol{sgn}(\boldsymbol{y}_l) \odot |\boldsymbol{y}_l|^{\boldsymbol{n}_l^*} \right), \end{aligned} \tag{32}$$

where

$$\boldsymbol{\Gamma}_l^* = \left(\boldsymbol{L}_l \boldsymbol{\Lambda}(\boldsymbol{v}_l) + \boldsymbol{\Lambda}(\boldsymbol{v}_l) \boldsymbol{L}_l^T \right). \tag{33}$$

Owing to $\boldsymbol{v}_l \in ker(\boldsymbol{L}_l)$, we have $\boldsymbol{\Gamma}_l^* \mathbf{1} = 0$, and thus the matrix $\boldsymbol{\Gamma}_l^*$ is positive semidefinite by Lemma 4.4. Hence, the function $\dot{V}_{\mathcal{D}}(\boldsymbol{y})$ is a summation of nonpositive terms, and it will be sufficient to show that there is at least one nonzero term. Recalling Proposition 4.4, the relation $\boldsymbol{y} \in \Psi^*_{(y_1,\ldots,y_m)} \setminus \{\boldsymbol{y}_e\}$ implies that $\boldsymbol{y}$ is not an equilibrium point of the system (14). Hence, there exists at least one SCC l' of G such that for the subvector $\boldsymbol{y}_{l'}$ of $\boldsymbol{y}$ we have $\boldsymbol{L}_{l'} \left(\boldsymbol{sgn}(\boldsymbol{y}_{l'}) \odot |\boldsymbol{y}_{l'}|^{\boldsymbol{n}_{l'}^*} \right) \neq 0$ or equivalently $\boldsymbol{L}_{l'} \boldsymbol{\Lambda}(\boldsymbol{v}_{l'}) \boldsymbol{z}_{l'} \neq 0$; that is to say that $\boldsymbol{z}_{l'} \notin ker(\boldsymbol{L}_{l'} \boldsymbol{\Lambda}(\boldsymbol{v}_{l'}))$. In addition, since the matrix $\boldsymbol{\Gamma}_{l'}^*$ is positive semidefinite, it has the following property: $\boldsymbol{w}_{l'}^T \boldsymbol{\Gamma}_{l'}^* \boldsymbol{w}_{l'} = 0$ if and only if $\boldsymbol{\Gamma}_{l'}^* \boldsymbol{w}_{l'} = 0$ for all $\boldsymbol{w}_{l'} \in \mathbb{R}^{M_{l'}}$. Given $\boldsymbol{w}_{l'} = \boldsymbol{z}_{l'}$, the conclusion $\dot{V}_{\mathcal{D}}(\boldsymbol{y}) < 0$ for $\boldsymbol{y} \in \Psi^*_{(y_1,\ldots,y_m)} \setminus \{\boldsymbol{y}_e\}$ can therefore be drawn from the following equality:

$$ker(\boldsymbol{L}_{l'} \boldsymbol{\Lambda}(\boldsymbol{v}_{l'})) = ker(\boldsymbol{\Gamma}_{l'}^*), \tag{34}$$

which will be proven as the next step of our proof. The matrix $\boldsymbol{\Lambda}(\boldsymbol{v}_{l'})$ is full rank, deduced from the fact that $\boldsymbol{v}_{l'} \in \mathbb{R}^{M_{l'}}_{>0}$. Thus, since $ker(\boldsymbol{L}_{l'})$ has dimension one according to Lemma 4.1, it follows that $ker(\boldsymbol{L}_{l'} \boldsymbol{\Lambda}(\boldsymbol{v}_{l'}))$ is also one-dimensional. Further, it is easily seen that $\boldsymbol{v}_{l'} \in ker(\boldsymbol{L}_{l'})$ implies $\mathbf{1} \in ker(\boldsymbol{L}_{l'} \boldsymbol{\Lambda}(\boldsymbol{v}_{l'}))$. Hence, to demonstrate the equality (34), it suffices to show that if $\boldsymbol{w}_{l'} \in ker(\boldsymbol{\Gamma}_{l'}^*)$, then for elements of $\boldsymbol{w}_{l'}$ we get $[\boldsymbol{w}_{l'}]_1 = [\boldsymbol{w}_{l'}]_2 = \ldots = [\boldsymbol{w}_{l'}]_{M_{l'}}$. Let $\boldsymbol{w}_{l'} \in ker(\boldsymbol{\Gamma}_{l'}^*)$, and thus given $\boldsymbol{\Gamma}_{l'}^* \mathbf{1} = 0$, it can be written

$$\boldsymbol{\Gamma}_{l'}^* \boldsymbol{w}_{l'} - \min_{1 \leq k \leq M_{l'}} ([\boldsymbol{w}_{l'}]_k)\, \boldsymbol{\Gamma}_{l'}^* \mathbf{1} = 0. \tag{35}$$

We define a set $U_{min} \subseteq \{1, 2, \ldots, M_{l'}\}$ such that if $[\boldsymbol{w}_{l'}]_{k^*} = \min_{1 \leq k \leq M_{l'}} ([\boldsymbol{w}_{l'}]_k)$, then the index k^* belongs to U_{min}. Due to $\boldsymbol{w}_{l'} \in \mathbb{R}^{M_{l'}}$, there is at least one element of $\boldsymbol{w}_{l'}$ whose index belongs to U_{min}, and thus this set is not empty. For $k^* \in U_{min}$, we can obtain the following equation using Eq. (35).

$$\sum_{\substack{k=1 \\ k \neq k^*}}^{M_{l'}} \left(-[\boldsymbol{L}_{l'}]_{k^* k} [\boldsymbol{v}_{l'}]_k - [\boldsymbol{v}_{l'}]_{k^*} [\boldsymbol{L}_{l'}]_{k k^*} \right) \left([\boldsymbol{w}_{l'}]_k - [\boldsymbol{w}_{l'}]_{k^*} \right) = 0, \tag{36}$$

where $[\boldsymbol{L}_{l'}]_{k^* k}$ denotes the entry in the k^*-th row and k-th column of $\boldsymbol{L}_{l'}$. Since $\boldsymbol{v}_{l'} \in \mathbb{R}^{M_{l'}}_{>0}$,

bioRxiv preprint doi: https://doi.org/10.1101/2023.02.04.527149; this version posted February 4, 2023. The copyright holder for this preprint (which was not certified by peer review) is the author/funder, who has granted bioRxiv a license to display the preprint in perpetuity. It is made available under aCC-BY-NC-ND 4.0 International license.

$[\boldsymbol{L}_{l'}]_{k_1k_2} \leq 0$ for all $k_1 \neq k_2$, and $[\boldsymbol{w}_{l'}]_k \geq [\boldsymbol{w}_{l'}]_{k^*}$ for all k, both terms of the summand in Eq. (36) are nonnegative. Besides, because the component l' of G is strongly connected, there is at least one edge from k^* to one of its other nodes. This implies that the first term of the summand in Eq. (36) is in fact strictly positive, and it can be deduced that $[\boldsymbol{w}_{l'}]_k = [\boldsymbol{w}_{l'}]_{k^*}$. As a result, the set U_{min} is closed under outgoing edges, and hence, we conclude that $U_{min} = \{1, 2, ..., M_{l'}\}$, which means $[\boldsymbol{w}_{l'}]_1 = [\boldsymbol{w}_{l'}]_2 = ... = [\boldsymbol{w}_{l'}]_{M_{l'}}$. □

It is now time to encapsulate our first finding regarding the convergence of solutions of the system (14) in Corollary 4.4.

Corollary 4.4. *Let $\boldsymbol{y}_e \in \mathbb{R}^M$ be an equilibrium point of the system (14), holding the condition (29) for all l. Then, for any initial state $\boldsymbol{y}(0)$ belonging to the positively invariant set $\tilde{\Psi}_{(y_1,...,y_m)} \supseteq \{\boldsymbol{y}_e\}$ (or $\tilde{\Psi}^*_{(y_1,...,y_m)} \supseteq \{\boldsymbol{y}_e\}$), the solution $\boldsymbol{y}(t)$ converges to $\boldsymbol{y}_e$ as t approaches infinity.*

Proof. It is concluded from Theorem 2.3, Corollary 4.3, and Proposition 4.5. □

In the case that the system (14) does not fulfill the condition (29), the convergence of solutions to equilibria can also be established in two steps. First, we will demonstrate that every solution of the system (14) with an arbitrary initial condition enters a specific subspace containing equilibrium points. Second, it will be shown that all solutions in that subspace converge to equilibria. The first step is accomplished by using the function $V(\boldsymbol{x}) = \|\boldsymbol{x}\|_1$ whose set-valued derivative, introduced in (3), with respect to the Filippov differential inclusion $\dot{\boldsymbol{x}} \in \{-\boldsymbol{\mathcal{L}}_G(\boldsymbol{x})\}$ is as follows:

$$\dot{\tilde{V}}(\boldsymbol{x}) = \bigcap_{\boldsymbol{\varsigma} \in \partial V(\boldsymbol{x})} \boldsymbol{\varsigma}^T \{-\boldsymbol{L}(\boldsymbol{sgn}(\boldsymbol{x}) \odot |\boldsymbol{x}|^{\boldsymbol{n}})\}, \tag{37}$$

where $\boldsymbol{\varsigma} \in \partial V(\boldsymbol{x})$ can be expressed elementwise as

$$\varsigma_i \in \begin{cases} \{+1\} & x_i > 0, \\ [-1, 1] & x_i = 0, \\ \{-1\} & x_i < 0. \end{cases}$$

Proposition 4.6. *Consider the differential inclusion $\dot{\boldsymbol{x}} \in \{-\boldsymbol{\mathcal{L}}_G(\boldsymbol{x})\}$ and the set-valued derivative $\dot{\tilde{V}}(\boldsymbol{x})$ in Eq. (37). If G is strongly connected, then*

$$\dot{\tilde{V}}(\boldsymbol{x}) \subseteq \begin{cases} \{0\} & x = 0, \\ \{0\} & x \in Int\ \mathbb{O}^M_{\boldsymbol{\varepsilon}}, with\ |\mathbf{1}^T\boldsymbol{\varepsilon}| = M, \\ \mathbb{R}^M_{<0} & x \in Int\ \mathbb{O}^M_{\boldsymbol{\varepsilon}}, with\ |\mathbf{1}^T\boldsymbol{\varepsilon}| < M, \\ \emptyset & elsewhere, \end{cases}$$

where $Int\ \mathbb{O}^M_{\boldsymbol{\varepsilon}}$ means the interior of the orthant $\mathbb{O}^M_{\boldsymbol{\varepsilon}}$, defined in Eq. (10).

bioRxiv preprint doi: https://doi.org/10.1101/2023.02.04.527149; this version posted February 4, 2023. The copyright holder for this preprint (which was not certified by peer review) is the author/funder, who has granted bioRxiv a license to display the preprint in perpetuity. It is made available under aCC-BY-NC-ND 4.0 International license.

Proof. Let us first rewrite Eq. (37) as follows:

$$\dot{\tilde{V}}(\boldsymbol{x}) = \bigcap_{\varsigma \in \partial V(\boldsymbol{x})} \{-\sum_{i=1}^{M} \sum_{\substack{j=1 \\ j \neq i}}^{M} sgn(x_i) |x_i|^{n_i} \omega_{ji} (\varsigma_i - \varsigma_j)\}. \tag{38}$$

For $\boldsymbol{x} = 0$, we have

$$\dot{\tilde{V}}(\boldsymbol{x}) = \bigcap_{\varsigma \in \partial V(\boldsymbol{x})} \{\sum_{i=1}^{M} \sum_{\substack{j=1 \\ j \neq i}}^{M} 0\} = \{0\}.$$

For the case $\boldsymbol{x} \in Int\ \mathbb{O}_{\boldsymbol{\varepsilon}}^{M}$ with $|\mathbf{1}^T \boldsymbol{\varepsilon}| = M$, it is obtained that

$$\dot{\tilde{V}}(\boldsymbol{x}) = \{-\sum_{i=1}^{M} \sum_{\substack{j=1 \\ j \neq i}}^{M} |x_i|^{n_i} \omega_{ji} (1 - sgn(x_i)\, sgn(x_j))\} = \{0\},$$

thanks to the fact that $sgn(x_i)\, sgn(x_j) = 1$ for all i and j.

For the case $\boldsymbol{x} \in Int\ \mathbb{O}_{\boldsymbol{\varepsilon}}^{M}$ with $|\mathbf{1}^T \boldsymbol{\varepsilon}| < M$, Eq. (38) can be written as

$$\dot{\tilde{V}}(\boldsymbol{x}) = \{-\sum_{i=1}^{M} \sum_{\substack{j=1 \\ j \neq i}}^{M} |x_i|^{n_i} \omega_{ji} (1 - sgn(x_i)\, sgn(x_j))\},$$

which is obviously nonpositive. Owing to the fact that G is strongly connected, it is deduced that $\dot{\tilde{V}}(\boldsymbol{x}) = 0$ if and only if $sgn(x_i)\, sgn(x_j) = 1$ when $i \neq j$. Indeed, this inference comes from the fact that there is a path passing through all nodes of G. Furthermore, since G is strongly connected, it follows from $|\mathbf{1}^T \boldsymbol{\varepsilon}| < M$ that there is an edge $i^* \to j^*$ for which $sgn(x_{i^*})\, sgn(x_{j^*}) = -1$. Thus, we have $\dot{\tilde{V}}(\boldsymbol{x}) = \{v\}$ with $v < 0$.

In the last case, $\boldsymbol{x}$ is a nonzero vector possessing at least one zero element. Hence, due to the fact that G is strongly connected, there is an edge $i^* \to j^*$ for which $x_{i^*} \neq 0$ and $x_{j^*} = 0$, and subsequently, it follows from Eq. (38) that

$$\begin{aligned} \dot{\tilde{V}}(\boldsymbol{x}) \subseteq & \bigcap_{\substack{\varsigma \in \partial V(\boldsymbol{x}) \\ \varsigma_{j^*} = 1}} \{Q + sgn(x_{i^*}) |x_{i^*}|^{n_{i^*}} \omega_{j^* i^*}\} \\ & \bigcap \bigcap_{\substack{\varsigma \in \partial V(\boldsymbol{x}) \\ \varsigma_{j^*} = -1}} \{Q - sgn(x_{i^*}) |x_{i^*}|^{n_{i^*}} \omega_{j^* i^*}\}, \end{aligned} \tag{39}$$

where

$$\begin{aligned} Q = & -\sum_{\substack{i=1 \\ i \neq i^*}}^{M} \sum_{\substack{j=1 \\ j \neq i}}^{M} sgn(x_i) |x_i|^{n_i} \omega_{ji} (\varsigma_i - \varsigma_j) \\ & - \sum_{\substack{j=i^* \\ j \neq j^*}}^{M} |x_{i^*}|^{n_{i^*}} \omega_{ji^*} (1 - sgn(x_{i^*})\, \varsigma_j) - |x_{i^*}|^{n_{i^*}} \omega_{j^* i^*}. \end{aligned}$$

bioRxiv preprint doi: https://doi.org/10.1101/2023.02.04.527149; this version posted February 4, 2023. The copyright holder for this preprint (which was not certified by peer review) is the author/funder, who has granted bioRxiv a license to display the preprint in perpetuity. It is made available under aCC-BY-NC-ND 4.0 International license.

According to (39), it is inferred that $\dot{\tilde{V}}(\boldsymbol{x}) \subseteq \emptyset$ since $x_i \neq 0$ and $\omega_{j^*i^*} > 0$. □

Corollary 4.5. *If G is strongly connected, then every solution of the system (9) with an arbitrary initial state converges to the largest invariant set in the union of $\mathbb{R}^M_{\geq 0}$ and $\mathbb{R}^M_{\leq 0}$.*

Proof. It follows from Propositions 4.1 and 4.6 and Theorem 2.4 that a solution $\boldsymbol{x}(t)$ of the system (9) with an initial state $\boldsymbol{x}(0) \in \mathbb{R}^M$ converges to the largest invariant set in the union of $\mathbb{R}^M_{\geq 0} \cap \Upsilon_\eta$ and $\mathbb{R}^M_{\leq 0} \cap \Upsilon_\eta$ where $\eta \geq \|\boldsymbol{x}(0)\|_1$. □

To prove that all solutions starting in $\mathbb{R}^M_{\geq 0}$ or $\mathbb{R}^M_{\leq 0}$ converge to equilibria, we will utilize a modified version of the "free-energy" function of the Becker-Döring model, describing the evolution of coagulation and fragmentation of clusters [74, 75]. Buhagiar [74] observed that this free-energy function is a Lyapunov function for the Becker-Döring cluster equations, and recently, it has been demonstrated that it is also a Lyapunov function for any system of differential equations generated by chemical reaction networks whose components are strongly connected [32]. Due to the fact that it is possible to derive a system of differential equations similar to Eq. (9), where all elements of the power vector $\boldsymbol{n}$ are nonnegative integers, from a chemical reaction network in which each reaction has identical reactants and also yields identical products, the mentioned free-energy function has assisted us to suggest the function $E_{\mathcal{D}} : \mathbb{R}^M_{\geq 0} \to \mathbb{R}$, defined by

$$E_{\mathcal{D}}(\boldsymbol{x}) = \boldsymbol{n}^T (\boldsymbol{x} \odot (\boldsymbol{ln}(\boldsymbol{x}) - \boldsymbol{ln}(\boldsymbol{x}_e)) - (\boldsymbol{x} - \boldsymbol{x}_e)), \tag{40}$$

to assess stability properties of an equilibrium point $\boldsymbol{x}_e \in \mathbb{R}^M_{>0}$ and the convergence of solutions of the system (9). It follows from Lemma 4.5 that $E_{\mathcal{D}}(\boldsymbol{x})$ is continuous on $\mathbb{R}^M_{\geq 0}$ as well as positive definite with respect to $\boldsymbol{x}_e$.

Lemma 4.5. *Assume that $E(x) = x(ln(x) - ln(y)) - (x - y)$ with $x \in \mathbb{R}_{\geq 0}$ and $y \in \mathbb{R}_{>0}$ where $E(0)$ is defined to be y. Then,*

- *$E(x)$ is continuous on $\mathbb{R}_{\geq 0}$;*
- *$E(x)$ is continuously differentiable on $\mathbb{R}_{>0}$;*
- *$E(x) > 0$ for all $x \neq y$, and $E(y) = 0$.*

Proof. Considering $\lim_{x \to 0^+} E(x) = y$, the first item is easy to spot. Due to $dE/dx = ln(x) - ln(y)$, the second item is also obvious. Since $d^2E/dx^2 = 1/x > 0$ for all $x > 0$, the function $E(x)$ is strictly convex on $\mathbb{R}_{>0}$, and thus, for all $x, y \in \mathbb{R}_{>0}$ when $x \neq y$, we have

$$E(x) > E(y) + \frac{dE}{dx}(y)(x - y).$$

Owing to the fact that $E(y) = (dE/dx)(y) = 0$ and $E(0) = y > 0$, the third item is deduced. □

Calculating the derivative of $E_{\mathcal{D}}(\boldsymbol{x})$ along the trajectories of the system (9) yields

$$\dot{E}_{\mathcal{D}}(\boldsymbol{x}) = -(\boldsymbol{x}^{\boldsymbol{n}})^T \boldsymbol{L}^T \boldsymbol{\Lambda}(\boldsymbol{n}) (\boldsymbol{ln}(\boldsymbol{x}) - \boldsymbol{ln}(\boldsymbol{x}_e)), \quad \boldsymbol{x} \in \mathbb{R}^M_{>0}. \tag{41}$$

bioRxiv preprint doi: https://doi.org/10.1101/2023.02.04.527149; this version posted February 4, 2023. The copyright holder for this preprint (which was not certified by peer review) is the author/funder, who has granted bioRxiv a license to display the preprint in perpetuity. It is made available under aCC-BY-NC-ND 4.0 International license.

Considering the equalities

$$\begin{aligned}
&\left(\boldsymbol{x}_e^{\boldsymbol{n}}\right)^T \boldsymbol{\Lambda}^{-1}\left(\boldsymbol{x}_e^{\boldsymbol{n}}\right) \boldsymbol{\Lambda}\left(\boldsymbol{x}^{\boldsymbol{n}}\right) = \left(\boldsymbol{x}^{\boldsymbol{n}}\right)^T, \\
&\left(\boldsymbol{x}_e^{\boldsymbol{n}}\right)^T \boldsymbol{L}^T \boldsymbol{\Lambda}^{-1}\left(\boldsymbol{x}_e^{\boldsymbol{n}}\right) \boldsymbol{x}^{\boldsymbol{n}} = 0, \\
&\boldsymbol{\Lambda}(\boldsymbol{n})\, \boldsymbol{ln}(\boldsymbol{x}) = \boldsymbol{ln}\left(\boldsymbol{x}^{\boldsymbol{n}}\right),
\end{aligned}$$

$\dot{E}_{\mathcal{D}}(\boldsymbol{x})$ in Eq. (41) can be written as

$$\begin{aligned}
\dot{E}_{\mathcal{D}}(\boldsymbol{x}) = &-\left(\boldsymbol{x}_e^{\boldsymbol{n}}\right)^T \boldsymbol{\Lambda}^{-1}\left(\boldsymbol{x}_e^{\boldsymbol{n}}\right) \boldsymbol{\Lambda}\left(\boldsymbol{x}^{\boldsymbol{n}}\right) \boldsymbol{L}^T\left(\boldsymbol{ln}\left(\boldsymbol{x}^{\boldsymbol{n}}\right) - \boldsymbol{ln}\left(\boldsymbol{x}_e^{\boldsymbol{n}}\right)\right) \\
&+\left(\boldsymbol{x}_e^{\boldsymbol{n}}\right)^T \boldsymbol{L}^T \boldsymbol{\Lambda}^{-1}\left(\boldsymbol{x}_e^{\boldsymbol{n}}\right) \boldsymbol{x}^{\boldsymbol{n}},
\end{aligned}$$

or as the elementwise summation

$$\dot{E}_{\mathcal{D}}(\boldsymbol{x}) = -\sum_{i=1}^{M} \sum_{\substack{j=1 \\ j \neq i}}^{M} x_{e_i}^{n_i} \omega_{ji} \left(x_i^* \left(ln\left(x_i^*\right) - ln\left(x_j^*\right)\right) - \left(x_i^* - x_j^*\right)\right), \tag{42}$$

where $x_i^* = x_i^{n_i} / x_{e_i}^{n_i}$.

Lemma 4.6. *If G is strongly connected, then*

$$\begin{aligned}
&\dot{E}_{\mathcal{D}}(\boldsymbol{x}_e) \leq 0, \qquad \forall \boldsymbol{x} \in \mathbb{R}_{>0}^M, \\
&\dot{E}_{\mathcal{D}}(\boldsymbol{x}_e) = 0, \\
&\dot{E}_{\mathcal{D}}(\boldsymbol{x}) < 0, \qquad \forall \boldsymbol{x} \in \mathbb{R}_{>0}^M \cap \Psi_{x_{tot}}^+ \setminus \{\boldsymbol{x}_e\},
\end{aligned}$$

where $x_{tot} = \mathbf{1}^T \boldsymbol{x}_e$.

Proof. Due to $x_{e_i}^{n_i} > 0$ and $\omega_{ji} \geq 0$, Lemma 4.5 implies that $\dot{E}_{\mathcal{D}}(\boldsymbol{x})$ in Eq. (42) is nonpositive for $\boldsymbol{x} \in \mathbb{R}_{>0}^M$. In addition, since G is strongly connected, the equality $\dot{E}_{\mathcal{D}}(\boldsymbol{x}) = 0$ occurs if and only if

$$\frac{x_1^{n_1}}{x_{e_1}^{n_1}} = \frac{x_2^{n_2}}{x_{e_2}^{n_2}} = \ldots = \frac{x_M^{n_M}}{x_{e_M}^{n_M}} = \gamma$$

or equivalently $\boldsymbol{x}^{\boldsymbol{n}} = \gamma \boldsymbol{x}_e^{\boldsymbol{n}}$ where $\gamma > 0$ using Lemma 4.5. If $\boldsymbol{x}$ simultaneously satisfies $\boldsymbol{x}^{\boldsymbol{n}} = \gamma \boldsymbol{x}_e^{\boldsymbol{n}}$ and $\mathbf{1}^T \boldsymbol{x} = \mathbf{1}^T \boldsymbol{x}_e$, then we must have

$$\left(\sqrt[n_1]{\gamma} - 1, \ldots, \sqrt[n_M]{\gamma} - 1\right)^T \boldsymbol{x}_e = 0. \tag{43}$$

Due to $n_i \geq 1$ and $\boldsymbol{x}_e \in \mathbb{R}_{>0}^M$, the equality (43) is only satisfied for $\gamma = 1$. □

Proposition 4.7. *Let $\boldsymbol{x}_e \in \mathbb{R}_{\geq 0}^M$ (resp., $\boldsymbol{x}_e \in \mathbb{R}_{\leq 0}^M$) be an equilibrium point of the system (9). If G is strongly connected, then $\boldsymbol{x}_e$ is stable, and every solution $\boldsymbol{x}(t)$ with an initial state belonging to $\Psi_{x_{tot}}^+$ (resp., $\Psi_{x_{tot}}^-$) with $x_{tot} = \mathbf{1}^T \boldsymbol{x}_e$ converges to $\boldsymbol{x}_e$ as t approaches infinity.*

Proof. It is sufficient to proceed only with $\boldsymbol{x}_e \in \mathbb{R}_{\geq 0}^M$ since the state space is symmetric under reflection through the origin. When G is strongly connected, we have either $\boldsymbol{x}_e = 0$ or $\boldsymbol{x}_e \in \mathbb{R}_{>0}^M$ by Lemma 4.1. For the trivial case $\boldsymbol{x}_e = 0$, the stability can be guaranteed by Proposition 4.1. Now, suppose that $\boldsymbol{x}_e \in \mathbb{R}_{>0}^M$. It follows from Lemmas 4.5 and 4.6 that there exists a

bioRxiv preprint doi: https://doi.org/10.1101/2023.02.04.527149; this version posted February 4, 2023. The copyright holder for this preprint (which was not certified by peer review) is the author/funder, who has granted bioRxiv a license to display the preprint in perpetuity. It is made available under aCC-BY-NC-ND 4.0 International license.

domain $X^* \subseteq \mathbb{R}^M_{>0}$ containing $\boldsymbol{x}_e$ in which $E_{\mathcal{D}}(\boldsymbol{x})$ and $\dot{E}_{\mathcal{D}}(\boldsymbol{x})$ satisfy the conditions of Theorem 2.2. Hence, $\boldsymbol{x}_e$ is stable. According to Proposition 4.2, the compact set $\Psi^+_{x_{tot}}$ is positively invariant. Now, we show that the function $E_{\mathcal{D}}(\boldsymbol{x}(t))$ on $\mathbb{R}_{\geq 0}$ is decreasing for all $\boldsymbol{x}(0) \in \Psi^+_{x_{tot}}$ with $x_{tot} = \mathbf{1}^T \boldsymbol{x}_e$. Note that $\boldsymbol{x}(0) \neq 0$ because of $x_{tot} > 0$. Due to the fact that the right-hand side of the system (9) is continuously differentiable, any initial condition $\boldsymbol{x}(0) \in \Psi^+_{x_{tot}}$ leads to a continuously differentiable solution $\boldsymbol{x}(t) \in \mathbb{R}^M_{>0} \cap \Psi^+_{x_{tot}}$ for all $t > 0$ using Proposition 4.3, and since the function $E_{\mathcal{D}}(\boldsymbol{x})$ and its derivative $\dot{E}_{\mathcal{D}}(\boldsymbol{x})$ are continuous on $\mathbb{R}^M_{\geq 0}$ and $\mathbb{R}^M_{>0}$, respectively, we can apply the second fundamental theorem of calculus (FTC) as follows:

$$E_{\mathcal{D}}(\boldsymbol{x}(t)) - E_{\mathcal{D}}(\boldsymbol{x}(t_0)) = \int_{t_0}^{t} \dot{E}_{\mathcal{D}}(\boldsymbol{x}(\tau))\,\tau, \quad \forall t_0 \in \mathbb{R}_{>0}, \forall t \geq t_0.$$

Because $E_{\mathcal{D}}(\boldsymbol{x}(t))$ is continuous on $\mathbb{R}_{\geq 0}$, we obtain

$$\begin{aligned}
\int_0^t \dot{E}_{\mathcal{D}}(\boldsymbol{x}(\tau))\,\tau &= \lim_{t_0 \to 0^+} \int_{t_0}^{t} \dot{E}_{\mathcal{D}}(\boldsymbol{x}(\tau))\,\tau \\
&= \lim_{t_0 \to 0^+} \left(E_{\mathcal{D}}(\boldsymbol{x}(t)) - E_{\mathcal{D}}(\boldsymbol{x}(t_0))\right) \\
&= E_{\mathcal{D}}(\boldsymbol{x}(t)) - E_{\mathcal{D}}(\boldsymbol{x}(0)),
\end{aligned}$$

and using Lemma 4.6, which implies $\dot{E}_{\mathcal{D}}(\boldsymbol{x}) \leq 0$ for all $\boldsymbol{x} \in \mathbb{R}^M_{>0}$, it can be deduced that for every initial state $\boldsymbol{x}(0) \in \Psi^+_{x_{tot}}$, we have

$$E_{\mathcal{D}}(\boldsymbol{x}(t)) \leq E_{\mathcal{D}}(\boldsymbol{x}(0)), \quad \forall t \geq 0.$$

Therefore, $E_{\mathcal{D}}(\boldsymbol{x}(t))$ is decreasing, and since $E_{\mathcal{D}}(\boldsymbol{x})$ is also lower bounded on the compact set $\Psi^+_{x_{tot}}$ due to its continuity, the function $E_{\mathcal{D}}(\boldsymbol{x}(t))$ converges to a limit as time goes to infinity, i.e.,

$$E_{\mathcal{D}}(\boldsymbol{x}(t)) \to E_\infty \; as \; t \to \infty. \tag{44}$$

Before going on, we want to recall two definitions. A point $\boldsymbol{p}$ is said to be in the positive limit set of a solution $\boldsymbol{x}(t)$ if there is a sequence t_n going to infinity with n and such that $\boldsymbol{x}(t_n) \to \boldsymbol{p}$ as $n \to \infty$. A set is called invariant if for any initial condition $\boldsymbol{x}(0)$ belonging to this set, the solution $\boldsymbol{x}(t)$ remains in it for all $t \in \mathbb{R}$. Now, let us resume our discussion. At this point, someone thinks of applying LaSalle's invariance principle [46] to investigate the convergence problem here. Owing to the fact that $\dot{E}_{\mathcal{D}}(\boldsymbol{x})$ is only continuous on $\mathbb{R}^M_{>0}$ but not $\mathbb{R}^M_{\geq 0}$, the function $\dot{E}_{\mathcal{D}}(\boldsymbol{x})$ is not continuous on whole $\Psi^+_{x_{tot}}$, and consequently, LaSalle's invariance theorem cannot be directly employed. However, we can take advantage of a fundamental result concerning positive limit sets which states that if a solution $\boldsymbol{x}(t)$ is bounded for all $t \geq 0$, then its positive limit sets is nonempty, compact, and invariant [46]. Let H^+ be the positive limit set of a solution $\boldsymbol{x}(t)$ with $\boldsymbol{x}(0) \in \Psi^+_{x_{tot}}$. Since the positively invariant set $\Psi^+_{x_{tot}}$ is closed, it follows

bioRxiv preprint doi: https://doi.org/10.1101/2023.02.04.527149; this version posted February 4, 2023. The copyright holder for this preprint (which was not certified by peer review) is the author/funder, who has granted bioRxiv a license to display the preprint in perpetuity. It is made available under aCC-BY-NC-ND 4.0 International license.

that $H^+ \subseteq \Psi^+_{x_{tot}}$. According to (44), it is deduced that

$$\forall \boldsymbol{p} \in H^+ \Rightarrow E_{\mathcal{D}}(\boldsymbol{p}) = E_\infty$$

because $E_{\mathcal{D}}(\boldsymbol{x})$ is continuous on $\Psi^+_{x_{tot}} \subset \mathbb{R}^M_{\geq 0}$. Consider a solution $\boldsymbol{x}^*(t)$ with $\boldsymbol{x}^*(0) \in H^+$. Thanks to the fact that H^+ is invariant, it is inferred that $\boldsymbol{x}^*(t) \in H^+ \cap \mathbb{R}^M_{>0}$ for all $t > 0$ by Proposition 4.3. Thus, recalling again the second FTC results in

$$\int_{t_0}^{t} \dot{E}_{\mathcal{D}}(\boldsymbol{x}(\tau))\,\tau = E_\infty - E_\infty = 0, \quad \forall t_0 \in \mathbb{R}_{>0}, \forall t \geq t_0.$$

Hence, since $\dot{E}_{\mathcal{D}}(\boldsymbol{x}^*(t))$ is continuous on $[t_0, t_1]$ for all $t_1 > t_0$, applying the first FTC implies

$$\dot{E}_{\mathcal{D}}(\boldsymbol{x}^*(t)) = \frac{d}{dt}(0) = 0. \quad \forall t \in (t_0, t_1),$$

and it follows that $\boldsymbol{x}^*(t) = \boldsymbol{x}_e$ because of the fact that $\dot{E}_{\mathcal{D}}(\boldsymbol{x})$ is only zero at $\boldsymbol{x}_e$ and is negative for all $\boldsymbol{x} \in \mathbb{R}^M_{>0} \cap \Psi^+_{x_{tot}} \setminus \{\boldsymbol{x}_e\}$ by Lemma 4.6. □

We now summarize our findings concerning the convergence of solutions of the system (14) as well as the stability of its equilibria in Corollary 4.6.

Corollary 4.6. *Suppose $\boldsymbol{y}_e \in \mathbb{R}^M$ is an equilibrium point of the system (14). Then, $\boldsymbol{y}_e$ is stable, and for any initial state $\boldsymbol{y}(0)$ belonging to the positively invariant set $\tilde{\Psi}_{(y_1,\ldots,y_m)} \supseteq \{\boldsymbol{y}_e\}$ (or $\tilde{\Psi}^*_{(y_1,\ldots,y_m)} \supseteq \{\boldsymbol{y}_e\}$), the solution $\boldsymbol{y}(t)$ converges to $\boldsymbol{y}_e$ as t approaches infinity.*

Proof. Considering Proposition 4.4, this conclusion can be drawn by applying Corollary 4.5 and Proposition 4.7 to each subsystem of the system (14). □

5. Extended FP Fisher-KPP reaction–diffusion equation on directed networks

Given a digraph $G \in \mathcal{G}_{\mathcal{T}}$ having M nodes, let us study a reaction-diffusion process on G that may be described by

$$\dot{\boldsymbol{x}} = \boldsymbol{\mathcal{R}}(\boldsymbol{x}) - \sigma \boldsymbol{\mathcal{L}}_G(\boldsymbol{x}), \quad \boldsymbol{x}(0) \in \mathbb{R}^M, \tag{45}$$

with

$$\boldsymbol{\mathcal{R}}(\boldsymbol{x}) = \boldsymbol{\alpha} \odot \boldsymbol{sgn}(\boldsymbol{x}) \odot |\boldsymbol{x}|^{\boldsymbol{\mu}} \odot (\boldsymbol{\rho} - |\boldsymbol{x}|^{\boldsymbol{\nu}}), \tag{46}$$

where $\sigma \in \mathbb{R}_{>0}$, $\boldsymbol{\alpha} \in \mathbb{R}^M_{\geq 0}$, $\boldsymbol{\rho} \in \mathbb{R}^M_{\geq 0}$, $\boldsymbol{\mu} \in \mathbb{R}^M_{\geq 1}$, $\boldsymbol{\nu} \in \mathbb{R}^M_{>0}$, which implies $\boldsymbol{\mathcal{R}} \in \mathbb{EF}(\mathbb{R}^M, \mathbb{R}^M)$, and the i-th element of $\boldsymbol{x}(t)$ is the concentration of a given species at node i at time t, denoted by $x_i(t)$. Accordingly, $x_{tot}(t) = \mathbf{1}^T \boldsymbol{x}(t)$ is the total concentration of that species on G at time t.

Lemma 5.1. *Let $\mathcal{R}(x) = sgn(x)\,|x|^{\mu}(\rho - |x|^{\nu})$ with $\rho \in \mathbb{R}_{\geq 0}$, $\mu \in \mathbb{R}_{\geq 1}$, and $\nu \in \mathbb{R}_{>0}$. Then,*

$$\mathcal{R}(x) \leq \left(\frac{\rho}{\mu + \nu}\right)^{\frac{\mu}{\nu}+1} \left(\mu^{\frac{\mu}{\nu}}\right) \nu, \quad \forall x \in \mathbb{R}_{\geq 0}, \tag{47}$$

bioRxiv preprint doi: https://doi.org/10.1101/2023.02.04.527149; this version posted February 4, 2023. The copyright holder for this preprint (which was not certified by peer review) is the author/funder, who has granted bioRxiv a license to display the preprint in perpetuity. It is made available under aCC-BY-NC-ND 4.0 International license.

and

$$\mathcal{R}(x)+\gamma\leq 0,\quad \forall\gamma\in\mathbb{R}_{\geq 0},\forall\beta\in\mathbb{R}_{>0},\forall x\geq max\{\left(\frac{\gamma}{\beta}\right)^{\frac{1}{\mu}},(\rho+\beta)^{\frac{1}{\nu}}\}. \tag{48}$$

Proof. The inequality (47) can be verified by the first derivative test. The derivative of $\mathcal{R}(x)$ with respect to x is given by

$$\frac{d\mathcal{R}(x)}{dx}=|x|^{\mu-1}\left(\rho\mu-(\mu+\nu)|x|^{\nu}\right). \tag{49}$$

For $\rho>0$, it is easy to spot that $x^*=\left(\frac{\rho\mu}{\mu+\nu}\right)^{\frac{1}{\nu}}$ is a critical point of $\mathcal{R}(x)$, and since we have $\frac{d\mathcal{R}(x)}{dx}>0$ for all x between zero and x^* and $\frac{d\mathcal{R}(x)}{dx}<0$ for all x greater than x^*, it follows that $\mathcal{R}(x^*)$, which is equal to the right-hand side of the inequality (47), is the maximum value of $\mathcal{R}(x)$ in $\mathbb{R}_{\geq 0}$. For the case $\rho=0$, it is obvious that $\mathcal{R}(x)\leq 0$ for $x\geq 0$. The inequality (48) can also be deduced by the following steps:

$$\begin{aligned}
&x\geq\left(\frac{\gamma}{\beta}\right)^{\frac{1}{\mu}}\overset{\beta>0}{\Longrightarrow}x^{\mu}\beta\geq\gamma,\\
&x\geq(\rho+\beta)^{\frac{1}{\nu}}\overset{\beta>0}{\Longrightarrow}x^{\nu}\geq\rho+\beta\overset{x>0}{\Longrightarrow}\\
&x^{\mu}\left(x^{\nu}-\rho\right)\geq x^{\mu}\beta\Rightarrow x^{\mu}\left(\rho-x^{\nu}\right)+\gamma\leq 0.
\end{aligned} \tag{50}$$

□

Proposition 5.1. *For the system (45), let us define the sets*

$$\begin{aligned}
&\Omega_1=\{1,...,M\},\\
&\Omega_2=\{i\in\Omega_1:\alpha_i=0\},\\
&\Omega_k=\{i\in\Omega_{k-1}:\sum_{j\in\Omega_1\setminus\Omega_{k-1}}\omega_{ji}=0\},\quad 3\leq k\leq M+1,
\end{aligned} \tag{51}$$

where α_i is the i-th element of $\boldsymbol{\alpha}$, and let M^* be the smallest positive integer for which $\Omega_{M^*+1}=\Omega_{M^*}$ or $\Omega_{M^*+1}=\emptyset$. Then, the sets

$$\begin{aligned}
&\Phi_{(V_1,...,V_{M^*})}=\{\boldsymbol{x}\in\mathbb{R}^M:\sum_{i\in\Omega_k}|x_i|\leq V_k,\forall k\in\{1,...,M^*\}\},\\
&\Phi^{+}_{(V_1,...,V_{M^*})}=\{\boldsymbol{x}\in\mathbb{R}^M_{\geq 0}:\sum_{i\in\Omega_k}x_i\leq V_k,\forall k\in\{1,...,M^*\}\},\\
&\Phi^{-}_{(V_1,...,V_{M^*})}=\{\boldsymbol{x}\in\mathbb{R}^M_{\leq 0}:\sum_{i\in\Omega_k}x_i\geq -V_k,\forall k\in\{1,...,M^*\}\},
\end{aligned} \tag{52}$$

with $(V_1,...,V_{M^*})^T\in\mathbb{R}^{M^*}_{\geq 0}$ is positively invariant with respect to the system (45) if V_k's satisfy for $M^*=1$ that

$$V_1\geq\begin{cases}0 & if\ \Omega_1=\Omega_2,\\ \sum\limits_{l\in\Omega_1\setminus\Omega_2}x^*_l & if\ \Omega_1\neq\Omega_2,\end{cases} \tag{53}$$

bioRxiv preprint doi: https://doi.org/10.1101/2023.02.04.527149; this version posted February 4, 2023. The copyright holder for this preprint (which was not certified by peer review) is the author/funder, who has granted bioRxiv a license to display the preprint in perpetuity. It is made available under aCC-BY-NC-ND 4.0 International license.

and for $M^* \geq 2$ *that*

$$\begin{aligned} V_{M^*} &\geq \sum_{l\in\Omega_{M^*}} x_l^*, \\ W_k &\geq \sum_{l\in\Omega_k\setminus\Omega_{k+1}} x_l^*, \quad 1 \leq k \leq M^*-1, \\ V_k &= V_{k+1} + W_k, \end{aligned} \tag{54}$$

where, for $l \in \Omega_1 \setminus \Omega_2$,

$$x_l^* = \begin{cases} \rho_l^{\frac{1}{\nu_l}} & if\ \{l\} = \Omega_1 \setminus \Omega_2, \\ max\{\left(\frac{\gamma_l^*}{\beta_l^*}\right)^{\frac{1}{\mu_l}}, (\rho_l + \beta_l^*)^{\frac{1}{\nu_l}}\} & if\ \{l\} \neq \Omega_1 \setminus \Omega_2, \end{cases} \tag{55}$$

with

$$\beta_l^* \in \mathbb{R}_{>0},\ \gamma_l^* = \left(\frac{1}{\alpha_l}\right) \sum_{\substack{i\in\Omega_1\setminus\Omega_2 \\ i\neq l}} \alpha_i \left(\frac{\rho_i}{\mu_i+\nu_i}\right)^{\frac{\mu_i}{\nu_i}+1} \left(\mu_i^{\frac{\mu_i}{\nu_i}}\right) \nu_i, \tag{56}$$

and, for $l \in \Omega_k \setminus \Omega_{k+1}$ *with* $k \geq 2$,

$$x_l^* = \begin{cases} 0 & if\ \Omega_{k+1} = \Omega_k, \\ \left(\frac{1}{\sum_{j\in\Omega_1\setminus\Omega_k}\omega_{jl}} \left(\sum_{i\in\Omega_1\setminus\Omega_k} \left(\sum_{j\in\Omega_k}\omega_{ji}\right)\left(\sum_{k'=1}^{k-1} W_{k'}\right)^{n_i}\right)\right)^{\frac{1}{n_l}} & if\ \Omega_{k+1} \neq \Omega_k, \end{cases} \tag{57}$$

where ρ_i, μ_i, ν_i, *and* n_i *represent the* i*-th elements of* $\boldsymbol{\rho}$, $\boldsymbol{\mu}$, $\boldsymbol{\nu}$, *and* $\boldsymbol{n}$.

Proof. Here, we will provide a proof for the set $\Phi_{(V_1,\ldots,V_{M^*})}$, and Consequently, since the right-hand side of Eq. (45) satisfies the positivity condition (4), it can be inferred that $\Phi^+_{(V_1,\ldots,V_{M^*})}$ is also positively invariant. Further, thanks to the fact that the system (45) is invariant under the change of variables $\boldsymbol{x} \to -\boldsymbol{x}$, we arrive at the same conclusion for $\Phi^-_{(V_1,\ldots,V_{M^*})}$.

Assume that $\boldsymbol{\varepsilon} = (\varepsilon_1, \ldots, \varepsilon_M)^T$ where ε_i is either -1 or 1. Each boundary segment $\sum_{i\in\Omega_k} \varepsilon_i x_i = V_k$ of the set $\Phi_{(V_1,\ldots,V_{M^*})}$ is entirely contained in the orthant $\mathbb{O}^M_{\boldsymbol{\varepsilon}}$, defined in Eq. (10), and it is easy to see that $\sum_{i\in\Omega_k} \varepsilon_i x_i \geq 0$ for $\boldsymbol{x} \in \mathbb{O}^M_{\boldsymbol{\varepsilon}}$ due to $\varepsilon_i x_i \geq 0$. Thus, it is sufficient by Theorem 2.1 to demonstrate that at any point $\boldsymbol{x} \in \mathbb{O}^M_{\boldsymbol{\varepsilon}}$ on the boundary segment $\sum_{i\in\Omega_k} \varepsilon_i x_i = V_k$, the summation $\sum_{i\in\Omega_k} \varepsilon_i x_i$ is nonincreasing along the trajectories of the system (45); that is,

$$\forall \boldsymbol{\varepsilon}, \forall \boldsymbol{x} \in \mathbb{O}^M_{\boldsymbol{\varepsilon}} : \sum_{i\in\Omega_k} \varepsilon_i x_i = V_k \Rightarrow \frac{d}{dt}\left(\sum_{i\in\Omega_k} \varepsilon_i x_i\right) \leq 0. \tag{58}$$

In other words, we intend to show that any solution $\boldsymbol{x}(t)$ with an initial state $\boldsymbol{x}(0) \in \Phi_{(V_1,\ldots,V_{M^*})}$ cannot leave the compact set $\Phi_{(V_1,\ldots,V_{M^*})}$ through the boundary segments $\sum_{i\in\Omega_k} \varepsilon_i x_i = V_k$, for all $k \in \{1, \ldots, M^*\}$.

Before we establish the claim (58), we verify the statements (59) and (60) which will be used

bioRxiv preprint doi: https://doi.org/10.1101/2023.02.04.527149; this version posted February 4, 2023. The copyright holder for this preprint (which was not certified by peer review) is the author/funder, who has granted bioRxiv a license to display the preprint in perpetuity. It is made available under aCC-BY-NC-ND 4.0 International license.

in the proof. For all $k \in \{1, ..., M^*\}$ and $k' > k$,

$$\forall \boldsymbol{x} \in \mathbb{O}_{\boldsymbol{\varepsilon}}^M \cap \Phi_{(V_1,...,V_{M^*})} : \sum_{i\in\Omega_k} \varepsilon_i x_i = V_k \Rightarrow \sum_{i\in\Omega_k\setminus\Omega_{k'}} \varepsilon_i x_i \geq V_k - V_{k'}, \tag{59}$$

and

$$\forall \boldsymbol{x} \in \mathbb{O}_{\boldsymbol{\varepsilon}}^M \cap \Phi_{(V_1,...,V_{M^*})} : \sum_{i\in\Omega_{k'}} \varepsilon_i x_i = V_{k'} \Rightarrow \sum_{i\in\Omega_k\setminus\Omega_{k'}} \varepsilon_i x_i \leq V_k - V_{k'}. \tag{60}$$

Note that $\Omega_{k'} \subseteq \Omega_k$ if $k' > k$ by definition. The statement (59) can be proved by contradiction, for if it was not true there would exist $\boldsymbol{x} \in \mathbb{O}_{\boldsymbol{\varepsilon}}^M \cap \Phi_{(V_1,...,V_{M^*})}$ such that $\sum_{i\in\Omega_k\setminus\Omega_{k'}} \varepsilon_i x_i < V_k - V_{k'}$. Using $\sum_{i\in\Omega_k} \varepsilon_i x_i = V_k$, we obtain

$$\sum_{i\in\Omega_k\setminus\Omega_{k'}} \varepsilon_i x_i < \sum_{i\in\Omega_k} \varepsilon_i x_i - V_{k'} \Rightarrow \sum_{i\in\Omega_{k'}} \varepsilon_i x_i > V_{k'}, \tag{61}$$

which contradicts the fact that $\boldsymbol{x} \in \Phi_{(V_1,...,V_{M^*})}$. The statement (60) can also be shown by contradiction. Suppose that there is a point $\boldsymbol{x} \in \mathbb{O}_{\boldsymbol{\varepsilon}}^M \cap \Phi_{(V_1,...,V_{M^*})}$ such that $\sum_{i\in\Omega_k\setminus\Omega_{k'}} \varepsilon_i x_i > V_k - V_{k'}$. Using $\sum_{i\in\Omega_{k'}} \varepsilon_i x_i = V_{k'}$, we have

$$\sum_{i\in\Omega_k\setminus\Omega_{k'}} \varepsilon_i x_i > V_k - \sum_{i\in\Omega_{k'}} \varepsilon_i x_i \Rightarrow \sum_{i\in\Omega_k} \varepsilon_i x_i > V_k, \tag{62}$$

which contradicts the fact that $\boldsymbol{x} \in \Phi_{(V_1,...,V_{M^*})}$.

To prove the claim (58), we start by calculating the derivative of $\sum_{i\in\Omega_1} \varepsilon_i x_i$ along the trajectories of the system (45).

$$\begin{aligned}
\frac{d}{dt}\left(\sum_{i\in\Omega_1} \varepsilon_i x_i\right) &= \sum_{i\in\Omega_1\setminus\Omega_2} \alpha_i \varepsilon_i sgn\left(x_i\right) |x_i|^{\mu_i} \left(\rho_i - |x_i|^{\nu_i}\right) \\
&\quad - \sigma \sum_{i\in\Omega_1} \sum_{\substack{j\in\Omega_1 \\ j\neq i}} sgn\left(x_i\right) |x_i|^{n_i} \omega_{ji} \left(\varepsilon_i - \varepsilon_j\right) \\
&= \sum_{i\in\Omega_1\setminus\Omega_2} \alpha_i |x_i|^{\mu_i} \left(\rho_i - |x_i|^{\nu_i}\right) \\
&\quad - \sigma \sum_{i\in\Omega_1} \sum_{\substack{j\in\Omega_1 \\ j\neq i}} |x_i|^{n_i} \omega_{ji} \left(1 - sgn\left(x_i\right) \varepsilon_j\right), \quad \forall \boldsymbol{x} \in \mathbb{O}_{\boldsymbol{\varepsilon}}^M
\end{aligned} \tag{63}$$

In the case $\Omega_1 = \Omega_2$, which implies $M^* = 1$, the derivative $\frac{d}{dt}\left(\sum_{i\in\Omega_1} \varepsilon_i x_i\right)$ in Eq. (63) is nonpositive for all $\boldsymbol{x} \in \mathbb{O}_{\boldsymbol{\varepsilon}}^M$ satisfying $\sum_{i\in\Omega_1} \varepsilon_i x_i = V_1$ with $V_1 \geq 0$; see Eq. (11). In fact, $\Omega_1 = \Omega_2$ means all reaction coefficients α_i's are equal to zero, which makes the system (45) equivalent to (9).

In the case $\Omega_1 \neq \Omega_2$ when $M^* = 1$, we have $\Omega_2 = \emptyset$ by definition, and it can be seen that the derivative $\frac{d}{dt}\left(\sum_{i\in\Omega_1} \varepsilon_i x_i\right)$ is nonpositive for all $\boldsymbol{x} \in \mathbb{O}_{\boldsymbol{\varepsilon}}^M$ satisfying $\sum_{i\in\Omega_1} \varepsilon_i x_i = V_1$ with $V_1 \geq \sum_{i\in\Omega_1} x_i^*$. To clarify, when Ω_1 has only one element x_1, it is easy to see that the derivative $\frac{d}{dt}\left(\sum_{i\in\Omega_1} \varepsilon_i x_i\right)$ is nonpositive for $x_1 \in \mathbb{O}_{\varepsilon_1}^1$ if $\varepsilon_1 x_1 \geq \rho_1^{(1/\nu_1)}$, and when Ω_1 has more than one

bioRxiv preprint doi: https://doi.org/10.1101/2023.02.04.527149; this version posted February 4, 2023. The copyright holder for this preprint (which was not certified by peer review) is the author/funder, who has granted bioRxiv a license to display the preprint in perpetuity. It is made available under aCC-BY-NC-ND 4.0 International license.

element, we obtain, for $\boldsymbol{x} \in \mathbb{O}_{\boldsymbol{\varepsilon}}^M$ and $l \in \Omega_1 \setminus \Omega_2$,

$$\begin{aligned}\frac{d}{dt}\left(\sum_{i\in\Omega_1}\varepsilon_i x_i\right) &= \alpha_l|x_l|^{\mu_l}\left(\rho_l - |x_l|^{\nu_l}\right) + \sum_{\substack{k\in\Omega_1\setminus\Omega_2\\k\neq l}}\alpha_k|x_k|^{\mu_k}\left(\rho_k - |x_k|^{\nu_k}\right)\\ &\quad - \sigma\sum_{i\in\Omega_1}\sum_{\substack{j\in\Omega_1\\j\neq i}}|x_i|^{n_i}\omega_{ji}\left(1 - sgn\left(x_i\right)\varepsilon_j\right)\\ &\leq \alpha_l|x_l|^{\mu_l}\left(\rho_l - |x_l|^{\nu_l}\right) + \sum_{\substack{k\in\Omega_1\setminus\Omega_2\\k\neq l}}\alpha_k\left(\frac{\rho_k}{\mu_k+\nu_k}\right)^{\frac{\mu_k}{\nu_k}+1}\left(\mu_k^{\frac{\mu_k}{\nu_k}}\right)\nu_k,\end{aligned} \tag{64}$$

using Lemma 5.1 and Eqs. (63) and (11). Hence, Lemma 5.1 guarantees that the derivative $\frac{d}{dt}\left(\sum_{i\in\Omega_1}\varepsilon_i x_i\right)$ in Eq. (64) is nonpositive for all $\boldsymbol{x} \in \mathbb{O}_{\boldsymbol{\varepsilon}}^M$ if

$$|x_l| \geq max\{\left(\frac{\gamma_l^*}{\beta_l^*}\right)^{\frac{1}{\mu_l}}, (\rho_l + \beta_l^*)^{\frac{1}{\nu_l}}\}, \tag{65}$$

where β_l^* and γ_l^* have been given by Eq. (56). Finally, due to $V_1 \geq \sum_{i\in\Omega_1} x_i^*$, there is at least one component x_l of $\boldsymbol{x} \in \mathbb{O}_{\boldsymbol{\varepsilon}}^M$ satisfying $\sum_{i\in\Omega_1}\varepsilon_i x_i = V_1$ such that $\varepsilon_l x_l \geq x_l^*$, which can be shown by contradiction. Suppose $\varepsilon_i x_i < x_i^*$ for all $i \in \Omega_1$, then $\sum_{i\in\Omega_1}\varepsilon_i x_i < \sum_{i\in\Omega_1} x_i^*$, which contradicts the assumption that $\sum_{i\in\Omega_1}\varepsilon_i x_i = V_1 \geq \sum_{i\in\Omega_1} x_i^*$.

In the case $M^* \geq 2$, evaluating that the derivative $\frac{d}{dt}\left(\sum_{i\in\Omega_1} x_i\right)$ in Eq. (64) is nonpositive for all $\boldsymbol{x} \in \mathbb{O}_{\boldsymbol{\varepsilon}}^M$ satisfying $\sum_{i\in\Omega_1}\varepsilon_i x_i = V_1$ is equivalent by the statement (59) to evaluating that it is nonpositive for all $\boldsymbol{x} \in \mathbb{O}_{\boldsymbol{\varepsilon}}^M$ satisfying $\sum_{i\in\Omega_1\setminus\Omega_2}\varepsilon_i x_i \geq V_1 - V_2 = W_1$, which can be concluded if $W_1 \geq \sum_{i\in\Omega_1\setminus\Omega_2} x_i^*$. Due to $W_1 \geq \sum_{i\in\Omega_1\setminus\Omega_2} x_i^*$, there exists at least one component x_l of $\boldsymbol{x} \in \mathbb{O}_{\boldsymbol{\varepsilon}}^M$ satisfying $\sum_{i\in\Omega_1\setminus\Omega_2}\varepsilon_i x_i \geq W_1$ such that $\varepsilon_l x_l \geq x_l^*$, which can be shown by contradiction similar to the previous argument.

To study the other boundary segments $\sum_{i\in\Omega_k}\varepsilon_i x_i = V_k$ with $k \geq 2$, we first calculate the derivative of $\sum_{i\in\Omega_k}\varepsilon_i x_i$, with $k \geq 2$, along the trajectories of the system (45).

$$\begin{aligned}\frac{d}{dt}\left(\sum_{i\in\Omega_k}\varepsilon_i x_i\right) &= -\sigma\sum_{i\in\Omega_k}\sum_{\substack{j\in\Omega_k\\j\neq i}} sgn\left(x_i\right)|x_i|^{n_i}\omega_{ji}\left(\varepsilon_i - \varepsilon_j\right)\\ &\quad - \sigma\sum_{i\in\Omega_k}\sum_{j\in\Omega_1\setminus\Omega_k} sgn\left(x_i\right)|x_i|^{n_i}\omega_{ji}\left(\varepsilon_i\right)\\ &\quad - \sigma\sum_{i\in\Omega_1\setminus\Omega_k}\sum_{j\in\Omega_k} sgn\left(x_i\right)|x_i|^{n_i}\omega_{ji}\left(-\varepsilon_j\right)\end{aligned} \tag{66}$$

bioRxiv preprint doi: https://doi.org/10.1101/2023.02.04.527149; this version posted February 4, 2023. The copyright holder for this preprint (which was not certified by peer review) is the author/funder, who has granted bioRxiv a license to display the preprint in perpetuity. It is made available under aCC-BY-NC-ND 4.0 International license.

Considering $\Omega_{k+1} \subseteq \Omega_k$, Eq. (66) can be rewritten as

$$\begin{aligned}\frac{d}{dt}\left(\sum_{i\in\Omega_k}\varepsilon_i x_i\right) &= -\sigma\sum_{i\in\Omega_k}\sum_{\substack{j\in\Omega_k\\ j\neq i}}|x_i|^{n_i}\omega_{ji}\left(1-sgn\left(x_i\right)\varepsilon_j\right)\\ &\quad-\sigma\sum_{i\in\Omega_k\setminus\Omega_{k+1}}|x_i|^{n_i}\sum_{j\in\Omega_1\setminus\Omega_k}\omega_{ji}\\ &\quad-\sigma\sum_{i\in\Omega_{k+1}}|x_i|^{n_i}\sum_{j\in\Omega_1\setminus\Omega_k}\omega_{ji}\\ &\quad+\sigma\sum_{i\in\Omega_1\setminus\Omega_k}\sum_{j\in\Omega_k}|x_i|^{n_i}\omega_{ji}\left(sgn\left(x_i\right)\varepsilon_j\right), \quad \forall \boldsymbol{x}\in\mathbb{O}_{\boldsymbol{\varepsilon}}^M.\end{aligned} \tag{67}$$

By the definition of Ω_k, the third summation in the right-hand side of Eq. (67) is identical to zero, and thus, we can obtain

$$\begin{aligned}\frac{d}{dt}\left(\sum_{i\in\Omega_k}\varepsilon_i x_i\right) &\leq -\sigma\sum_{i\in\Omega_k\setminus\Omega_{k+1}}|x_i|^{n_i}\sum_{j\in\Omega_1\setminus\Omega_k}\omega_{ji}\\ &\quad+\sigma\sum_{i\in\Omega_1\setminus\Omega_k}|x_i|^{n_i}\sum_{j\in\Omega_k}\omega_{ji}, \quad \forall \boldsymbol{x}\in\mathbb{O}_{\boldsymbol{\varepsilon}}^M.\end{aligned} \tag{68}$$

When $\Omega_{k+1}=\Omega_k$, it can be demonstrated that $\frac{d}{dt}\left(\sum_{i\in\Omega_k}\varepsilon_i x_i\right)$ is nonpositive for all $\boldsymbol{x}\in\mathbb{O}_{\boldsymbol{\varepsilon}}^M$. Assuming $\Omega_{k+1}=\Omega_k$, we have

$$\omega_{ji}=0, \quad \forall j\in\Omega_1\setminus\Omega_k, \forall i\in\Omega_k,$$

due to $\omega_{ji}\geq 0$ and consequently, since all SCCs of G are terminal, it is deduced that

$$\omega_{ji}=0, \quad \forall j\in\Omega_k, \forall i\in\Omega_1\setminus\Omega_k,$$

which leads to the conclusion that $\frac{d}{dt}\left(\sum_{i\in\Omega_k}\varepsilon_i x_i\right)$ is nonpositive for $\boldsymbol{x}\in\mathbb{O}_{\boldsymbol{\varepsilon}}^M$ if $\Omega_{k+1}=\Omega_k$, using the inequality (68). Now supposing that $\Omega_{k+1}\neq\Omega_k$, it can be seen for the inequality (68) and $l\in\Omega_k\setminus\Omega_{k+1}$ that

$$\begin{aligned}\frac{d}{dt}\left(\sum_{i\in\Omega_k}\varepsilon_i x_i\right) &\leq -\sigma|x_l|^{n_l}\sum_{j\in\Omega_1\setminus\Omega_k}\omega_{jl}-\sigma\sum_{\substack{i\in\Omega_k\setminus\Omega_{k+1}\\ i\neq l}}|x_i|^{n_i}\sum_{j\in\Omega_1\setminus\Omega_k}\omega_{ji}\\ &\quad+\sigma\sum_{i\in\Omega_1\setminus\Omega_k}|x_i|^{n_i}\sum_{j\in\Omega_k}\omega_{ji},\\ &\leq -\sigma|x_l|^{n_l}\sum_{j\in\Omega_1\setminus\Omega_k}\omega_{jl}+\sigma\sum_{i\in\Omega_1\setminus\Omega_k}|x_i|^{n_i}\sum_{j\in\Omega_k}\omega_{ji}, \quad \forall \boldsymbol{x}\in\mathbb{O}_{\boldsymbol{\varepsilon}}^M.\end{aligned} \tag{69}$$

Verifying that the derivative $\frac{d}{dt}\left(\sum_{i\in\Omega_k}\varepsilon_i x_i\right)$ for $2\leq k\leq M^*-1$ (resp., $k=M^*$) is nonpositive for all $\boldsymbol{x}\in\mathbb{O}_{\boldsymbol{\varepsilon}}^M\cap\Phi_{(V_1,\ldots,V_{M^*})}$ satisfying $\sum_{i\in\Omega_k}\varepsilon_i x_i=V_k$ is equivalent by the statements (59) and (60) (resp., the statement (60)) to verifying that it is nonpositive for all $\boldsymbol{x}\in\mathbb{O}_{\boldsymbol{\varepsilon}}^M\cap\Phi_{(V_1,\ldots,V_{M^*})}$ satisfying

bioRxiv preprint doi: https://doi.org/10.1101/2023.02.04.527149; this version posted February 4, 2023. The copyright holder for this preprint (which was not certified by peer review) is the author/funder, who has granted bioRxiv a license to display the preprint in perpetuity. It is made available under aCC-BY-NC-ND 4.0 International license.

both $\sum_{i\in\Omega_1\setminus\Omega_k}\varepsilon_i x_i \le V_1 - V_k$ and $\sum_{i\in\Omega_k\setminus\Omega_{k+1}}\varepsilon_i x_i \ge V_k - V_{k+1}$ (resp., $\sum_{i\in\Omega_1\setminus\Omega_k}\varepsilon_i x_i \le V_1 - V_k$). Thus, due to $\sum_{i\in\Omega_1\setminus\Omega_k}\varepsilon_i x_i \le V_1 - V_k$, it follows from Eq. (69) that

$$\begin{aligned}\frac{d}{dt}\left(\sum_{i\in\Omega_j}\varepsilon_i x_i\right) \le & -\sigma|x_l|^{n_l}\sum_{j\in\Omega_1\setminus\Omega_k}\omega_{jl} \\ & +\sigma\sum_{i\in\Omega_1\setminus\Omega_k}\left(\sum_{k'=1}^{k-1}W_{k'}\right)^{n_k}\sum_{j\in\Omega_k}\omega_{ji}, \quad \forall \boldsymbol{x}\in\mathbb{O}_{\boldsymbol{\varepsilon}}^M.\end{aligned} \tag{70}$$

where $W_{k'} = V_{k'} - V_{k'+1}$. Note by definition that $V_1 - V_k = \sum_{k'=1}^{k-1} W_{k'}$. Hence, it is easy to see that $\frac{d}{dt}\left(\sum_{i\in\Omega_k}\varepsilon_i x_i\right)$ in the inequality (70) is nonpositive if $x_l \ge x_l^*$ where x_l^* is given in Eq. (57) when $\Omega_{k+1}\neq\Omega_k$. Using a contradiction argument similar to the previous one, it can be shown that $\frac{d}{dt}\left(\sum_{i\in\Omega_k}\varepsilon_i x_i\right)$ with $2\le k\le M^*-1$ (resp., $k=M^*$) is nonpositive for $\boldsymbol{x}\in\mathbb{O}_{\boldsymbol{\varepsilon}}^M\cap\Phi_{(V_1,\ldots,V_{M^*})}$ satisfying $\sum_{i\in\Omega_k}\varepsilon_i x_i = V_k$ if $W_k \ge \sum_{l\in\Omega_k\setminus\Omega_{k+1}} x_l^*$ (resp., $V_{M^*}\ge\sum_{l\in\Omega_{M^*}} x_l^*$). □

Corollary 5.1. *For any initial condition $\boldsymbol{x}(0)\in\mathbb{R}_{\ge 0}^M$ (resp., $\boldsymbol{x}(0)\in\mathbb{R}_{\le 0}^M$), the system (45) has a unique solution $\boldsymbol{x}(t)$ remaining entirely in $\mathbb{R}_{\ge 0}^M$ (resp., $\mathbb{R}_{\le 0}^M$) for all $t\ge 0$.*

Proof. Since the state space is symmetric under reflection through the origin, we only proceed with the nonnegative orthant. For every solution $\boldsymbol{x}(t)$ of the system (45) with $\boldsymbol{x}(0)\in\mathbb{R}_{\ge 0}^M$, we can choose a vector $(V_1,\ldots,V_{M^*})^T$ such that a set $\Phi^+_{(V_1,\ldots,V_{M^*})}$ satisfying the conditions of Proposition 5.1 and also $V_j\ge\sum_{i\in\Omega_j}x_i(0)$ for all $j\in\{1,\ldots,M^*\}$, which implies $\boldsymbol{x}(0)\in\Phi^+_{(V_1,\ldots,V_{M^*})}$. Hence, Theorem 2.1 ensures the existence and uniqueness of the solution $\boldsymbol{x}(t)$ for all $t\ge 0$. □

Corollary 5.2. *For any initial condition $\boldsymbol{x}(0)\in\mathbb{R}^M$, the system (45) has a unique bounded solution $\boldsymbol{x}(t)$ that is defined for all $t\ge 0$.*

Proof. According to the definition (52) of the set $\Phi_{(V_1,\ldots,V_{M^*})}$, we can find a vector $(V_1,\ldots,V_{M^*})^T\in\mathbb{R}_{\ge 0}^{M^*}$ such that $\boldsymbol{x}(0)\in\Phi_{(V_1,\ldots,V_{M^*})}$ by choosing sufficiently large V_k's. The rest of the proof follows from Proposition 5.1 and Theorem 2.1. □

6. Nonlinear diffusion on a directed one-dimensional lattice

Cytoskeletal motor proteins are responsible for directional transportation along microfilaments or microtubules within the cell. Among the prominent motor proteins associated with microtubules, kinesins crawl anterogradely, whereas dyneins slide retrogradely along microtubules by converting the chemical energy produced from ATP hydrolysis to mechanical energy [76]. It was experimentally demonstrated that the movement of microtubule-associated motors can be an anomalous subdiffusion process, especially at long times [77]. In addition, to investigate the motion of motor proteins, recent studies have modeled microtubules as one-dimensional lattices [78–80]. Hence, it may be of potential interest to examine nonlinear diffusion processes governed by the proposed equation (9) on a directed one-dimensional lattice.

bioRxiv preprint doi: https://doi.org/10.1101/2023.02.04.527149; this version posted February 4, 2023. The copyright holder for this preprint (which was not certified by peer review) is the author/funder, who has granted bioRxiv a license to display the preprint in perpetuity. It is made available under aCC-BY-NC-ND 4.0 International license.

Consider a directed one-dimensional lattice G with M nodes and weights

$$\omega_{ik} = \begin{cases} 1 & i = k+1, \\ r & k = i+1, \\ 0 & elsewhere, \end{cases} \tag{71}$$

where $0 < r \leq 1$. Here, we conduct a qualitative study of particle diffusion on G governed by

$$\dot{\boldsymbol{c}} = -\sigma \boldsymbol{\mathcal{L}}_G(\boldsymbol{c}), \quad \boldsymbol{c}(0) \in \mathbb{R}^M_{\geq 0}, \tag{72}$$

where $\sigma \in \mathbb{R}_{>0}$ and $\boldsymbol{n} = n\mathbf{1}$ for the Laplacian operator given in Eq. (7). Fig. 1 displays the simulation results of Eq. (72) with $M = 101$ at 10 different points in the parameter space when the initial concentration at each node was set to zero except either for Node 14 or for Node 51, which has been set to 1. As demonstrated by the first and last columns of images in Fig. 1, decreasing r results in an anterograde-bias in the diffusion pattern. Furthermore, as seen in the second and third columns of images in Fig. 1, while both shrinking σ and growing n contribute to more localized diffusion over the simulation period, the tail of the distribution of particles diffused under a regime with an increased n is sharper and smaller compared to that of particles diffused under a regime with a reduced σ.

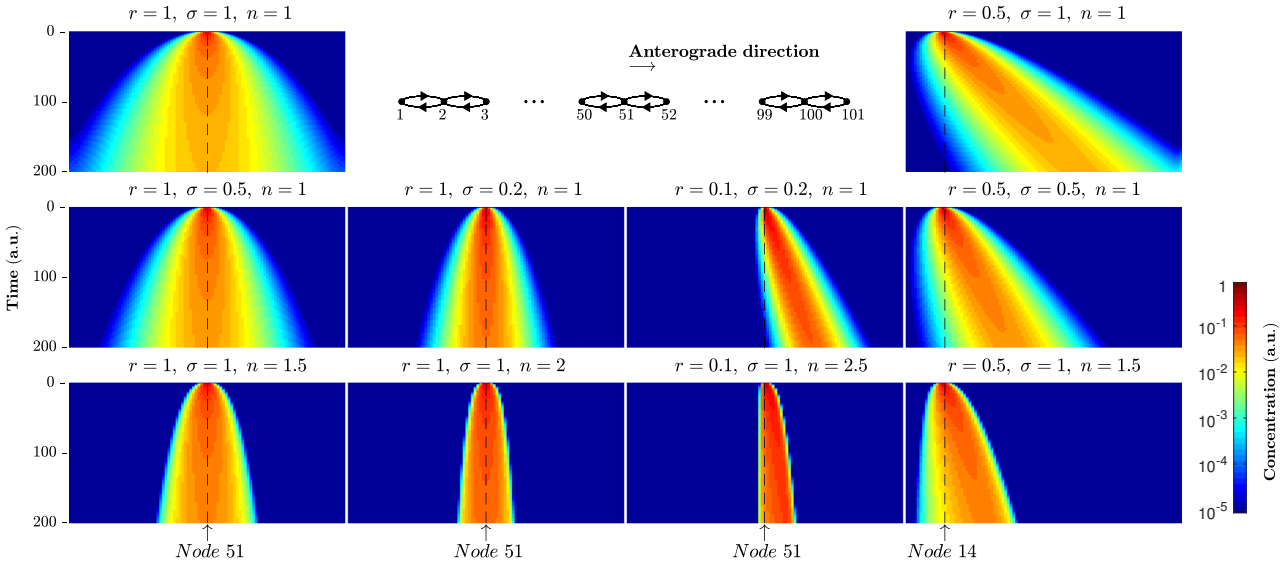

Figure 1: It illustrates a directed one-dimensional lattice with 101 nodes and the simulation results of Eq. (72) for 10 different scenarios when the initial concentration at each node was set to zero except either for Node 14 or for Node 51, which has been set to 1.

Using simulation, we will now demonstrate that, regardless of directionality, diffusion is normal if $n = 1$, and subdiffusion occurs when $n > 1$, but let us first recall two definitions pertaining to anomalous diffusion. The average position of N particles and the variance of the

bioRxiv preprint doi: https://doi.org/10.1101/2023.02.04.527149; this version posted February 4, 2023. The copyright holder for this preprint (which was not certified by peer review) is the author/funder, who has granted bioRxiv a license to display the preprint in perpetuity. It is made available under aCC-BY-NC-ND 4.0 International license.

position or mean squared displacement with respect to the average position are as follows [81]:

$$\begin{aligned} AVG\left(t\right) &= \frac{1}{N}\sum_{k=1}^{N} q_k\left(t\right), \\ MSD\left(t\right) &= \frac{1}{N}\sum_{k=1}^{N} \left|q_k\left(t\right) - AVG\left(t\right)\right|^2, \end{aligned} \tag{73}$$

respectively, where $q_k\left(t\right)$ is the position of the k-th particle at time t. Assuming c_i denotes the concentration of particles at node i, the probability of finding particles at node i can be represented as $c_i/\mathbf{1}^T\boldsymbol{c}$, and subsequently, some calculations leads to the formulae

$$\begin{aligned} AVG\left(t\right) &= \frac{1}{\mathbf{1}^T\boldsymbol{c}\left(t\right)}\sum_{i=1}^{M} ic_i\left(t\right), \\ MSD\left(t\right) &= \frac{1}{\mathbf{1}^T\boldsymbol{c}\left(t\right)}\sum_{i=1}^{M} i^2c_i - \left(AVG\left(t\right)\right)^2, \end{aligned} \tag{74}$$

which are simple the mean and the variance of a discrete stochastic process on the set of M nodes. Simulation results for two directionally unbiased regimes ($r = 1$) and two anterograde-biased regimes with $r = 0.1$ when the initial concentration at all 101 nodes was set to zero except node 51, which was set to 1, are depicted in Fig. 2. For both directionally unbiased and anterograde-biased regimes with $n = 1$, there is a linear relationship between $MSD\left(t\right)$ and time t, indicating normal diffusion, and for the other two regimes with $n > 1$, $MSD\left(t\right)$ is approximately proportional to t^{ζ} with $\zeta < 1$, exhibiting subdiffusion. See Fig. 2A2,B2. Note, however, that this conclusion is confined to a finite time interval before particles accumulate on the lattice's end points. Moreover, for both directionally unbiased regimes with $n = 1$ and $n = 2.5$, $AVG\left(t\right)$ remains unchanged at 51 (see Fig. 2A1), while it increases linearly for the anterograde-biased regime with $n = 1$ and nonlinearly for the anterograde-biased regime with $n = 2.5$ (see Fig. 2B1). Notice that the diffusion coefficient σ is simply a time-scaling factor.

7. Modeling tauopathy progression in the mouse brain

First discovered in 1975, tau is a multifunctional microtubule-associated protein (MAP) in the neuron, which many researchers have extensively studied its function to stabilize microtubules and encourage axonal prolongation [82, 83]. Tau protein is natively unfolded, and in physiological conditions its tendency for aggregation is low. However, there are modifications, such as phosphorylation and truncation [82], which may enable monomeric tau proteins to make aggregates. Tau aggregation characterizes neurodegenerative diseases known as tauopathies, including Alzheimer's disease (AD), Huntington disease (HD), Pick disease (PiD), progressive supranuclear palsy (PSP), argyrophilic grain disease (AGD), corticobasal degeneration (CBD), and frontotemporal dementia with parkinsonism-17 (FTDP -17). Although the potential of tau protein to induce such diseases has been confirmed by the identification of tau mutants in patients with FTDP-17 [84], the mechanisms and pathways by which tau protein forms

bioRxiv preprint doi: https://doi.org/10.1101/2023.02.04.527149; this version posted February 4, 2023. The copyright holder for this preprint (which was not certified by peer review) is the author/funder, who has granted bioRxiv a license to display the preprint in perpetuity. It is made available under aCC-BY-NC-ND 4.0 International license.

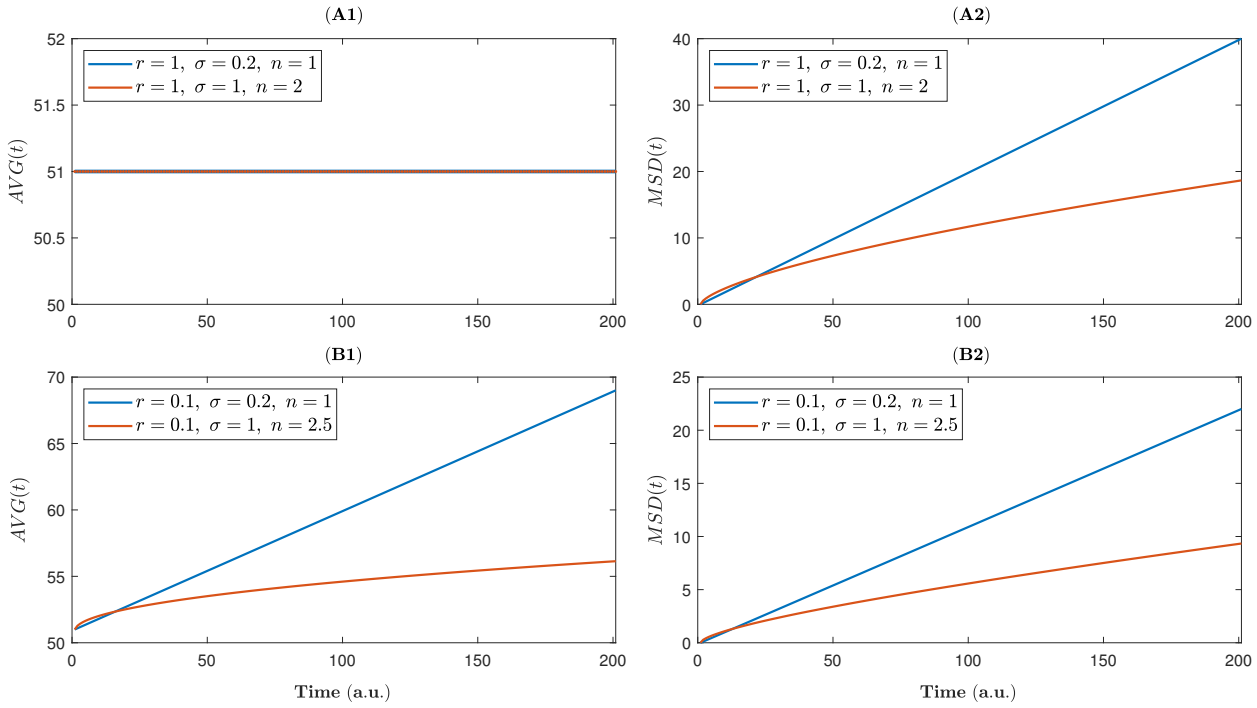

Figure 2: (A1) and (A2) present the average position $AVG\,(t)$ and the mean squared displacement with respect to the average position $MSD\,(t)$, respectively, for two directionally unbiased regimes ($r = 1$), and (B1) and (B2) also show $AVG\,(t)$ and $MSD\,(t)$, respectively, for two anterograde-biased regimes with $r = 0.1$ when the initial concentration at all 101 nodes was set to zero except node 51, which was set to 1.

aggregates in tauopathies are not sufficiently comprehended.

Tau pathology induced by the injection of tau seeds into the mouse brain supports the idea that the harmful species can be transmitted from the inoculation sites to synaptically connected brain regions [85, 86]. Actually, the spreading of toxic tau species is chiefly attributed to the axonal transportation [87], and thus, due to the porous structure of axonal bundles [88–90], it is expected that, at the mesoscale, tau pathology is propagated by a nonlinear diffusion process. Further, cell culture and animal model studies have indicated that misfolded tau species can be transmitted trans-synaptically among neurons, both anterogradely and retrogradely [91, 92], and recently, researchers have also investigated directionally biased spreading of tauopathies using an in-silico model mimicking the two-neuron system [93] and a diffusion equation with the linear Laplacian operator on the mouse connectome [94]. This section proposes a model that captures the effects of both nonlinearity and directionality of spreading on the spatiotemporal evolution of tau pathology.

7.1. Constructing the Laplacian matrix using the Allen Mouse Brain Connectome

Here, we aim to take advantage of the publicly available data from the Allen Mouse Brain Connectivity Atlas (AMBCA) [95] (connectivity.brain-map.org) to construct a Laplacian matrix that meets our objectives. The inter-region connectivity matrix $\left[\boldsymbol{W}_{ipsi}^{T}\ \boldsymbol{W}_{contra}^{T}\right]^{T}$ of the Allen Mouse Brain Connectome provides strength estimates of the mutual connections from 213 regions of interest (ROIs) in the right hemisphere to 426 (2×213) ROIs in the right (ipsilateral) and left (contralateral) hemispheres. Since the strength values resulted from a linear regression, a

bioRxiv preprint doi: https://doi.org/10.1101/2023.02.04.527149; this version posted February 4, 2023. The copyright holder for this preprint (which was not certified by peer review) is the author/funder, who has granted bioRxiv a license to display the preprint in perpetuity. It is made available under aCC-BY-NC-ND 4.0 International license.

p-value was also assigned to each connection [95]. Fig. 3A. depicts this matrix for the maximum accepted p-value (the significance level) of 0.5.

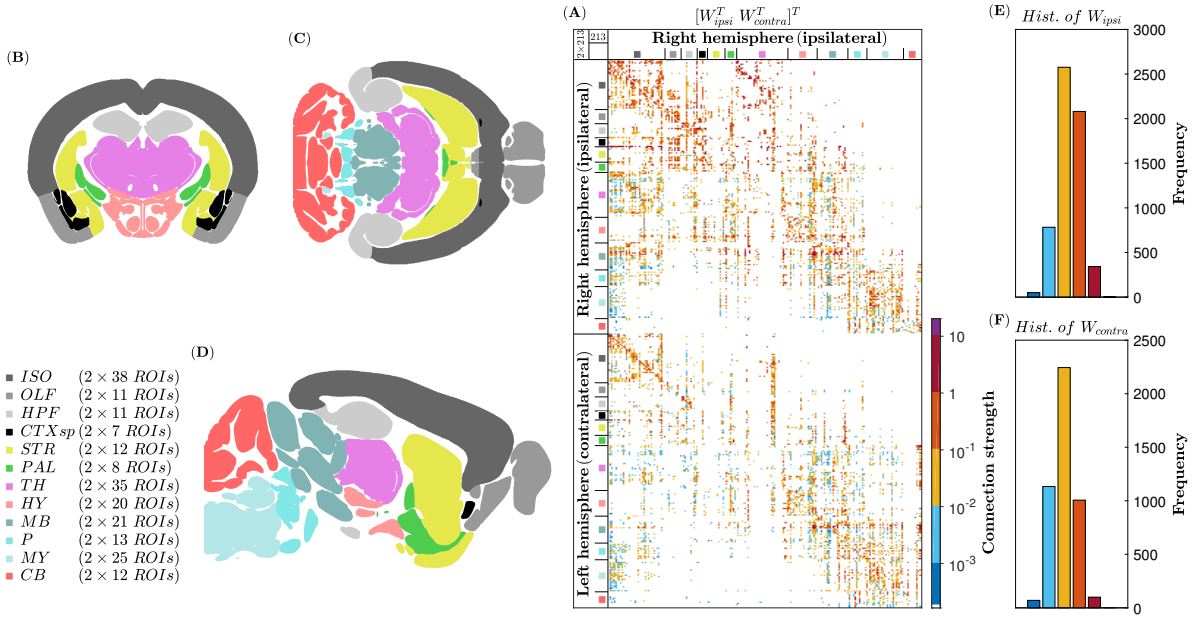

Figure 3: (A) Graphical representation of $\left[\boldsymbol{W}_{ipsi}^T\ \boldsymbol{W}_{contra}^T\right]^T$ for the significance level of 0.5. Images (B), (C), and (D) show coronal, axial, and sagittal views of the mouse brain, respectively, which demonstrate the 12 major regions of the gray matter: isocortex (ISO), olfactory areas (OLF), hippocampal formation (HPF), cortical subplate (CTXsp), striatum (STR), pallidum (PAL), thalamus (TH), hypothalamus (HY), midbrain (MB), pons (P), medulla (MY), and cerebellum (CB). To generate this result, we used the dataset of the Allen Mouse Common Coordinate Framework (CCFv3) [96] (help.brain-map.org/display/mouseconnectivity/API, specifically annotation/ccf_2017). (E) and (F) also display the histograms of $\boldsymbol{W}_{ipsi}$ and $\boldsymbol{W}_{contra}$, respectively.

In the AMBCA project, axonal projections were traced by injecting recombinant adeno-associated virus (AAV) expressing enhanced green fluorescent protein (EGFP), which is known as an anterograde tracer. In this sense, based on the assumption that hemispheric symmetry holds, one can define an anterograde weighted adjacency matrix in the following way:

$$\boldsymbol{W}_{an} = \begin{pmatrix} \boldsymbol{W}_{ipsi} & \boldsymbol{W}_{contra} \\ \boldsymbol{W}_{contra} & \boldsymbol{W}_{ipsi} \end{pmatrix}, \tag{75}$$

and, consequently, it makes sense to suggest a retrograde weighted adjacency matrix $\boldsymbol{W}_{re} = r\boldsymbol{W}_{an}^T$ with $r \in \mathbb{R}_{>0}$. The two weighted adjacency matrices may eventually be combined into a single matrix

$$\boldsymbol{W} = \boldsymbol{W}_{an} + \boldsymbol{W}_{re}. \tag{76}$$

Now, let us construct the adjacency matrix $\boldsymbol{A}$ by replacing the nonzero elements of $\boldsymbol{W}$ with 1. Using mathematical induction, it can be shown that the number of different paths of length k from node i to node j, where k is a positive integer, equals to (j,i)-th entry of $\boldsymbol{A}^k$. Thus, there exists at least one path of length lower than or equal to p^* from each node to every other node if the matrix $\sum_{k=1}^{p^*} \boldsymbol{A}^k$ has positive values in all its off-diagonal entries. The minimum value of

bioRxiv preprint doi: https://doi.org/10.1101/2023.02.04.527149; this version posted February 4, 2023. The copyright holder for this preprint (which was not certified by peer review) is the author/funder, who has granted bioRxiv a license to display the preprint in perpetuity. It is made available under aCC-BY-NC-ND 4.0 International license.

p^* for different significance levels are illustrated in Table 1, which ensures that the weighted connectivity matrix $\boldsymbol{W}$ represents a strongly connected symmetric digraph for significance levels greater than or equal to 10^{-5}.

Table 1: Percentage of nonzero elements of the adjacency matrix $\boldsymbol{A}$ and the corresponding minimum value p^* for different maximum accepted p-values of the connection strengths.

The significance level	Percentage of non-zero elements of $\boldsymbol{A}$	The minimum value of p^*
≤ 0.5	19.34%	3
≤ 0.3	15.72%	4
≤ 0.1	11.89%	4
≤ 0.01	8.6%	4
$\leq 10^{-5}$	5.12%	5

Normalizing the matrix $\boldsymbol{W}$ requires taking into account the fact that the resulting Laplacian matrix must satisfy the condition $\mathbf{1}^T\boldsymbol{L} = 0$, ensuring that the total concentration will be preserved during a diffusion process. Thus, one may propose two methods to normalize $\boldsymbol{W}$: either by converting $\boldsymbol{W}$ into a left stochastic matrix, i.e., a matrix with each column summing to 1, or by dividing $\boldsymbol{W}$ by $\|\boldsymbol{W}\|_1$ where $\|.\|_1$ denotes the maximum absolute column sum of the matrix. It is more preferable to go with the latter option, which is simply scaling $\boldsymbol{W}$ by a coefficient, as the ratio of any two elements from different columns of $\boldsymbol{W}$ remains unchanged after normalizing. Moreover, since $\|\boldsymbol{W}\|_1$ depends on r, $\|\boldsymbol{W}_{an} + \boldsymbol{W}_{an}^T\|_1$ will be substituted here for $\|\boldsymbol{W}\|_1$ to ensure that the scaling coefficient is continuously differentiable with respect to r, which is necessary to calculate the sensitivity function that will be discussed in Subsection 7.3. Lastly, the normalized weighted adjacency matrix

$$\boldsymbol{W}_{no} = \frac{\boldsymbol{W}_{an} + r\boldsymbol{W}_{an}^T}{\|\boldsymbol{W}_{an} + \boldsymbol{W}_{an}^T\|_1} \tag{77}$$

yields the Laplacian matrix

$$\boldsymbol{L}_r = \boldsymbol{\Lambda}(\mathbf{1}^T\boldsymbol{W}_{no}) - \boldsymbol{W}_{no}. \tag{78}$$

7.2. Simulation results

Taking into account the Laplacian matrix $\boldsymbol{L}_r$, let us rewrite Eq. (45) for the mouse connectome G as follows:

$$\dot{\boldsymbol{c}} = \boldsymbol{\mathcal{R}}(\boldsymbol{c}) - \sigma\boldsymbol{\mathcal{L}}_G(\boldsymbol{c}), \quad \boldsymbol{c}(0) = \boldsymbol{c}_0 \in \mathbb{R}_{\geq 0}^{426}, \tag{79}$$

where $\boldsymbol{\alpha} = \alpha\mathbf{1}$, $\boldsymbol{\rho} = \rho\mathbf{1}$, $\boldsymbol{\mu} = \mu\mathbf{1}$, $\boldsymbol{\nu} = \nu\mathbf{1}$, $\boldsymbol{n} = n\mathbf{1}$, and the parameter vector $\boldsymbol{\theta} = (\alpha, \rho, \mu, \nu, \sigma, r, n)^T$ belongs to the set

$$\Theta = \mathbb{R}_{\geq 0} \times \mathbb{R}_{\geq 0} \times \mathbb{R}_{\geq 1} \times \mathbb{R}_{>0} \times \mathbb{R}_{>0} \times \mathbb{R}_{>0} \times \mathbb{R}_{\geq 1}. \tag{80}$$

Having analyzed the data from transgenic tau P301S mice, which represent animal models

bioRxiv preprint doi: https://doi.org/10.1101/2023.02.04.527149; this version posted February 4, 2023. The copyright holder for this preprint (which was not certified by peer review) is the author/funder, who has granted bioRxiv a license to display the preprint in perpetuity. It is made available under aCC-BY-NC-ND 4.0 International license.

of tauopathy, for up to 4 months, Meisl et al. [97] reported a doubling time of approximately 2 weeks in the brain stem, neocortex, and frontal lobe. This gives us a crude estimate of α, which is $ln(2)/2 \approx 0.35$. In animal experiments examining tauopathy progression, tau prion strains are commonly injected into the ROIs of the hippocampal formation (HPF) such as $CA1$ [98]. In our simulations, we therefore consider the following initial concentrations:

$$\begin{cases} 1 & for \;\; CA1, \\ 0 & for \; the \; other \; ROIs. \end{cases} \tag{81}$$

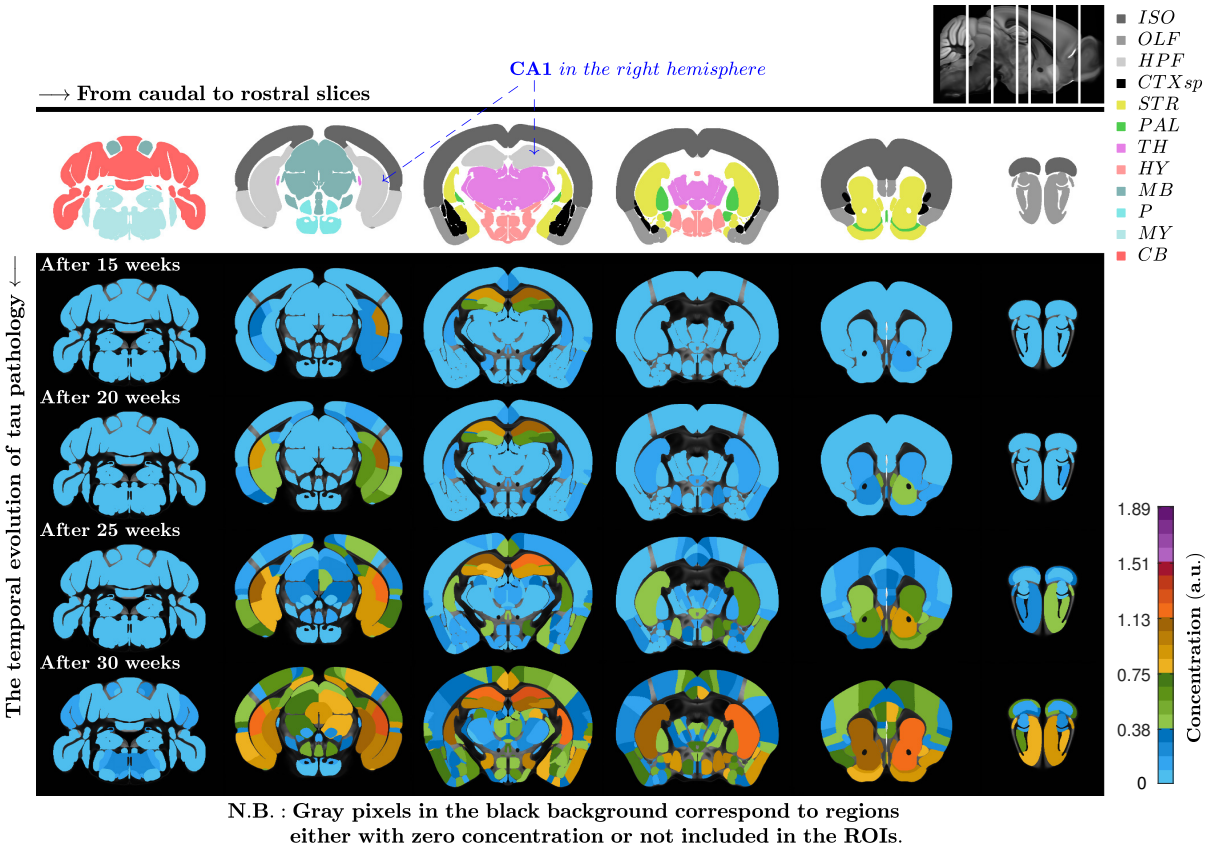

Figure 4: It displays the in-silico spatiotemporal evolution of tau pathology for the initial concentrations given in Eq. (81) when $(\alpha, \rho, \mu, \nu, \sigma, r, n) = (0.35, 1, 1, 1, 0.1, 1)$. To generate this result, we used the dataset of the Allen Mouse Common Coordinate Framework (CCFv3) [96] (help.brain-map.org/display/mouseconnectivity/API, specifically annotation/ccf_2017).

We conducted two in-silico experiments to examine the effect of nonlinear diffusion on the spatiotemporal evolution of tauopathy. First, a simulation was carried out for an anterograde-biased regime with $r = 0.1$ and the initial concentrations specified in Eq. (81), where $\alpha = 0.35$, and all the other parameters were set to 1; See Fig. 4. The simulation was then repeated with the same initial conditions and parameters, except that n was changed to 1.5. Fig. 5 illustrates how tauopathy evolved in the second in-silico experiment relative to that in the first. As shown in Fig. 5, increasing n slowed down the spreading of tau pathology. In fact, it resulted in tauopathy progression being localized more significantly to the ROIs adjacent to the in-silico injection site $CA1$ during the simulation period. One may note that decreasing the diffusion

bioRxiv preprint doi: https://doi.org/10.1101/2023.02.04.527149; this version posted February 4, 2023. The copyright holder for this preprint (which was not certified by peer review) is the author/funder, who has granted bioRxiv a license to display the preprint in perpetuity. It is made available under aCC-BY-NC-ND 4.0 International license.

coefficient σ can also lead to a similar result. To address this claim and investigate the effect of parameter variations on the progression of tauopathy, we intend to perform a sensitivity analysis.

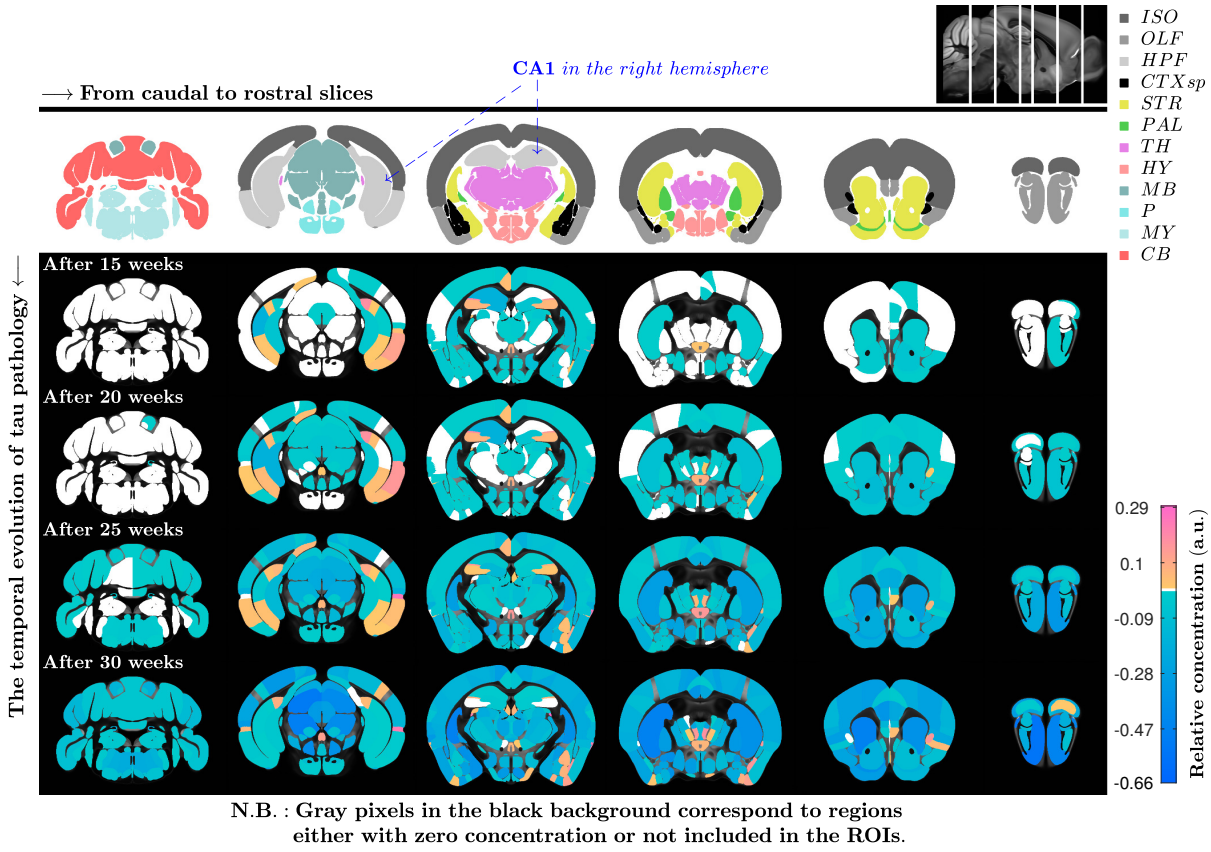

Figure 5: It exhibits the relative spatiotemporal evolution of tauopathy for the initial concentrations given in Eq. (81) in the in-silico experiment with the parameters $(\alpha, \rho, \mu, \nu, \sigma, r, n) = (0.35, 1, 1, 1, 0.1, 1.5)$ in comparison with that of one with the same parameters, except that $n = 1$. To generate this result, we used the dataset of the Allen Mouse Common Coordinate Framework (CCFv3) [96] (help.brain-map.org/display/mouseconnectivity/API, specifically annotation/ccf_2017).

7.3. Sensitivity analysis

Let $\boldsymbol{\mathcal{P}}(\boldsymbol{c}, \boldsymbol{\theta}) = \boldsymbol{\mathcal{R}}(\boldsymbol{c}) - \sigma \boldsymbol{\mathcal{L}}_G(\boldsymbol{c})$; then, by integration, the system (79) can be written as

$$\boldsymbol{c}(t, \boldsymbol{\theta}) = \boldsymbol{c}_0 + \int_0^t \boldsymbol{\mathcal{P}}(\boldsymbol{c}(\tau, \boldsymbol{\theta}), \boldsymbol{\theta})\, d\tau \tag{82}$$

having a unique solution $\boldsymbol{c}(t, \boldsymbol{\theta})$ for an initial concentration $\boldsymbol{c}_0 \in \mathbb{R}^{426}_{\geq 0}$ and a parameter vector $\boldsymbol{\theta} \in \Theta$ by Corollary 5.1. Calculating the partial derivatives of $\boldsymbol{\mathcal{P}}(\boldsymbol{c}, \boldsymbol{\theta})$ with respect to $\boldsymbol{c}$ and $\boldsymbol{\theta}$ yields

$$\begin{aligned}
\frac{\partial \boldsymbol{\mathcal{P}}}{\partial \boldsymbol{c}} &= \alpha \boldsymbol{\Lambda}\left(|\boldsymbol{c}|^{\mu-1}\right)\left(\mu\rho\mathbf{1} - (\mu+\nu)\,\boldsymbol{\Lambda}\left(|\boldsymbol{c}|^{\nu}\right)\right) - n\sigma \boldsymbol{L}_r \boldsymbol{\Lambda}\left(|\boldsymbol{c}|^{n-1}\right), \\
\frac{\partial \boldsymbol{\mathcal{P}}}{\partial \alpha} &= \boldsymbol{sgn}(\boldsymbol{c}) \odot |\boldsymbol{c}|^{\mu} \odot \left(\rho\mathbf{1} - |\boldsymbol{c}|^{\nu}\right), \\
\frac{\partial \boldsymbol{\mathcal{P}}}{\partial \rho} &= \alpha \boldsymbol{sgn}(\boldsymbol{c}) \odot |\boldsymbol{c}|^{\mu},
\end{aligned}$$

bioRxiv preprint doi: https://doi.org/10.1101/2023.02.04.527149; this version posted February 4, 2023. The copyright holder for this preprint (which was not certified by peer review) is the author/funder, who has granted bioRxiv a license to display the preprint in perpetuity. It is made available under aCC-BY-NC-ND 4.0 International license.

$$
\begin{aligned}
\frac{\partial \boldsymbol{\mathcal{P}}}{\partial \mu} &= \alpha \boldsymbol{sgn}\left(\boldsymbol{c}\right) \odot \boldsymbol{ln}\left(|\boldsymbol{c}|\right) \odot |\boldsymbol{c}|^{\mu} \odot \left(\rho \mathbf{1} - |\boldsymbol{c}|^{\nu}\right), \\
\frac{\partial \boldsymbol{\mathcal{P}}}{\partial \nu} &= -\alpha \boldsymbol{sgn}\left(\boldsymbol{c}\right) \odot \boldsymbol{ln}\left(|\boldsymbol{c}|\right) \odot |\boldsymbol{c}|^{\mu+\nu}, \\
\frac{\partial \boldsymbol{\mathcal{P}}}{\partial \sigma} &= -\boldsymbol{L}_r \left(\boldsymbol{sgn}\left(\boldsymbol{c}\right) \odot |\boldsymbol{c}|^{n}\right), \\
\frac{\partial \boldsymbol{\mathcal{P}}}{\partial r} &= -\frac{\sigma}{\|\boldsymbol{W}_{an} + \boldsymbol{W}_{an}^{T}\|_1} \left(\boldsymbol{\Lambda}(\mathbf{1}^T \boldsymbol{W}_{an}^{T}) - \boldsymbol{W}_{an}^{T}\right) \left(\boldsymbol{sgn}\left(\boldsymbol{c}\right) \odot |\boldsymbol{c}|^{n}\right), \\
\frac{\partial \boldsymbol{\mathcal{P}}}{\partial n} &= -\sigma \boldsymbol{L}_r \left(\boldsymbol{sgn}\left(\boldsymbol{c}\right) \odot \boldsymbol{ln}\left(|\boldsymbol{c}|\right) \odot |\boldsymbol{c}|^{n}\right),
\end{aligned}
\tag{83}
$$

where are continuous for all $(\boldsymbol{c}, \boldsymbol{\theta}) \in \mathbb{R}^{426} \times \Theta^{*}$ with

$$
\Theta^{*} = \mathbb{R} \times \mathbb{R} \times \mathbb{R}_{>1} \times \mathbb{R}_{>0} \times \mathbb{R} \times \mathbb{R} \times \mathbb{R}_{>1}. \tag{84}
$$

Note that $\lim_{\boldsymbol{c} \to 0} \boldsymbol{ln}\left(|\boldsymbol{c}|\right) \odot |\boldsymbol{c}|^{n} = 0$ for $n > 0$. Thanks to the continuous differentiability of $\boldsymbol{\mathcal{P}}\left(\boldsymbol{c}, \boldsymbol{\theta}\right)$ with respect to $\boldsymbol{c}$ and $\boldsymbol{\theta}$, the solution $\boldsymbol{c}\left(t, \boldsymbol{\theta}\right)$ is differentiable with respect to $\boldsymbol{\theta}$ near a nominal value $\boldsymbol{\theta}_0 \in \Theta^{*}$. Thus, we can obtain the following equation by taking partial derivatives of Eq. (82) with respect to $\boldsymbol{\theta}$.

$$
\frac{\partial \boldsymbol{c}}{\partial \boldsymbol{\theta}}\left(t, \boldsymbol{\theta}\right) = \int_0^t \left(\frac{\partial \boldsymbol{\mathcal{P}}}{\partial \boldsymbol{c}}\left(\boldsymbol{c}\left(\tau, \boldsymbol{\theta}\right), \boldsymbol{\theta}\right) \frac{\partial \boldsymbol{c}}{\partial \boldsymbol{\theta}}\left(\tau, \boldsymbol{\theta}\right) + \frac{\partial \boldsymbol{\mathcal{P}}}{\partial \boldsymbol{\theta}}\left(\boldsymbol{c}\left(\tau, \boldsymbol{\theta}\right), \boldsymbol{\theta}\right) \right) d\tau \tag{85}
$$

For a nominal solution $\boldsymbol{c}\left(t, \boldsymbol{\theta}_0\right)$ with $\boldsymbol{\theta}_0 \in \Theta \cap \Theta^{*}$, differentiating both sides of Eq. (85) with respect to t gives the sensitivity equation

$$
\dot{\boldsymbol{S}}\left(t\right) = \frac{\partial \boldsymbol{\mathcal{P}}}{\partial \boldsymbol{c}}\left(\boldsymbol{c}, \boldsymbol{\theta}\right)\Big|_{\substack{\boldsymbol{\theta} = \boldsymbol{\theta}_0 \\ \boldsymbol{c} = \boldsymbol{c}\left(t, \boldsymbol{\theta}_0\right)}} \boldsymbol{S}\left(t\right) + \frac{\partial \boldsymbol{\mathcal{P}}}{\partial \boldsymbol{\theta}}\left(\boldsymbol{c}, \boldsymbol{\theta}\right)\Big|_{\substack{\boldsymbol{\theta} = \boldsymbol{\theta}_0 \\ \boldsymbol{c} = \boldsymbol{c}\left(t, \boldsymbol{\theta}_0\right)}}, \quad \boldsymbol{S}\left(0\right) = 0, \tag{86}
$$

where $\boldsymbol{S}\left(t\right) = \frac{\partial \boldsymbol{c}}{\partial \boldsymbol{\theta}}\left(t, \boldsymbol{\theta}_0\right)$. The sensitivity function $\boldsymbol{S}\left(t\right)$ provides a first-order estimate of the effect of parameter variations on the solution $\boldsymbol{c}\left(t, \boldsymbol{\theta}_0\right)$. In other words, for $\boldsymbol{\theta}$ sufficiently close to $\boldsymbol{\theta}_0$, the solution $\boldsymbol{c}\left(t, \boldsymbol{\theta}\right)$ can be approximated by a Taylor series about the solution $\boldsymbol{c}\left(t, \boldsymbol{\theta}_0\right)$, i.e.,

$$
\boldsymbol{c}\left(t, \boldsymbol{\theta}\right) = \boldsymbol{c}\left(t, \boldsymbol{\theta}_0\right) + \boldsymbol{S}\left(t\right)\left(\boldsymbol{\theta} - \boldsymbol{\theta}_0\right) + \textit{higher-order terms}.
$$

Due to the large number of elements in the sensitivity function $\boldsymbol{S}\left(t\right)$, i.e., 426×7, it is difficult to scrutinize the simulation results for this function, and therefore a version of $\boldsymbol{S}\left(t\right)$ with a lower dimension is required. For the solution $\boldsymbol{c}\left(t, \boldsymbol{\theta}\right)$, let us now define the spatial average concentration at time t

$$
SAC\left(t, \boldsymbol{\theta}\right) = \frac{\boldsymbol{b}^T \boldsymbol{c}\left(t, \boldsymbol{\theta}\right)}{\mathbf{1}^T \boldsymbol{b}}, \tag{87}
$$

where the i-th element of the vector $\boldsymbol{b}$ is the number of voxels occupied by the i-th ROI, according to the dataset of the Allen Mouse Common Coordinate Framework (CCFv3) [96] (help.brain-map.org/display/mouseconnectivity/API, specifically annotation/ccf_2017). The

bioRxiv preprint doi: https://doi.org/10.1101/2023.02.04.527149; this version posted February 4, 2023. The copyright holder for this preprint (which was not certified by peer review) is the author/funder, who has granted bioRxiv a license to display the preprint in perpetuity. It is made available under aCC-BY-NC-ND 4.0 International license.

spatial average concentration approximately represents the spatial average of the distribution of the species concentration over the entire brain. It is easy to see that the sensitivity function for the spatial average concentration is derived as follows:

$$\frac{\partial SAC}{\partial \boldsymbol{\theta}}(t, \boldsymbol{\theta}_0) = \frac{\boldsymbol{b}^T \boldsymbol{S}(t)}{\mathbf{1}^T \boldsymbol{b}}. \tag{88}$$

Taking into account the initial concentrations given in Eq. (81), we computed the sensitivity function $\boldsymbol{S}(t)$ and its corresponding function $\partial SAC/\partial \boldsymbol{\theta}(t, \boldsymbol{\theta}_0)$ at 16 different points $\boldsymbol{\theta}_0$ in the parameter space. The maximum absolute value over time of each element of $\partial SAC/\partial \boldsymbol{\theta}(t, \boldsymbol{\theta}_0)$ have been reported in Table 2 for the chosen parameter values. Fig. 6 also illustrates the simulation results from which we derived the maximum absolute values in the first two rows of Table 2. As outlined in Table 2, the spatial average concentration of tauopathy generally appears to be more sensitive to variations in the parameter μ than to variations in the other parameters. Among the reaction term coefficients, including α, ρ, μ, and ν, the variation in ν also has the least impact on the model output at the selected points in the parameter space, and in general, there is a greater sensitivity to variations in α than that to variations in ρ. However, as indicated in Fig. 6, variations in ρ can substantially change the steady state of the spatial average concentration. According to Table 2, when restricting ourselves to the diffusion term coefficients, namely, σ, r, and n, the average concentration of tau pathology seems chiefly to be most sensitive to r at the points in the parameter space with an anterograde-biased regime ($r = 0.1$) and to n at the points with a directionally unbiased regime ($r = 1$). Additionally, among all the seven parameters considered, variations in the parameter σ have the least influence on the model output.

8. Conclusion

In this manuscript, the extended FP diffusion and Fisher-KPP reaction-diffusion equations on weighted digraphs whose SCCs are terminals were introduced. For the extended FP diffusion equation, it was shown that all solutions remain bounded and converge to equilibria which are stable. Further, we found positively invariant sets containing exactly one equilibrium point. Indeed, the domain of attraction of each equilibrium point was obtained. We also presented a family of positively invariant sets for the extended FP Fisher-KPP reaction-diffusion equation. Since a weighted undirected graph can be considered as a symmetric digraph, our results are also applicable to any arbitrary weighted undirected graph. To assess the practical significance of the proposed equations, it was first illustrated that the extended FP diffusion equation can generate a directionally-biased anomalous subdiffusion process on a one-dimensional lattice, which can be applied to describe the motion of motor proteins on microtubules. Moreover, we modeled tauopathy progression in the mouse brain connectome using the extended FP Fisher-KPP equation and then conducted a sensitivity analysis to estimate the effect of model parameter variations on solutions.

Here, the active concentration was also introduced. By definition, the active concentration

bioRxiv preprint doi: https://doi.org/10.1101/2023.02.04.527149; this version posted February 4, 2023. The copyright holder for this preprint (which was not certified by peer review) is the author/funder, who has granted bioRxiv a license to display the preprint in perpetuity. It is made available under aCC-BY-NC-ND 4.0 International license.

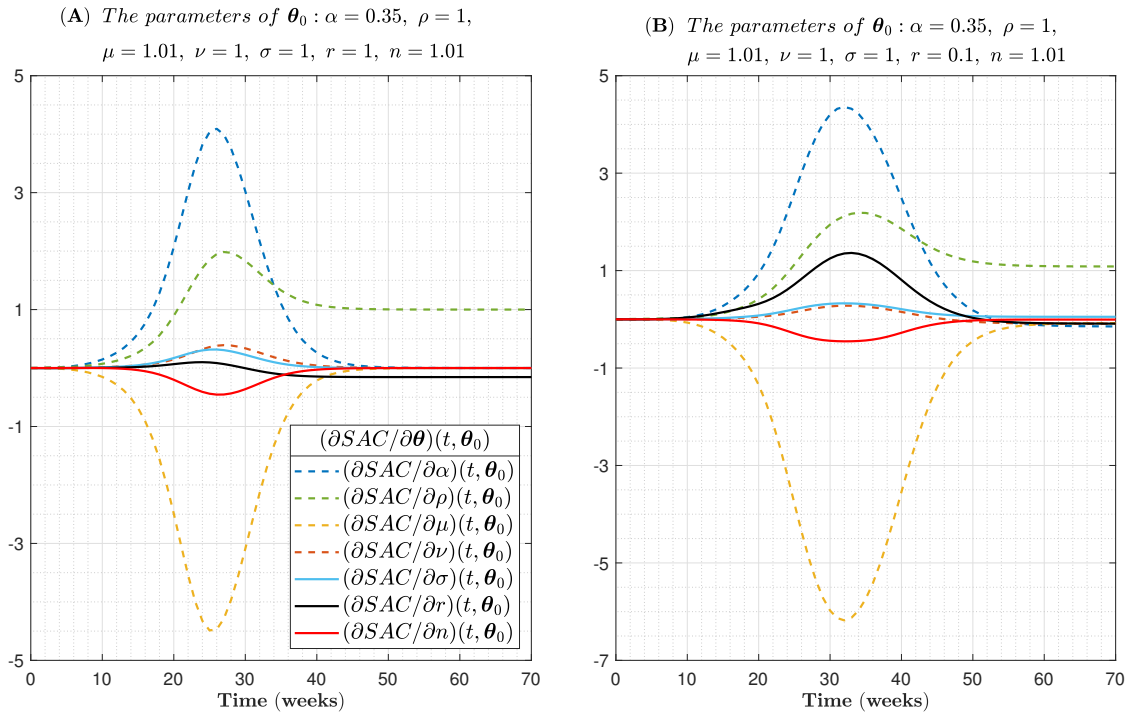

Figure 6: The elements of $\partial SAC/\partial \boldsymbol{\theta}\,(t, \boldsymbol{\theta}_0)$ are depicted in (A) for a directionally unbiased regime and in (B) for an anterograde-biased regime with r=0.1, where the initial concentrations are taken as Eq. (81).

of a given species can take a negative value, indicating the dominance of an antibody of that species. The concept of active concentration combined with the proposed extended FP equations enables us to capture the dynamics of a given species in presence of its antibody, which provides a useful framework for future research on studying antibodies, such as anti-tau and anti-amyloid antibodies for Alzheimer's disease.

Declaration of competing interest

The authors declare that the research was conducted in the absence of any commercial or financial relationships that could be construed as a potential conflict of interest.

Data availability

In this research project, we drew on the publicly available data from the Allen Mouse Brain Connectivity Atlas (AMBCA) [95] (connectivity.brain-map.org) and the dataset of the Allen Mouse Common Coordinate Framework (CCFv3) [96] (help.brain-map.org/display/mouse connectivity/API, specifically annotation/ccf_2017). All computations, including numerical solution of differential equations, were also done using MATLAB.

Acknowledgments

We acknowledge the support of the Natural Sciences and Engineering Research Council of Canada (NSERC) and GCS Faculty Research Support, Concordia University.

bioRxiv preprint doi: https://doi.org/10.1101/2023.02.04.527149; this version posted February 4, 2023. The copyright holder for this preprint (which was not certified by peer review) is the author/funder, who has granted bioRxiv a license to display the preprint in perpetuity. It is made available under aCC-BY-NC-ND 4.0 International license.

Table 2: The maximum absolute value over time of the elements of $\partial SAC/\partial \boldsymbol{\theta}\,(t, \boldsymbol{\theta}_0)$ for some different nominal values $\boldsymbol{\theta}_0$, where the initial concentrations are taken as Eq. (81).

$\boldsymbol{\theta}_0$							The maximum absolute value over time of						
α	ρ	μ	ν	σ	r	n	$\frac{\partial SAC}{\partial \alpha}$	$\frac{\partial SAC}{\partial \rho}$	$\frac{\partial SAC}{\partial \mu}$	$\frac{\partial SAC}{\partial \nu}$	$\frac{\partial SAC}{\partial \sigma}$	$\frac{\partial SAC}{\partial r}$	$\frac{\partial SAC}{\partial n}$
0.35	1	1.01	1	1	1	1.01	4.09	1.98	**4.49**	0.39	0.32	0.15	**0.45**
0.35	1	1.01	1	1	0.1	1.01	4.36	2.19	**6.18**	0.28	0.33	**1.36**	0.45
1	1	1.01	1	1	1	1.01	1.5	2.04	**5.53**	0.34	0.32	0.13	**0.51**
1	1	1.01	1	1	0.1	1.01	1.56	2.14	**7.25**	0.25	0.31	**1.12**	0.54
0.35	**0.5**	1.01	1	1	1	1.01	1.89	1.88	**2.29**	0.44	0.15	0.1	**0.26**
0.35	**0.5**	1.01	1	1	0.1	1.01	2.1	2.16	**3.22**	0.43	0.16	**0.8**	0.25
0.35	1	**1.3**	1	1	1	1.01	**5.04**	2.73	3.9	0.63	**0.5**	0.23	0.13
0.35	1	**1.3**	1	1	0.1	1.01	**4.5**	2.68	4.49	0.39	0.44	**3.05**	0.39
0.35	1	1.01	**0.3**	1	1	1.01	3.01	**3.45**	3.17	2.31	0.16	0.23	**0.31**
0.35	1	1.01	**0.3**	1	0.1	1.01	3.98	4.34	**5.45**	2.63	0.24	**0.82**	0.43
0.35	1	1.01	**2.5**	1	1	1.01	5.02	1.97	**5.44**	0.07	0.45	0.19	**0.47**
0.35	1	1.01	**2.5**	1	0.1	1.01	4.3	1.74	**6.09**	0.03	0.34	**1.55**	0.4
0.35	1	1.01	1	**1.5**	1	1.01	4.06	1.96	**4.18**	0.41	0.2	0.18	**0.42**
0.35	1	1.01	1	**1.5**	0.1	1.01	4.37	2.2	**5.87**	0.29	0.22	**1.49**	0.4
0.35	1	1.01	1	1	1	**1.5**	**3.89**	2.02	**3.89**	0.42	**0.3**	0.12	**0.3**
0.35	1	1.01	1	1	0.1	**1.5**	4.37	2.26	**5.48**	0.34	0.34	**1.15**	0.31

References

[1] R. A. Fisher, The wave of advance of advantageous genes, Annals of eugenics 7 (4) (1937) 355–369. doi:https://doi.org/10.1111/j.1469-1809.1937.tb02153.x.

[2] V. Tikhomirov, A study of the diffusion equation with increase in the amount of substance, and its application to a biological problem, in: Selected works of AN Kolmogorov, Springer, 1991, pp. 242–270. doi:10.1007/978-94-011-3030-1_38.

[3] S. Fornari, A. Schäfer, M. Jucker, A. Goriely, E. Kuhl, Prion-like spreading of Alzheimer's disease within the brain's connectome, Journal of the Royal Society Interface 16 (159) (2019) 20190356. doi:https://doi.org/10.1098/rsif.2019.0356.

[4] A. Schäfer, E. C. Mormino, E. Kuhl, Network diffusion modeling explains longitudinal tau pet data, Frontiers in Neuroscience 14 (2020) 566876. doi:https://doi.org/10.3389/fnins.2020.566876.

[5] P. Putra, T. B. Thompson, P. Chaggar, A. Goriely, A. D. N. Initiative, et al., Braiding braak

bioRxiv preprint doi: https://doi.org/10.1101/2023.02.04.527149; this version posted February 4, 2023. The copyright holder for this preprint (which was not certified by peer review) is the author/funder, who has granted bioRxiv a license to display the preprint in perpetuity. It is made available under aCC-BY-NC-ND 4.0 International license.

and braak: Staging patterns and model selection in network neurodegeneration, Network Neuroscience 5 (4) (2021) 929–956. doi:https://doi.org/10.1162/netn_a_00208.

[6] P. S. Putra, H. Oliveri, T. B. Thompson, A. Goriely, Front propagation and arrival times in networks with application to neurodegenerative diseases, bioRxiv (2022). doi:https://doi.org/10.1101/2022.01.04.474911.

[7] I. Mirzaev, J. Gunawardena, Laplacian dynamics on general graphs, Bull. Math. Biol. 75 (11) (2013) 2118–2149. doi:https://doi.org/10.1007/s11538-013-9884-8.

[8] M. Asllani, J. D. Challenger, F. S. Pavone, L. Sacconi, D. Fanelli, The theory of pattern formation on directed networks, Nature communications 5 (1) (2014) 1–9. doi:https://doi.org/10.1038/ncomms5517.

[9] J. Veerman, E. Kummel, Diffusion and consensus on weakly connected directed graphs, Linear Algebra and its Applications 578 (2019) 184–206. doi:https://doi.org/10.1016/j.laa.2019.05.014.

[10] J. Veerman, R. Lyons, A primer on Laplacian dynamics in directed graphs, NONLINEAR PHENOMENA IN COMPLEX SYSTEMS 23 (2) (2020) 196–206. doi:https://doi.org/10.33581/1561-4085-2020-23-2-196-206.

[11] F. Chung, Laplacians and the cheeger inequality for directed graphs, Annals of Combinatorics 9 (1) (2005) 1–19. doi:https://doi.org/10.1007/s00026-005-0237-z.

[12] D. Zhou, J. Huang, B. Schölkopf, Learning from labeled and unlabeled data on a directed graph, in: Proceedings of the 22nd international conference on Machine learning, 2005, pp. 1036–1043. doi:https://doi.org/10.1145/1102351.1102482.

[13] F. Chung, Random walks and local cuts in graphs, Linear Algebra and its applications 423 (1) (2007) 22–32. doi:https://doi.org/10.1016/j.laa.2006.07.018.

[14] Y. Li, Z.-L. Zhang, Digraph laplacian and the degree of asymmetry, Internet Mathematics 8 (4) (2012) 381–401. doi:https://doi.org/10.1080/15427951.2012.708890.

[15] Y. Yoshida, Nonlinear Laplacian for digraphs and its applications to network analysis, in: Proceedings of the Ninth ACM International Conference on Web Search and Data Mining, 2016, pp. 483–492. doi:https://doi.org/10.1145/2835776.2835785.

[16] E. J. Friedman, A. S. Landsberg, Duality and nonlinear graph Laplacians, Theoretical Computer Science 713 (2018) 21–30. doi:https://doi.org/10.1016/j.tcs.2017.12.034.

[17] Y. Yoshida, Cheeger inequalities for submodular transformations, in: Proceedings of the Thirtieth Annual ACM-SIAM Symposium on Discrete Algorithms, SIAM, 2019, pp. 2582–2601. doi:https://doi.org/10.1137/1.9781611975482.160.

bioRxiv preprint doi: https://doi.org/10.1101/2023.02.04.527149; this version posted February 4, 2023. The copyright holder for this preprint (which was not certified by peer review) is the author/funder, who has granted bioRxiv a license to display the preprint in perpetuity. It is made available under aCC-BY-NC-ND 4.0 International license.

[18] M. Ikeda, A. Miyauchi, Y. Takai, Y. Yoshida, Finding cheeger cuts in hypergraphs via heat equation, Theoretical Computer Science 930 (2022) 1–23. doi:https://doi.org/10.1016/j.tcs.2022.07.006.

[19] A. P. Riascos, J. L. Mateos, Fractional dynamics on networks: Emergence of anomalous diffusion and lévy flights, Physical Review E 90 (3) (2014) 032809. doi:https://doi.org/10.1103/PhysRevE.90.032809.

[20] L. Aceto, P. Novati, Rational approximation to the fractional Laplacian operator in reaction-diffusion problems, SIAM Journal on Scientific Computing 39 (1) (2017) A214–A228. doi:https://doi.org/10.1137/16M1064714.

[21] M. Benzi, D. Bertaccini, F. Durastante, I. Simunec, Non-local network dynamics via fractional graph Laplacians, Journal of Complex Networks 8 (3) (2020) cnaa017. doi:https://doi.org/10.1093/comnet/cnaa017.

[22] D. Bertaccini, F. Durastante, Nonlocal diffusion of variable order on complex networks, International Journal of Computer Mathematics: Computer Systems Theory 7 (3) (2022) 172–191. doi:https://doi.org/10.1080/23799927.2022.2114381.

[23] E. Estrada, Path laplacian matrices: introduction and application to the analysis of consensus in networks, Linear algebra and its applications 436 (9) (2012) 3373–3391. doi:https://doi.org/10.1016/j.laa.2011.11.032.

[24] E. Estrada, E. Hameed, N. Hatano, M. Langer, Path Laplacian operators and superdiffusive processes on graphs. I. One-dimensional case, Linear Algebra and its Applications 523 (2017) 307–334. doi:https://doi.org/10.1016/j.laa.2017.02.027.

[25] E. Estrada, E. Hameed, M. Langer, A. Puchalska, Path Laplacian operators and superdiffusive processes on graphs. II. Two-dimensional lattice, Linear Algebra and its Applications 555 (2018) 373–397. doi:https://doi.org/10.1016/j.laa.2018.06.026.

[26] E. Estrada, Path laplacians versus fractional laplacians as nonlocal operators on networks, New Journal of Physics 23 (7) (2021) 073049. doi:10.1088/1367-2630/ac14ac.

[27] F. Diaz-Diaz, E. Estrada, Time and space generalized diffusion equation on graph/networks, Chaos, Solitons & Fractals 156 (2022) 111791. doi:https://doi.org/10.1016/j.chaos.2022.111791.

[28] A. Elmoataz, O. Lezoray, S. Bougleux, Nonlocal discrete regularization on weighted graphs: a framework for image and manifold processing, IEEE transactions on Image Processing 17 (7) (2008) 1047–1060. doi:10.1109/TIP.2008.924284.

[29] F. Lozes, A. Elmoataz, O. Lézoray, Partial difference operators on weighted graphs for image processing on surfaces and point clouds, IEEE Transactions on Image Processing 23 (9) (2014) 3896–3909. doi:10.1109/TIP.2014.2336548.

bioRxiv preprint doi: https://doi.org/10.1101/2023.02.04.527149; this version posted February 4, 2023. The copyright holder for this preprint (which was not certified by peer review) is the author/funder, who has granted bioRxiv a license to display the preprint in perpetuity. It is made available under aCC-BY-NC-ND 4.0 International license.

[30] T. Carletti, M. Asllani, D. Fanelli, V. Latora, Nonlinear walkers and efficient exploration of congested networks, Physical Review Research 2 (3) (2020) 033012. doi:https://doi.org/10.1103/PhysRevResearch.2.033012.

[31] C. Falcó, From random walks on networks to nonlinear diffusion, Physical Review E 106 (5) (2022) 054103. doi:https://doi.org/10.1103/PhysRevE.106.054103.

[32] J. Veerman, T. Whalen-Wagner, E. Kummel, Chemical reaction networks in a Laplacian framework, Chaos, Solitons & Fractals 166 (2023) 112859. doi:https://doi.org/10.1016/j.chaos.2022.112859.

[33] M. Feinberg, Chemical reaction network structure and the stability of complex isothermal reactors—i. the deficiency zero and deficiency one theorems, Chemical engineering science 42 (10) (1987) 2229–2268. doi:https://doi.org/10.1016/0009-2509(87)80099-4.

[34] M. Feinberg, Foundations of chemical reaction network theory (2019). doi:https://doi.org/10.1007/978-3-030-03858-8.

[35] D. S. Banks, C. Fradin, Anomalous diffusion of proteins due to molecular crowding, Biophysical journal 89 (5) (2005) 2960–2971. doi:https://doi.org/10.1529/biophysj.104.051078.

[36] I. Golding, E. C. Cox, Physical nature of bacterial cytoplasm, Physical review letters 96 (9) (2006) 098102. doi:https://doi.org/10.1103/PhysRevLett.96.098102.

[37] J. Szymanski, M. Weiss, Elucidating the origin of anomalous diffusion in crowded fluids, Physical review letters 103 (3) (2009) 038102. doi:https://doi.org/10.1103/PhysRevLett.103.038102.

[38] S. C. Weber, A. J. Spakowitz, J. A. Theriot, Bacterial chromosomal loci move subdiffusively through a viscoelastic cytoplasm, Physical review letters 104 (23) (2010) 238102. doi:https://doi.org/10.1103/PhysRevLett.104.238102.

[39] J.-H. Jeon, V. Tejedor, S. Burov, E. Barkai, C. Selhuber-Unkel, K. Berg-Sørensen, L. Oddershede, R. Metzler, In vivo anomalous diffusion and weak ergodicity breaking of lipid granules, Physical review letters 106 (4) (2011) 048103. doi:https://doi.org/10.1103/PhysRevLett.106.048103.

[40] E. Barkai, Y. Garini, R. Metzler, Strange kinetics of single molecules in living cells, Phys. Today 65 (8) (2012) 29. doi:10.1063/PT.3.1677.

[41] F. Höfling, T. Franosch, Anomalous transport in the crowded world of biological cells, Reports on Progress in Physics 76 (4) (2013) 046602. doi:10.1088/0034-4885/76/4/046602.

[42] H. Li, Z. Wu, J. Yin, J. Zhao, Nonlinear diffusion equations, World Scientific, 2001.

bioRxiv preprint doi: https://doi.org/10.1101/2023.02.04.527149; this version posted February 4, 2023. The copyright holder for this preprint (which was not certified by peer review) is the author/funder, who has granted bioRxiv a license to display the preprint in perpetuity. It is made available under aCC-BY-NC-ND 4.0 International license.

[43] J. L. Vázquez, The porous medium equation: mathematical theory, Oxford University Press on Demand, 2007.

[44] R. A. Horn, C. R. Johnson, Matrix analysis, 2nd Edition, Cambridge University Press, 2012. doi:https://doi.org/10.1017/CBO9780511810817.

[45] H. K. Khalil, Nonlinear systems, 3rd Edition, Prentice Hall, Upper Saddle River, NJ, 2002.

[46] J. LaSalle, Some extensions of Liapunov's second method, IRE Trans. circuit theory 7 (4) (1960) 520–527. doi:https://doi.org/10.1109/TCT.1960.1086720.

[47] A. Filippov, Differential Equations with Discontinuous Righthand Sides: Control Systems, Vol. 18, Springer Science & Business Media, 1988. doi:https://doi.org/10.1007/978-94-015-7793-9.

[48] B. Paden, S. Sastry, A calculus for computing filippov's differential inclusion with application to the variable structure control of robot manipulators, IEEE transactions on circuits and systems 34 (1) (1987) 73–82. doi:10.1109/TCS.1987.1086038.

[49] D. Shevitz, B. Paden, Lyapunov stability theory of nonsmooth systems, IEEE Transactions on automatic control 39 (9) (1994) 1910–1914. doi:10.1109/9.317122.

[50] A. Bacciotti, F. Ceragioli, Stability and stabilization of discontinuous systems and nonsmooth lyapunov functions, ESAIM: Control, Optimisation and Calculus of Variations 4 (1999) 361–376. doi:https://doi.org/10.1051/cocv:1999113.

[51] F. H. Clarke, Generalized gradients and applications, Transactions of the American Mathematical Society 205 (1975) 247–262. doi:https://doi.org/10.1090/S0002-9947-1975-0367131-6.

[52] D. G. Luenberger, Introduction to dynamic systems; theory, models, and applications, Wiley, 1979.

[53] P. De Leenheer, Stabiliteit, regeling en stabilisatie van positieve systemen, Ph.D. thesis, University of Gent (2000).

[54] J. Bang-Jensen, G. Z. Gutin, Digraphs: theory, algorithms and applications, 2nd Edition, Springer, London, 2009. doi:https://doi.org/10.1007/978-1-84800-998-1.

[55] W. D. Blizard, Multiset theory, Notre Dame J. Form. Log. 30 (1) (1989) 36–66. doi:https://doi.org/10.1305/ndjfl/1093634995.

[56] L. Gillman, M. Jerison, Rings of continuous functions, Springer, originally published by Van Nostrand, 1960. doi:https://doi.org/10.1007/978-1-4615-7819-2.

[57] P. Royston, D. G. Altman, Regression using fractional polynomials of continuous covariates: parsimonious parametric modelling, J. R. Stat. Soc., C: Appl. Stat. 43 (3) (1994) 429–453. doi:https://doi.org/10.2307/2986270.

bioRxiv preprint doi: https://doi.org/10.1101/2023.02.04.527149; this version posted February 4, 2023. The copyright holder for this preprint (which was not certified by peer review) is the author/funder, who has granted bioRxiv a license to display the preprint in perpetuity. It is made available under aCC-BY-NC-ND 4.0 International license.

[58] P. Royston, W. Sauerbrei, Multivariable model-building: a pragmatic approach to regression anaylsis based on fractional polynomials for modelling continuous variables, Vol. 777, Wiley, 2008. doi:https://doi.org/10.1002/9780470770771.

[59] T. Abdeljawad, On Riemann and Caputo fractional differences, Comput. Math. Appl. 62 (3) (2011) 1602–1611. doi:https://doi.org/10.1016/j.camwa.2011.03.036.

[60] M. Rivero, S. V. Rogosin, J. A. Tenreiro Machado, J. J. Trujillo, Stability of fractional order systems, Math. Probl. Eng. 2013 (2013). doi:https://doi.org/10.1155/2013/356215.

[61] M. Müller, D. Schleicher, How to add a non-integer number of terms, and how to produce unusual infinite summations, J. Comput. Appl. Math. 178 (1-2) (2005) 347–360. doi:https://doi.org/10.1016/j.cam.2004.08.009.

[62] M. Müller, D. Schleicher, How to add a noninteger number of terms: From axioms to new identities, Am. Math. Mon. 118 (2) (2011) 136–152. doi:https://doi.org/10.4169/amer.math.monthly.118.02.136.

[63] B. Ü. Uzun, On the fractional sums of some special functions, Results Math. 74 (1) (2019) 1–11. doi:https://doi.org/10.1007/s00025-019-0964-4.

[64] T. Yano, On the theory of b-functions, Publ. Res. Inst. Math. Sci. 14 (1) (1978) 111–202. doi:https://doi.org/10.2977/prims/1195189282.

[65] G. Blanco, Yano's conjecture, Invent. Math. 226 (2) (2021) 421–465. doi:https://doi.org/10.1007/s00222-021-01052-2.

[66] L. Frerick, L. Loosveldt, J. Wengenroth, Continuously differentiable functions on compact sets, Results Math. 75 (4) (2020) 1–19. doi:https://doi.org/10.1007/s00025-020-01303-3.

[67] J. M. Lee, Smooth manifolds, in: Introduction to Smooth Manifolds, Springer, New York, NY, 2013, pp. 1–31. doi:https://doi.org/10.1007/978-1-4419-9982-5_1.

[68] H. Whitney, Differentiable functions defined in closed sets. I, Trans. Am. Math. Soc. 36 (2) (1934) 369–387. doi:https://doi.org/10.2307/1989844.

[69] H. Whitney, Analytic extensions of differentiable functions defined in closed sets, Trans. Am. Math. Soc. 36 (1) (1934) 63–89. doi:https://doi.org/10.2307/1989708.

[70] G. Glaeser, Étude de Quelques Algèbres Tayloriennes, J. Anal. Math. 6 (1) (1958) 1–124. doi:https://doi.org/10.1007/BF02790231.

[71] E. Bierstone, P. D. Milman, W. Pawłucki, Differentiable functions defined in closed sets. a problem of Whitney, Invent. math. 151 (2) (2003) 329–352. doi:https://doi.org/10.1007/s00222-002-0255-6.

bioRxiv preprint doi: https://doi.org/10.1101/2023.02.04.527149; this version posted February 4, 2023. The copyright holder for this preprint (which was not certified by peer review) is the author/funder, who has granted bioRxiv a license to display the preprint in perpetuity. It is made available under aCC-BY-NC-ND 4.0 International license.

[72] C. Fefferman, Whitney's extension problem for C^m, Ann. Math. 164 (2006) 313–359. doi:https://doi.org/10.4007/annals.2006.164.313.

[73] M. Thomson, J. Gunawardena, The rational parameterisation theorem for multisite post-translational modification systems, J. Theor. Biol. 261 (4) (2009) 626–636. doi:https://doi.org/10.1016/j.jtbi.2009.09.003.

[74] A. Buhagiar, Kinetics of phase segregation in a quenched alloy, Ph.D. thesis, The Open University (1981). doi:https://doi.org/10.21954/ou.ro.0000fc91.

[75] J. M. Ball, J. Carr, O. Penrose, The Becker-Döring cluster equations: basic properties and asymptotic behaviour of solutions, Commun. Math. Phys. 104 (4) (1986) 657–692. doi:https://doi.org/10.1007/BF01211070.

[76] J. Howard, Molecular motors: structural adaptations to cellular functions, Nature 389 (6651) (1997) 561–567. doi:https://doi.org/10.1038/39247.

[77] A. Caspi, R. Granek, M. Elbaum, Diffusion and directed motion in cellular transport, Physical Review E 66 (1) (2002) 011916. doi:https://doi.org/10.1103/PhysRevE.66.011916.

[78] L. Reese, A. Melbinger, E. Frey, Crowding of molecular motors determines microtubule depolymerization, Biophysical journal 101 (9) (2011) 2190–2200. doi:https://doi.org/10.1016/j.bpj.2011.09.009.

[79] M. Rank, E. Frey, Crowding and pausing strongly affect dynamics of kinesin-1 motors along microtubules, Biophysical journal 115 (6) (2018) 1068–1081. doi:https://doi.org/10.1016/j.bpj.2018.07.017.

[80] S. D. Ryan, Z. McCarthy, M. Potomkin, Motor protein transport along inhomogeneous microtubules, Bulletin of Mathematical Biology 83 (2) (2021) 1–29. doi:https://doi.org/10.1007/s11538-020-00838-4.

[81] L. Olivares-Quiroz, O. Resendis-Antonio, Quantitative models for microscopic to macroscopic biological macromolecules and tissues, Springer, 2018. doi:https://doi.org/10.1007/978-3-319-73975-5.

[82] Y. Wang, E. Mandelkow, Tau in physiology and pathology, Nature reviews neuroscience 17 (1) (2016) 22–35. doi:https://doi.org/10.1038/nrn.2015.1.

[83] P. W. Baas, L. Qiang, Tau: it's not what you think, Trends in cell biology 29 (6) (2019) 452–461. doi:https://doi.org/10.1016/j.tcb.2019.02.007.

[84] M. Hutton, C. L. Lendon, P. Rizzu, M. Baker, S. Froelich, H. Houlden, S. Pickering-Brown, S. Chakraverty, A. Isaacs, A. Grover, et al., Association of missense and 5'-splice-site mutations in tau with the inherited dementia FTDP-17, Nature 393 (6686) (1998) 702–705. doi:https://doi.org/10.1038/31508.

bioRxiv preprint doi: https://doi.org/10.1101/2023.02.04.527149; this version posted February 4, 2023. The copyright holder for this preprint (which was not certified by peer review) is the author/funder, who has granted bioRxiv a license to display the preprint in perpetuity. It is made available under aCC-BY-NC-ND 4.0 International license.

[85] F. Clavaguera, T. Bolmont, R. A. Crowther, D. Abramowski, S. Frank, A. Probst, G. Fraser, A. K. Stalder, M. Beibel, M. Staufenbiel, et al., Transmission and spreading of tauopathy in transgenic mouse brain, Nat. Cell Biol. 11 (7) (2009) 909–913. doi:https://doi.org/10.1038/ncb1901.

[86] L. Liu, V. Drouet, J. W. Wu, M. P. Witter, S. A. Small, C. Clelland, K. Duff, Trans-synaptic spread of tau pathology in vivo, PloS one 7 (2) (2012) e31302. doi:https://doi.org/10.1371/journal.pone.0031302.

[87] G. I. Hallinan, M. Vargas-Caballero, J. West, K. Deinhardt, Tau misfolding efficiently propagates between individual intact hippocampal neurons, Journal of Neuroscience 39 (48) (2019) 9623–9632. doi:https://doi.org/10.1523/JNEUROSCI.1590-19.2019.

[88] P. N. Sen, P. J. Basser, Modeling diffusion in white matter in the brain: a composite porous medium, Magnetic resonance imaging 23 (2) (2005) 215–220. doi:https://doi.org/10.1016/j.mri.2004.11.014.

[89] D. S. Novikov, E. Fieremans, S. N. Jespersen, V. G. Kiselev, Quantifying brain microstructure with diffusion mri: Theory and parameter estimation, NMR in Biomedicine 32 (4) (2019) e3998. doi:https://doi.org/10.1002/nbm.3998.

[90] M. Vidotto, M. Pederzani, A. Castellano, V. Pieri, A. Falini, D. Dini, E. De Momi, Integrating diffusion tensor imaging and neurite orientation dispersion and density imaging to improve the predictive capabilities of ced models, Annals of Biomedical Engineering 49 (2) (2021) 689–702. doi:https://doi.org/10.1007/s10439-020-02598-7.

[91] J. W. Wu, M. Herman, L. Liu, S. Simoes, C. M. Acker, H. Figueroa, J. I. Steinberg, M. Margittai, R. Kayed, C. Zurzolo, et al., Small misfolded tau species are internalized via bulk endocytosis and anterogradely and retrogradely transported in neurons, Journal of Biological Chemistry 288 (3) (2013) 1856–1870. doi:https://doi.org/10.1074/jbc.M112.394528.

[92] S. Takeda, S. Wegmann, H. Cho, S. L. DeVos, C. Commins, A. D. Roe, S. B. Nicholls, G. A. Carlson, R. Pitstick, C. K. Nobuhara, et al., Neuronal uptake and propagation of a rare phosphorylated high-molecular-weight tau derived from Alzheimer's disease brain, Nat. Commun. 6 (1) (2015) 1–15. doi:https://doi.org/10.1038/ncomms9490.

[93] J. Torok, P. D. Maia, P. Verma, C. Mezias, A. Raj, Emergence of directional bias in tau deposition from axonal transport dynamics, PLoS computational biology 17 (7) (2021) e1009258. doi:https://doi.org/10.1371/journal.pcbi.1009258.

[94] C. Mezias, A. Raj, The role of directionality in determining spatiotemporal tau pathology differs between AD-like and non-AD-like mouse models, bioRxiv (2020). doi:https://doi.org/10.1101/2020.11.06.371625.

bioRxiv preprint doi: https://doi.org/10.1101/2023.02.04.527149; this version posted February 4, 2023. The copyright holder for this preprint (which was not certified by peer review) is the author/funder, who has granted bioRxiv a license to display the preprint in perpetuity. It is made available under aCC-BY-NC-ND 4.0 International license.

[95] S. W. Oh, J. A. Harris, L. Ng, B. Winslow, N. Cain, S. Mihalas, Q. Wang, C. Lau, L. Kuan, A. M. Henry, et al., A mesoscale connectome of the mouse brain, Nature 508 (7495) (2014) 207–214. doi:https://doi.org/10.1038/nature13186.

[96] Q. Wang, S.-L. Ding, Y. Li, J. Royall, D. Feng, P. Lesnar, N. Graddis, M. Naeemi, B. Facer, A. Ho, et al., The allen mouse brain common coordinate framework: a 3d reference atlas, Cell 181 (4) (2020) 936–953. doi:https://doi.org/10.1016/j.cell.2020.04.007.

[97] G. Meisl, E. Hidari, K. Allinson, T. Rittman, S. L. DeVos, J. S. Sanchez, C. K. Xu, K. E. Duff, K. A. Johnson, J. B. Rowe, et al., In vivo rate-determining steps of tau seed accumulation in Alzheimer's disease, Science advances 7 (44) (2021) eabh1448. doi:10.1126/sciadv.abh1448.

[98] S. K. Kaufman, D. W. Sanders, T. L. Thomas, A. J. Ruchinskas, J. Vaquer-Alicea, A. M. Sharma, T. M. Miller, M. I. Diamond, Tau prion strains dictate patterns of cell pathology, progression rate, and regional vulnerability in vivo, Neuron 92 (4) (2016) 796–812. doi:https://doi.org/10.1016/j.neuron.2016.09.055.